iScience

CellPress
OPEN ACCESS

Review

State-of-the-art in carbides/carbon composites for electromagnetic wave absorption

Bo Hu,[1] Lixue Gai,[1] Yonglei Liu,[1] Pan Wang,[1] Shuping Yu,[1] Li Zhu,[1] Xijiang Han,[1,*] and Yunchen Du[1,*]

SUMMARY

Electromagnetic wave absorbing materials (EWAMs) have made great progress in the past decades, and are playing an increasingly important role in radiation prevention and antiradar detection due to their essential attenuation toward incident EM wave. With the flourish of nanotechnology, the design of high-performance EWAMs is not just dependent on the intrinsic characteristics of single-component medium, but pays more attention to the synergistic effects from different components to generate rich loss mechanisms. Among various candidates, carbides and carbon materials are usually labeled with the features of chemical stability, low density, tunable dielectric property, and diversified morphology/microstructure, and thus the combination of carbides and carbon materials will be a promising way to acquire new EWAMs with good practical application prospects. In this review, we introduce EM loss mechanisms related to dielectric composites, and then highlight the state-of-the-art progress in carbides/carbon composites as high-performance EWAMs, including silicon carbide/carbon, MXene/carbon, molybdenum carbide/carbon, as well as some uncommon carbides/carbon composites and multicomponent composites. The critical information regarding composition optimization, structural engineering, performance reinforcement, and structure-function relationship are discussed in detail. In addition, some challenges and perspectives for the development of carbides/carbon composites are also proposed after comparing the performance of some representative composites.

INTRODUCTION

Electromagnetic (EM) pollution refers to the interference and harmful radiation from natural and man-made EM wave. The extensive developments of radio, television, communication, and microwave technologies multiply various radiofrequency equipment, and especially with the arrival of 5G era, EM radiation on the ground will be increased significantly, which may even reach the level of a direct threat to human health.[1–3] In virtue of the characteristic function in energy dissipation, EM wave absorbing materials (EWAMs) have been considered as one of the most promising candidates for the precaution of EM pollution.[4–7] What's more, EWAMs also play an extremely important role in the field of military stealth, because they can effectively reduce the cross-section of a target under Radar detection to achieve the goal of confusing the enemy.[8,9] The intrinsic attenuation mechanisms of EWAMs originate from their interactions with the magnetic and electric field branches of incident EM wave, and thus EWAMs, in most cases, are customarily divided into magnetic loss materials and dielectric loss materials.[10,11] Magnetic loss materials ever dominated the practical application of EWAMs due to their powerful EM absorption, and some of them, such as ferrite, carbonyl iron, and Fe-Si-Al alloy, have been successfully developed as commercial EWAMs.[12–14] However, the attenuation amplitude of incident EM wave is highly dependent on the filler loading of magnetic EWAMs in resin matrix,[15] and thus an excellent EM absorption coating usually has very large areal density due to extremely high filler loading even up to 80 wt %.[16] In addition, some native drawbacks, including weak oxidative resistance and low corrosion potential, as well as the limitation of Curie temperature, make it impossible for magnetic EWAMs to serve for a long time under harsh conditions.[13,17,18] These difficulties force the related researchers to have to reorient their attention to dielectric loss materials in order to explore the oncoming generation of EWAMs that can meet high-performance and durable application requirements.

As compared with magnetic loss materials, the family of dielectric loss materials is very large, and many members, e.g., carbon materials,[19,20] conductive polymers,[21,22] metal oxides,[23,24] metal sulfides,[25,26] carbides,[27,28] can consume incident EM energy to a certain extent through conductive loss and polarization loss. Thanks to good chemical stability, tailorable dielectric property and low density, carbon materials attract wide-ranging interest in the past decade and are always recommended as potential substitutes for conventional magnetic EWAMs.[29–31] However, in most cases, single-component carbon materials easily suffer from mismatched impedance and insufficient loss capability,[32,33] and thus the construction of carbon-based composites by introducing some other components with compatible and compensatory EM functions has become a very popular mode to realize desirable EM absorption performance.[30,34,35] Of note is that although it is still

[1]MIIT Key Laboratory of Critical Materials Technology for New Energy Conversion and Storage, School of Chemistry and Chemical Engineering, Harbin Institute of Technology, Harbin 150001, China
*Correspondence: hanxijiang@hit.edu.cn (X.H.), yunchendu@hit.edu.cn (Y.D.)
https://doi.org/10.1016/j.isci.2023.107876

of great interest to fabricate various magnetic carbon-based composites as high-performance EWAMs, magnetic components therein cannot produce effective magnetic contribution as expected, especially in the case of low filler loading, because the coupling effect among different magnetic particles will be drastically weakened by non-magnetic carbon matri×.[36,37] In this context, dielectric carbon-based composites are receiving more and more attention, and many combinations, such as conductive polymers/carbon, metal oxides/carbon, metal sulfides/carbon, carbides/carbon, and even carbon/carbon, have demonstrated their significant contribution to the dissipation of EM energy.[38–42]

Carbides are a kind of compounds from carbon and other elements with similar or inferior electronegativity, and both covalent carbides (e.g., SiC) and interstitial carbides (e.g., ZrC, WC, TiC) usually have strong corrosion resistance, ultra-high melting point, excellent hardness, and mechanical strength.[43,44] The research on the EM absorption of carbides was launched at the end of last century,[45,46] while the relative complex permittivity of pristine carbides was usually small in gigahertz range at room temperature, resulting in insufficient dielectric loss and undesirable EM absorption performance.[28,47–49] Therefore, carbides were ever considered as potential high-temperature EWAMs.[50–52] Along with the flourish of nanotechnology, many effective strategies, including phase engineering, morphology design, size control, heteroatom doping, have been successfully applied to the regulation on EM properties of carbides,[49,53–55] and the emergency of some new carbides, e.g., MXenes, further provides tremendous potential for the application of carbides as high-performance EWAMs.[27,56,57] In particular when carbides are rationally integrated with carbon materials, there will be comprehensive performance improvements, not limited to EM absorption characteristics.[58–60] Literature search results indicate that more and more articles are focusing on the fabrication of carbides/carbon composites in the field of EM absorption, and thus a state-of-the art summary will be very helpful to understand and further promote the development of carbides/carbon composites as a new generation of EWAMs. In this review, we not only introduce the related loss mechanisms of carbides/carbon composites, but also pay more attention to the recent advances of some typical carbides/carbon composites, i.e., SiC/carbon, MXene/carbon, and Mo_2C/carbon, as well as the composites with some rare carbides and with some additional electromagnetic components. Furthermore, the shortcomings, challenges, and prospects of carbides/carbon composites are also proposed and discussed.

BRIEF ELECTROMAGNETIC ABSORPTION MECHANISMS

As we mentioned above, dielectric loss and magnetic loss are two main pathways for EWAMs to consume the energy of incident EM wave. However, in the family of carbides, except for a few members, such as Fe_3C, Ni_3C, and Co_3C, most of them cannot produce obvious magnetic response characteristics under room temperature.[61] Even for the carbides with magnetic properties, their saturation magnetization and magnetic loss capacity are usually less than those of their corresponding magnetic metals.[62] Therefore, magnetic loss is not the primary mode that we pursue in carbides/carbon composites, and in contrast, the regulation on dielectric loss is the key point for the design of carbides/carbon composites in most cases, which makes us pay more attention to the mechanism of dielectric loss in this review.

Classical theory in solid-state physics believes that dielectric loss originates from conductive loss and polarization loss.[63–65] When a dielectric medium is placed in an electric field, the residual carriers (usually electrons) therein will generate a weak current (i.e., leakage current) through directional migration or hopping driven by this external field,[63,66,67] as illustrated in a conductive network from crosslinked multi-walled carbon nanotubes (MWCNTs, Figure 1A).[63] Such a process can continuously consume the energy of the applied field. In carbides/carbon composites, carbon components often undertake the formation and transmission of leakage current due to their unique structural properties. Although strong leakage current is favorable for highly effective EM absorption from a theoretical perspective, the actual performance of EWAMs does not always depend on the strength of leakage current. This is because there is another important concept, impedance matching, related to the performance of EWAMs.[68] In usual, the prerequisite for EM absorption is that EM wave can enter a loss medium, and however, if this medium does not have good impedance matching, EM wave will be reflected off at the transmission interface.[11] As a result, no matter how strong leakage current or dielectric loss capability is generated in EWAMs, their absorption performance will be limited. This is the reason why many single-component carbon materials, such as CNTs, carbon black (CB), carbon fibers (CFs), graphite, cannot produce desirable EM absorption performance.[33,69–71] The ideal situation for good impedance matching is that EWAMs can produce very close complex permittivity and complex permeability,[31] while it can be only achieved in wave-transparent materials with negligible absorption characteristics. In most EWAMs, especially for dielectric EWAMs, their complex permittivity is obviously larger than complex permeability, and thus the key to improve impedance matching is to control the gap between complex permittivity and complex permeability.[66] The overlarge gap leads to poor impedance matching and EM absorption.

According to the categories of dipoles, polarization loss is generally divided into electronic polarization, ionic polarization, dipole orientation polarization, and interfacial polarization.[64,74] Electronic polarization and ionic polarization are caused by the displacements of electrons or ions under the action of an applied electric field, and both of them are elastic and complete in a very short time (10^{-15}~10^{-12} s),[11,62] which means that they hardly produce obvious contribution to EM absorption. Dipole orientation polarization can be described as the process that many permanent dipoles in a dielectric medium overcome thermal motion and gradually tend to be in the same direction with the guidance of an applied electric field (Figure 1B).[11] However, when an alternating EM field is employed, permanent dipoles cannot reorient themselves in time with the frequency of the EM field, and especially with the increase of the frequency, the lag will be longer, resulting in an obvious decrease of relative complex permittivity in high-frequency range, which is also known as frequency dispersion effect.[35,75] Interfacial polarization is a loss mechanism due to the different electrical properties (e.g., dielectric constant and conductivity) of two phases in a medium, the uneven accumulation of free charges occurs at the interface of these two phases caused by an applied electric field (Figure 1C), thus contributing to the overall polarization response.[65,76,77] The formation of interfacial polarization is not limited at the interface of two phases with different chemical compositions or physical states, but can be even created at the interface of two same phases as long as they have distinguishable crystalline structures and crystallinities.[78,79] Dipole orientation polarization and interfacial polarization can make solid

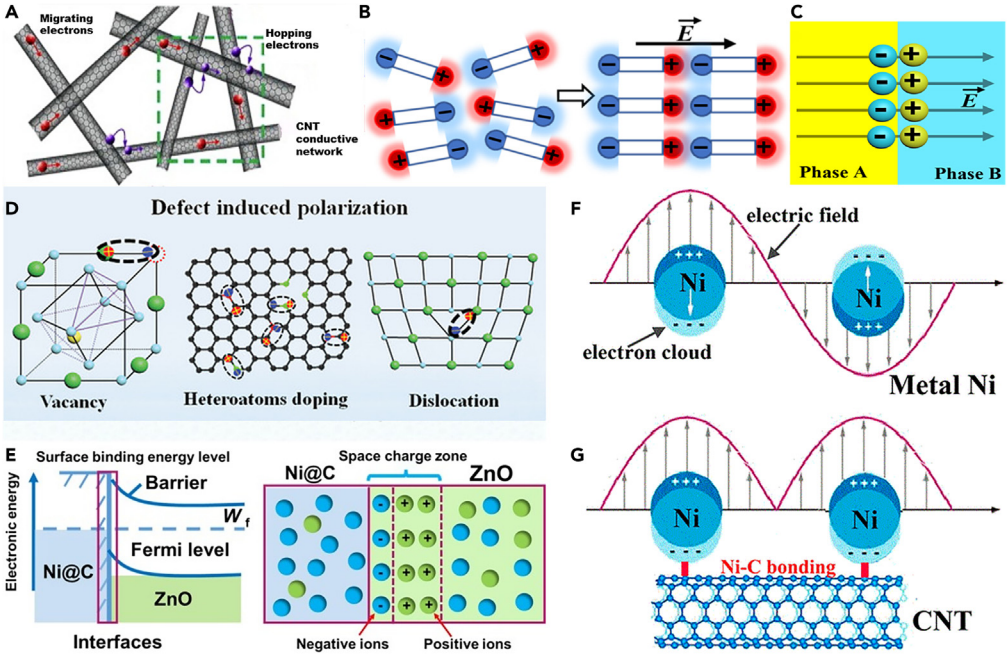

Figure 1. Schematic illustrations of some dielectric loss mechanisms

(A) Electron transport in MWCNT network. Reproduced with permission.[63] Copyright 2013, Elsevier Ltd.

(B) Dipole orientation polarization.

(C) Interfacial polarization.

(D) Defect induced polarization. Reproduced with permission.[65] Copyright 2022, Wiley-VCH.

(E) Electron transfer from ZnO to Ni@C. Reproduced with permission.[72] Copyright 2020, Elsevier Ltd. Surface electric fields of (F) metal nickel and (G) Ni-C bonded Ni-CNT composite. Reproduced with permission.[73]

(F and G) Copyright 2017, American Chemical Society.

contribution to the consumption of EM energy in gigahertz range, and thereby, they are two important factors that should be concerned in the design process of EWAMs.

Apart from these conventional mechanisms, some new dielectric loss pathways are also proposed in recent years. First, defect-induced polarization gains more and more attention in EM absorption. It is well known that defect sites, including vacancy, heteroatom, dislocation, can play the role of carrier traps, which suggests that they can break the balance of charge distribution in EWAMs and then induce various polarization processes to dissipate EM energy (Figure 1D).[65,80,81] The introduction of more defect sites in semiconductors and carbon materials has been proved to be an effective strategy for the improvement of EM absorption.[82–86] Second, Schottky heterojunction, a common unit consisted of metal and semiconductor, not only works for the regulation on electron transfer widely in catalysis field,[87,88] but also is found to be highly contributive to EM absorption.[89–91] Wang et al. designed multiple core-shell Ni@C@ZnO as EWAMs, and proposed that Ni@C unit with high conductivity could be regarded as a metalloid, and thus Schottky heterojunction was created at the interface between Ni@C and ZnO.[72] The irreversible electron transfer from ZnO to Ni@C brought obvious charge unbalance at the interface (Figure 1E), which could be understood as another form of interface polarization. Of note is that carbon materials usually have good conductivity and many types of carbides also have the characteristics of semiconductors,[92–94] and thus it is very feasible to construct Schottky heterojunction in carbide/carbon composites. Third, plasmon resonance was recently utilized to explain the consolidation of EM absorption in some recent studies.[95,73] Sha et al. even proclaimed that they enhanced such surface plasmon resonances through a chemical interaction between metal Ni and CNTs (Figures 1F and 1G), thus harvesting better EM absorption performance.[73] By considering that plasmon resonance usually occurs in visible region or near-infrared region, this is still a temporary speculation obtained through the size-dependent EM properties, and more convincing data are needed to be acquired to validate this conclusion. If it is true, the prospect of carbides/carbon composites in EM absorption can be further expected because some transition metal carbides, such as WC and Mo_2C, possess comparable plasmon resonance effect as those metal-based plasmonic absorbers.[96,97]

In this section, we briefly introduce some potential dielectric loss mechanisms that may work for EM absorption in carbides/carbon composites, and with respect to the mechanisms related to magnetic loss, they can be consulted in other references about magnetic EWAMs.[11,98]

SiC/C COMPOSITES

As one of the typically functional ceramic materials, SiC receives considerable attention in the past decades because it shows some amazing superiorities of light weight, good chemical inertness, wide band gap, controllable thermal conductivity, low thermal expansion, high wear

resistance, and strong hardness, which endow it with very wide applications ranging from separation and purification to thermal regulation, catalysis, corrosion protection, lubrication, wafer, and so on.[99–102] In addition to those conventional applications, the utilization of SiC in EM attenuation is also gradually recognized in recent years,[28,47,49,103] while the polarization loss caused by the inherent dipoles and defects alone cannot generate powerful EM absorption. The introduction of other EM components is a popular way to strengthen EM absorption performance of SiC.[50,104–107] Among various combinations, SiC/C composites almost account for more than half of SiC-related composites applied for EM absorption, not only for good chemical stability of carbon materials and their significant contribution to dielectric loss, but also for their abundant resource and diversified forms, as well as designable microstructure.[20,108–110] In this section, we will introduce the application of SiC/C composites as high-performance EWAMs in terms of their combination mode and microstructure design.

Physical mixing-prepared SiC/C composites

Both SiC powder and carbon powder (e.g., CB, CNTs, graphite) are commercially available raw materials, and thus the simplest and the most direct method for the preparation of SiC/C composites is physical mixing.[111–114] For example, Liu et al. mixed commercial SiC and CB through ball milling, and investigated the change of EM properties dependent on their filler loadings in epoxide resin.[69] They found that CB had much higher relative complex permittivity than SiC, and as a result, the introduction of CB could enhance dielectric loss of the final composites remarkably. When the mass fractions of SiC and CB in epoxide resin were 50 wt % and 5 wt %, respectively, the minimum reflection loss (RL) intensity would be as low as −41.0 dB at 9.0 GHz. Li et al. and Hu et al. finely regulated the content of MWCNTs in the composites from 0 to 20 wt %, and both two groups confirmed the optimum mass ratio of SiC to MWCNTs was about 250.[115,116] Under such circumstances, SiC/MWCNTs composites could produce minimum RL intensity less than −40.0 dB and effective absorption bandwidth (EAB, the frequency range with RL less than −10 dB) more than 2.0 GHz with an absorber thickness of only 1.6 mm. Although the facilitation of carbon materials to dielectric loss and EM absorption have been witnessed in many SiC/C composites, it is still difficult for a physical method to disperse SiC and carbon materials uniformly in final composites,[113,117] which suggests that such EM enhancement is more dependent on the intrinsic loss capabilities of individual components, and the synergy between SiC and carbon materials have not been developed effectively. Therefore, some advanced methods are always considered to be the key for the fabrication of high-performance SiC/C composites in the follow-up studies.

In situ derived SiC/C composites

Polymer-derived ceramics (PDCs) process is one of the important methods to prepare SiC/C composites and the pyrolysis of single-source precursor, polycarbosilane (PCS), can *in situ* generate SiC nanoparticles in carbon matrix, resulting in much better chemical homogeneity than those composites from physical mixing.[118–120] Li et al. pioneered the investigation on the dielectric and EM absorption properties of SiC/C composites derived from a liquid PCS with highly branched Si-CH_2-Si chain, and Si-H, Si-CH_3, CH = CH_2 functionalities.[121] They found that dielectric loss tangent of the resultant SiC/C composites would gradually increase with the pyrolysis temperature from 1100 to 1500°C, and became inferior when the temperature was further increased to 1600°C. However, the composite from 1400°C generated the best EM absorption with the average RL intensity of −9.97 dB in the X band, and they attributed the enhanced EM performance to sufficient interfacial polarization induced by numerous SiC nanocrystals (*ca.* 3.5 nm). Wang and his co-works employed commercial PCS powder as the precursor, and they revealed that the transformation of residual carbon from amorphous to turbostratic structure would cause regional carbon enrichment (Figures 2A–2C).[122] Meanwhile, the growth of SiC nanocrystals and the increased graphitization degree of carbon species played two important factors to affect EM parameters and impedance matching, and the minimum RL intensity would reach −35.0 dB due to the balance between dielectric loss and impedance matching (Figure 2D). Jia et al. also reported that SiC/C composites from PDCs process could also exhibit good EM absorption performance in the Ka band,[123] whose strongest RL intensity and EAB were −53.1 dB and 2.43 GHz, respectively. Of note is that PDCs process is a flexible strategy for SiC/C composites, and the chemical composition of final composites can be easily regulated by introducing different additives before the pyrolysis of PCS.[124–129] For example, Han et al. manipulated the carbon content in PCS-derived SiC/C composite through the pre-addition of GO, and thus promoted the minimum RL intensity from less than −5.0 to −69.3 dB.[124] Yu et al. even prepared multicomponent CNTs/Fe_3Si/Fe/SiOCN ceramic nanocomposites by pyrolyzing the mixture of poly(methylvinyl) silazane, ferric acetylacetonate, and carboxylic functionalized CNTs.[130] The reinforcement of interfacial polarization and the formation of magnetic loss were believed to be responsible for strong RL of −65.3 dB and broad EAB of 6.0 GHz.

Along with the flourish of nanotechnology, electrospinning is widely couple with PDCs to produce SiC/C composites in recent years.[133–136] On one hand, the utilization of electrospinning technology can retain the advantages of PDCs, and on the other hand, electrospinning can endow final composites with uniform one-dimensional (1D) morphology, facilitate the construction of conductive network, and achieve synchronous composition manipulation by screening organic additives. For example, Huo et al. dissolved PCS and polyvinylpyrrolidone (PVP) in a mixed solution of tetrahydrofuran/ethanol, and then this solution was inhaled into a medical syringe equipped in an electrospinning machine (Figure 2E).[131] After electrospinning and high-temperature pyrolysis, crosslinked 1D SiC/C fibers could be obtained (Figures 2F and 2G). SiC nanocrystals with average particle size of about 15 nm were evenly distributed in the fibers, and amorphous carbon derived from PVP could be easily identified high-resolution TEM image (Figure 2H). The final composite not only displayed satisfactory EM absorption characteristics, but also keep its performance in a very broad frequency range (Figure 2I). EM analysis disclosed that the energy consumption of incident EM wave came from electron migration and hopping in the conductive network assembled by 1D fibers, as well as interfacial polarization between SiC nanoparticles and carbon scaffold (Figure 2J). Similarly, such a combined technology can also accommodate other inorganic additives, such as rGO and CNTs, in order to further optimize the EM properties of final composites.[137,138]

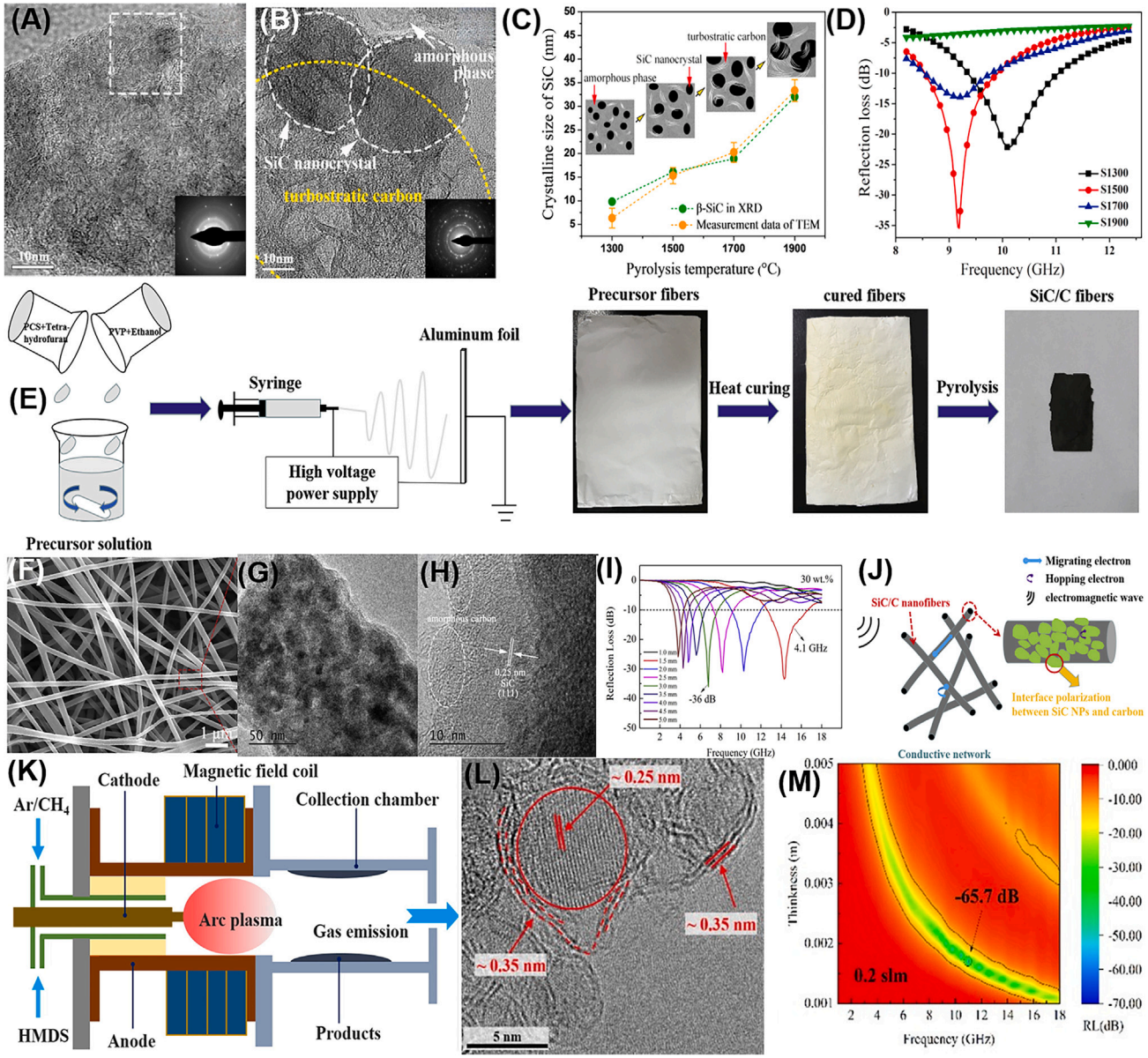

Figure 2. Characterization results, preparative process diagrams, EM absorption performance, and possible absorption mechanism of SiC/C composites from PDCs

(A and B) HRTEM images for the microstructure of SiC nanocrystals and carbon phase in PCS-derived SiC/C composites.

(C) The size of SiC nanocrystals pyrolyzed at different temperatures and schematic illustration of microstructural evolution of PCS-derived SiC/C composites.

(D) RL curves of PCS-derived PCS-derived SiC/C composites with a thickness of 1.5 mm.

(E) Preparative process.

(F) SEM.

(G) TEM.

(H) HRTEM images.

(I and J) (I) RL curves, and (J) EM absorption mechanism of SiC/C nanofiber from electrospinning.

(K) Schematic diagram of plasma-synthesis process.

(L and M) (L) TEM images and (M) 2D RL map of EM absorption performance of SiC/C composites.

(A–D) Reproduced with permission.[122] Copyright 2018, Elsevier Ltd.

(E–J) Reproduced with permission.[131] Copyright 2020, Elsevier Ltd.

(K–M) Reproduced with permission.[132] Copyright 2022, Taylor & Francis.

Although PDCs process, including the one combined with electrospinning, has been established as an effective strategy for the production of SiC/C composites, pre-crosslinking at moderate temperature (200–400°C) and pyrolysis at ultra-high temperature (over 1300°C) are always necessary steps to induce the formation of SiC nanocrystals,[121,122,131,133] which determine the characteristics of large energy consumption and high time cost of PDCs process. More recently, a new technique that can convert small organic molecules to SiC/C composites with the assistance of atmospheric plasmas has been successfully developed by Xia's group.[132,139,140] The schematic diagram of this process can be observed in Figure 2K, where hexamethyldisilane (HMDS) and methane are the precursors for SiC/C composites and Ar is utilized to generate atmospheric plasmas. Very interestingly, SiC/C composites from this way usually present desirable core-shell configuration (Figure 2L), resulting in full contact between SiC nanoparticles and carbon shells. The composition and EM characteristics of SiC/C composites can be easily tuned by the methane flowrate and the arc current.[132,139] The optimized SiC/C composite can also give considerable EM absorption performance, whose minimum RL intensity and EAB of the optimized SiC/C composite reach −65.7 dB and 4.6 GHz, respectively (Figure 2M).

It is universally acknowledged that microstructure design plays a vital role in the reinforcement of EM absorption performance.[141] If EWAMs have some special microstructures such as hollow structure, yolk-shell structure, porous structure and so on, better EM absorption performance will be achieved through multiple scattering, improved impedance matching and enhanced dielectric loss.[142–145] The abundant voids in the medium can intensify the reflection of incident EM wave, which results in the repeated consumption of EM energy. Besides, complex interior structure is also beneficial for impedance matching, which allows a major portion of EM wave to pass through the interface between the free space and EWAMs.[11] Microstructure design is conducive to strengthen dielectric loss as well. Massive microcurrents will be formed when the EM wave interact with the conductive networks formed by complex structure, transforming EM energy to joule heat.[42] Moreover, abundant interfaces, defects and surface functional groups result in enhanced polarization loss under alternative electric field.[20] With core-shell SiO_2@RF microspheres as the precursor, Liu et al. successfully fabricated hollow mesoporous SiC/C microspheres through high-temperature pyrolysis and acid etching.[146] EM analysis revealed that the synergy between carbon shells and SiC nanoparticles was mainly responsible for good EM absorption performance (minimum RL: −55.4 dB, maximum EAB: 5.6 GHz), while the hollow mesoporous structure was also greatly beneficial to impedance matching, interfacial polarization, and multiple reflections of EM wave.

Post-modified SiC/C composites

Although *in-situ* derived process significantly improves the dilemma of the random distributions of SiC and carbon components in the composites from physical mixing, the microscopic heterostructure between SiC and C is still difficult to regulate, because the temperature required for PDCs process is very high (over 1300°C), which easily leads to phase segregation in many cases.[122] In this context, the post-synthesis scheme is developed in order to further strengthen the interaction between SiC and carbon components. There are two common kinds of modes to conduct the post-synthesis scheme. One is to induce the growth of nanoscaled SiC units on CFs,[147–150] and the other is to create carbonaceous attachments on SiC fibers.[110,151–153]

CFs have high electrical conductivity and powerful intrinsic loss capability, while the mismatched impedance with free space always brings intensive reflection of incident EM wave rather than desirable absorption, and thus the core purpose of SiC growth on their surface is to improve the impedance matching to allow the heterogeneous propagation of EM wave from free space to EWAMs.[154–156] Su et al. coated CFs with PCS layers and then converted the PCS layers in SiC nanowires.[157] The results indicated that the formation of SiC nanowires indeed narrowed the gap between relative complex permittivity and relative complex permeability, and thus the front-end reflection of EM wave was largely suppressed. The EM characteristics of final products could be tailored by the times of PCS impregnation, and the optimum one exhibited strong RL of −41.1 dB and EAB of 3.82 GHz. Of note is that such a method is still based on the PDCs process, which makes the growth of SiC nanowires disordered, losing the advantages of CFs in uniformity and orderliness. Therefore, some groups attempt to plant SiC nanowires on CFs through chemical vapor reaction.[70,147,148] As shown in Figure 3A, Yan et al. impregnated pre-treated CFs in $Ni(NO_3)_2$ solution and then reduced Ni^{2+} into Ni nanoparticles, and after feeding CH_3SiCl_3 as both Si and C sources in this chemical vapor infiltration (CVI) system, SiC nanowires would be finally harvested on the surface of CFs with the assistance of Ni nanoparticles.[148] SEM images confirmed that this was an effective way to modify CFs with SiC nanowires, and the intersectional SiC nanowires loosely wrapped smooth CFs (Figures 3B–3D). TEM image identified a small droplet at the end of a single SiC nanowire (Figure 3E), indicating that the growth of SiC nanowires was in a vapor−liquid−solid mode.[158] The comparison in EM absorption manifested that the formation of SiC nanowires reinforced the performance of CFs remarkably, where the minimum RL was decreased from less than −5.6 to −33.1 dB and the EAB was correspondingly broadened from 0 to 3.1 GHz with an absorber thickness of 1.5 mm (Figures 3F and 3G). Zhou et al. deposited Ni nanoparticles on CFs (Toray T700) with an electroplating method, and then introduced CH_3SiCl_3 at 1000°C under the pressure of 600 Pa for 4h.[70] The as-prepared SiC/CFs composite also showed good EM absorption characteristics (minimum RL: −28.3 dB, maximum EAB: 2.5 GHz), and the improvement on impedance matching and electron hopping was considered to be primarily responsible for such performance.

In contrast to the first mode mentioned above, the growth of carbonaceous attachments on the SiC matrix is dedicated to the consolidation of dielectric loss (conductive loss exactly) capability, because carbonaceous attachments are usually more favorable for electron migration and hopping than SiC materials.[151,152,159–161] It has been reported that 1D SiC materials, e.g., nanowires and fibers, could produce better EM absorption than those bulky and disordered SiC particles,[28,162] and thus they are widely selected as the scaffolds for carbonaceous attachments. Liang and Wang coated SiC nanowires with resorcinol-formaldehyde (RF) polymers and then turned the immediate composite of SiC@RF into final SiC@C nanowires under high-temperature inert atmosphere (Figure 3H).[110] The final composites exhibited typical core-shell configuration and the relative content of carbon shells could be adjusted by the mass ratio of SiC to RF (Figure 3I). When the mass ratio

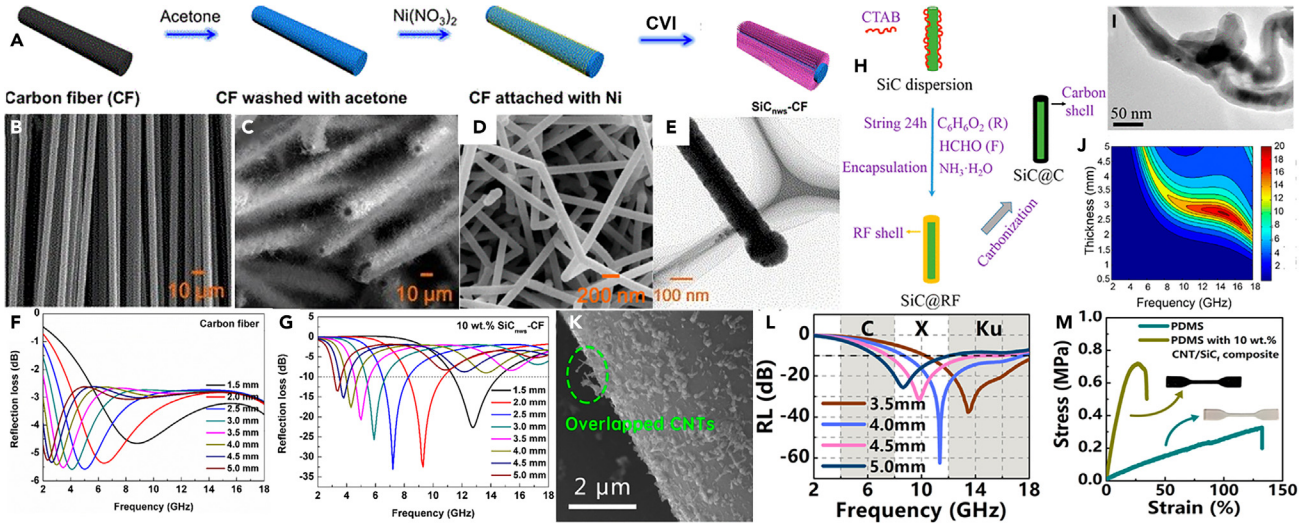

Figure 3. Preparative process, microstructure characterization, and EM absorption performance of SiC/C composites from post-synthesis

(A) Schematic illustration for the fabrication of SiCnws-CF.

(B–D) SEM images of CFs, SiCnws-CF, and SiC nanowires respectively.

(E) TEM image of a single SiC nanowire.

(F and G) RL curves of CFs and SiCnws-CF.

(H) Synthetic route of SiC@C core-shell nanowires.

(I) TEM image of SiC@C nanowires.

(J) 2D RL map of EM absorption performance of SiC@C nanowires.

(K) SEM image of CNTs on SiC fibers.

(L) RL curves of CNTs/SiC_f composite.

(M) Engineering tensile stress-strain curves of pure PDMS and CNTs/SiC_f/PDMS composite.

(A–G) Reproduced with permission.[142] Copyright 2017, American Chemical Society.

(H–J) Reproduced with permission.[110] Copyright 2017, American Chemical Society.

(K–M) Reproduced with permission.[147] Copyright 2020, American Chemical Society.

was 2:1, the resultant SiC@C nanowires could generate very strong RL of −50.0 dB at 12.0 GHz and considerable EAB as broad as 8.0 GHz (Figure 3J). More importantly, the authors addressed the significance of core-shell configuration to EM absorption by testing the performance of a physical mixture of SiC nanowires and carbon. Although carbon shells derived RF enhance dielectric loss capability to some extent, the overall loss capability of these composites is still limited due to their amorphous nature and inadequate thickness (less than 20 nm). To further improve the situation, CNTs are being taken as promising carbon attachments on SiC matrix, because they have excellent conductivity and desirable space extension.[163] For example, Xu et al. directed the growth of CNTs on SiC fibers with the assistance of ferrocene (Figure 3K), and they found that even if the loading of CNTs was only 0.72 wt %, the final composite could increase EM absorption characteristics by tens of times, especially for the EAB up to 8.8 GHz (Figure 3L). It was very interesting that the authors also mixed these SiC/CNTs composites with polydimethylsiloxane (PDMS) to manufacture a flexible EM absorption film with good mechanical property (Figure 3M). More recently, Huang et al. optimized the process for the growth of CNTs and harvested vertical carbon nanotubes arrays as thick as 46 μm on SiC fibers.[164] Although these unique composites have temporarily failed to achieve greater breakthroughs in EM absorption (minimum RL: −56.2 dB, maximum EAB: 4.3 GHz), this interesting growth style of CNTs might be highly attractive and greatly helpful for the design of high-performance EWAMs in the following studies. After analyzing the performance of these SiC/C composites prepared by the so-called post-synthesis scheme, one can find the formation of carbonaceous attachments on SiC matrix seems a better strategy for EM absorption, which is possibly attributed to stronger conductive loss benefited from external carbon species.

As compared with the physical mixing method and *in situ* derived method, the microstructure design in SiC/C composites through post-synthesis will be relatively easy, and thus become a hot topic to enhance their EM absorption capabilities in the latest research. Lan et al. impregnated porous SiC skeleton into CNTs paste and obtained binary porous SiC/C composites through high-temperature pyrolysis in the presence of Si/SiO_2 powder.[165] Such binary porous composites displayed excellent high-temperature EM absorption performance in X band. Chen et al. directed the growth of SiC whiskers on the external of hollow carbon microspheres, and they concluded that hollow microstructure in carbon microspheres made a significant contribution to polarization loss and EM absorption enhancement.[166]

Among conventional micro/nanostructures, aerogels are evolving into a fascinating architecture for EWAMs, not only for their highly open skeleton contributive to EM wave propagation and multiple reflections, but also for their crosslinked network that may generate induced current by promoting electron migration.[29,167,168] Such a situation greatly drives the research to develop SiC/C composite aerogels. Cai et al. incubated SiC nanowires in glucose solution, and then obtained well-interconnected SiC@C nanowire foams (SCNFs) through partial-hot-

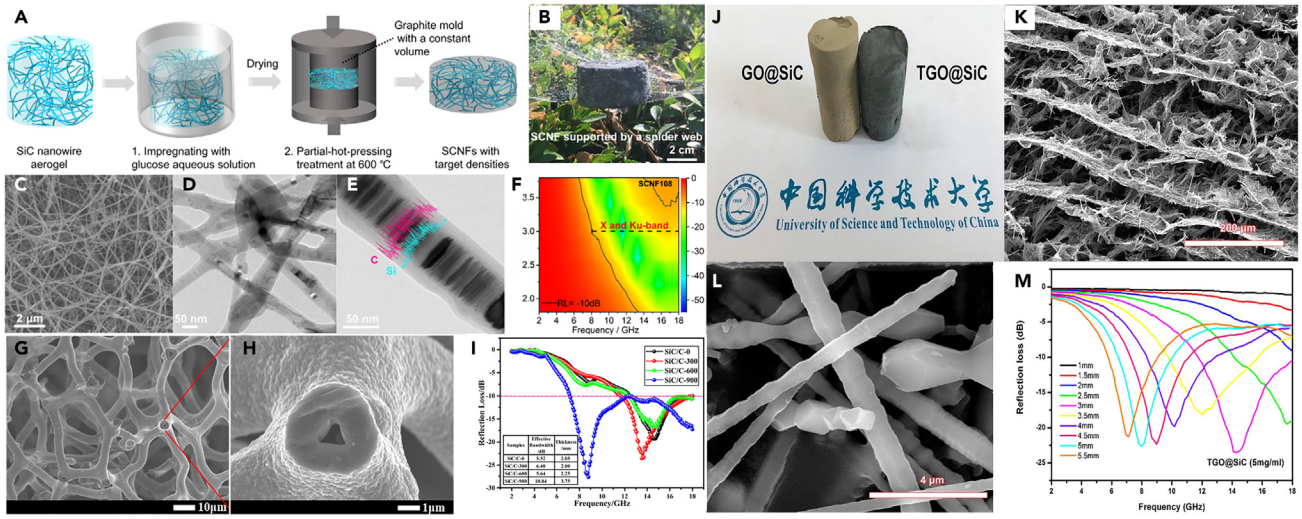

Figure 4. Preparative process, microstructure characterization, and EM absorption performance of SiC/C aerogels

(A) Schematic illustration for the fabrication of SiC/C aerogel (SCNF).

(B) Digital photograph of SCNF with a volume of ~25 cm^3 being supported by a spider web.

(C) SEM (Scale bar: 2 μm) and (D) TEM images (Scale bar: 50 nm) of SCNF.

(E) Linear EDS scanning of an individual SiC@C nanowire (Scale bar: 50 nm).

(F) 2D RL map of SCNF.

(G and H) SEM images of the SiC/C composite aerogel.

(I) The RL curves of SiC/C composite aerogel.

(J) Digital photographs of GO@SiC and TGO@SiC aerogels.

(K and L) SEM images of TGO@SiC and GO@SiC aerogels.

(M) RL curves of TGO@SiC aerogel.

(A–F) Reproduced with permission.[169] Copyright 2020, American Chemical Society.

(G–I) Reproduced with permission.[181] Copyright 2019, American Chemical Society.

(J–M) Reproduced with permission.[108] Copyright 2017, Elsevier Ltd.

pressing treatment (Figure 4A).[169] The density of final SCNFs could be manipulated from 36 to 180 mg/cm^3, and the low density made SCNFs be supported on a spider web (Figure 4B). The interconnected SiC nanowires therein were uniformly coated with amorphous carbon shells, resulting in a profitable core-shell configuration (Figures 4C–4E). The structural effect and multiscale dissipation mechanisms rendered SCNFs as high-performance EWAMs with ultra-wide EM response bandwidth (maximum EAB: 10.1 GHz, Figure 4F), which was obviously better than single core-shell SiC@C nanowires (8.0 GHz, Figure 3L).[110] The formation of SiC-based aerogels usually requires some special treatment technique (e.g., hot pressing), and thus most studies on SiC/C composite aerogels prefer to employ carbon aerogel or foam as the structural scaffold. Some carbon scaffolds or scaffold precursors, such as expanded graphite, commercial carbon foam, biomass, polyacrylamide, and cellulose, have exhibited their potential in the construction of SiC/C composite aerogels.[170–174] Among them, melamine foam receives much more attention due to its extremely high porosity, open-cell network, commercial availability, and low cost.[175,176] Chen's group carried out extensive relevant research and investigated the growth of SiC coatings on melamine-derived carbon foams in detail.[175,177–181] Finally, they concluded that a two-step heat treatment was necessary to achieve desirable EM absorption performance, where melamine foam was firstly pyrolyzed at 1100°C and SiC/C composite aerogels after chemical vapor deposition were further treated at 900°C, and besides, they also confirmed the optimum gas flow ratio of methyltrichlorosilane (MTS): H_2: Ar was 40:250:120.[181] With these optimum conditions, the resultant SiC/C composite aerogel could maintain open skeleton structure and present a cladding configuration with sufficient heterogeneous contact (Figures 4G and 4H). These salutary features broadened the EM response frequency range of SiC/C composites effectively, and the maximum EAB could reach up to 10.84 GHz (Figure 4I).

In addition to the utilization of pre-obtained carbon scaffolds, some groups also developed a self-assembly strategy for SiC/C composite aerogels through foaming or freeze-drying.[182–184] For example, Jiang et al. assembled GO and SiC whiskers through directional freeze-casting and then obtained rGO/SiC aerogels (TGO@SiC) by thermal reduction (Figure 4J).[108] The final TGO@SiC presented typical spongy bone-like hierarchical microstructure, and SiC whiskers were found to be closely attached on the skeleton of rGO (Figures 4K and 4L). The dielectric properties of final aerogels could be easily controlled by the content of GO in initial SiC slurry, and when the concentration of GO was 5 mg/mL, the corresponding TGO@SiC could produce good EM response in a broad frequency range (Figure 4M).

SiC is a kind of typical ceramics with good hardness and high temperature resistance, and it is also the first carbide for the application of EM absorption. The combination of SiC and carbon materials not only boosts intrinsic EM absorption performance of final composites, but also brings more opportunities for the microstructure design to increase the pathways of EM attenuation. In terms of EM absorption performance

alone, some SiC/C composites can already meet the requirement of some specific application scenarios, while few studies comprehensively evaluate the practical application potential of SiC/C composites. Besides, the presence of carbon components significantly reduces the possibility of the application of SiC/C composites under high temperature condition, and thus how to improve the thermal stability of carbon components in SiC matrix is a challenging task in the following studies.

MXene/C COMPOSITES

MXene is the latest family of two-dimensional transition metal carbides and/or nitrides, and it is usually denoted with the formula of $M_{n+1}X_nT_x$, where M is an early transition metal, such as Ti, V, Zr, Mo, and so forth, X is either C or N, and T represents constitute the surface terminating functional atoms or molecules (OH, O, and/or F groups).[185] Since the discovery of MXene by exfoliating layered transition metal carbide Ti_3AlC_2 with hydrofluoric acid (HF), this new kind of materials has quickly attracted the attention of researchers around the world and become a super star in many hot fields, including energy conversion and storage, catalysis, and sensor.[186–189] Very interestingly, the inherent conductivity, good mechanical properties, and abundant surface terminations also make MXene good candidates for EM radiation pollution prevention and control.[190–192] Although MXene can interact with electric field branch of incident EM wave and even produce desirable EM attenuation to some extent,[1] the total shielding effect is still established on EM reflection rather than EM absorption in most cases. Some effective strategies, e.g., surface modification, element doping, defect control, microstructure design, have been successfully developed to regulate EM characteristics of MXene and realize good EM absorption performance.[193–197] Apart from these modification methods on MXene itself, recent progress indicates that the combination of MXene and carbon materials may provide an alternative pathway to significantly promote EM absorption performance of MXene through synergistic attenuation mechanism and improved impedance matching.[198–200] By considering the complex preparation process of MXene, it is difficult to *in situ* direct the growth of MXene in carbon matrix, and thus most MXene/C composites are constructed in the way of physical combination. In this section, we mainly discuss the EM absorption performance of different MXene/C composites which are classified according to the dimension of carbon materials, and as for multicomponent MXene/C composites with other additives, we will mention them in subsequent chapters.

Composites of MXene and 0 D carbon materials

The good electrical conductivity of MXene is a double-edged sword for its EM absorption performance. On one hand, it enables MXene with powerful intrinsic loss capability, and on the other hand, it induces mismatched impedance with free space, resulting in strong reflection of EM wave at their heterogeneous interface. Carbon nanoparticles with relatively low graphitization degree can appropriately suppress rather than completely blocking carrier transmission in MXene, and thus they are taken as potential candidates to couple with MXene. For example, Fan et al. embedded CB nanoparticles with an average size of 10 nm into MXene film, and they found that the dispersion of CB nanoparticles brought porous structure, increased BET surface, and prevented intensive interface reflection.[201] With increasing the dosage of CB nanoparticles from 0 to 90 mg, the contribution of EM absorption in X band would enhance from −31 to −47 dB correspondingly. Xu et al. directed the polymerization of polyaniline (PANI) on the surface of exfoliated MXene nanosheets, and then converted PANI into N-doped carbon nanoparticles under high-temperature inert atmosphere.[202] The formation of carbon nanoparticles not only optimized impedance matching of the final composite, but also created additional polarization loss mechanisms, which effectively broadened its EAB to 5.0 GHz with a thin thickness of 1.72 mm. Similarly, Huyan et al. replaced PANI with polydopamine (PDA) and tailored the loading amount of carbon nanoparticles through the dosage of dopamine hydrochloride.[203] It was clear that carbon nanoparticles were densely attached on the surface of MXene nanosheets, and there were many heterointerfaces between crystalline and amorphous regions, as well as abundant lattice defects and discontinuous grain boundaries (Figures 5A–5C). By regulating the pyrolysis temperature and dopamine hydrochloride dosage, the strongest RL intensity and the broadest EAB of the optimal composite could reach −48 dB and 7.01 GHz, respectively (Figure 5D). Although carbon nanoparticles promote EM absorption performance of MXene as expected, the large gap between their sizes determines that carbon nanoparticles cannot modulate electron migration and hopping among different MXene nanosheets effectively, and thus the related studies on the composites of MXene and carbon nanoparticles are still limited.

Composites of MXene and 1 D carbon materials

1D carbon nanomaterials, *i.e.*, CNTs and CNFs, also have excellent electrical conductivity such as MXene, and thus in principle, the combination of MXene and 1D carbon nanomaterials cannot realize the optimization on impedance matching, but may further strengthen EM attenuation ability through some synergistic effects. There have been some reports that attributed to the enhancement of EM shielding effectiveness to the dominant absorption contribution in MXene-based composites with 1D carbon nanomaterials.[206–210] In addition, 1D carbon nanomaterials are well-known for their reasonable mechanical strength, which offers a great potential to fabricate various MXene-based electronic devices to meet the requirements in practical applications.[211–213] However, simply physical mixing of MXene and 1D carbon nanomaterials only brings small EM reinforcement, because the synergy from the randomly dispersed components is very limited,[214] and thus rational design on the composite mode is usually necessary to achieve remarkable EM performance. Cui et al. demonstrated the synthesis of porous MXene/CNTs microspheres through ultrasonic atomization and freeze drying.[204] MXene and CNTs could uniformly dispersed in each microsphere (Figures 5E–5G), and their weight ratio could be manipulated from 1:1 to 5:1, which affected EM properties of the final composites in turn. The best weight ratio of MXene to CNTs was 3:1 in these microspheres, and the minimum RL intensity and the maximum EAB under this circumstance were −45.0 dB and 4.9 GHz, respectively (Figure 5H). Another common method is to decorate the pre-prepared

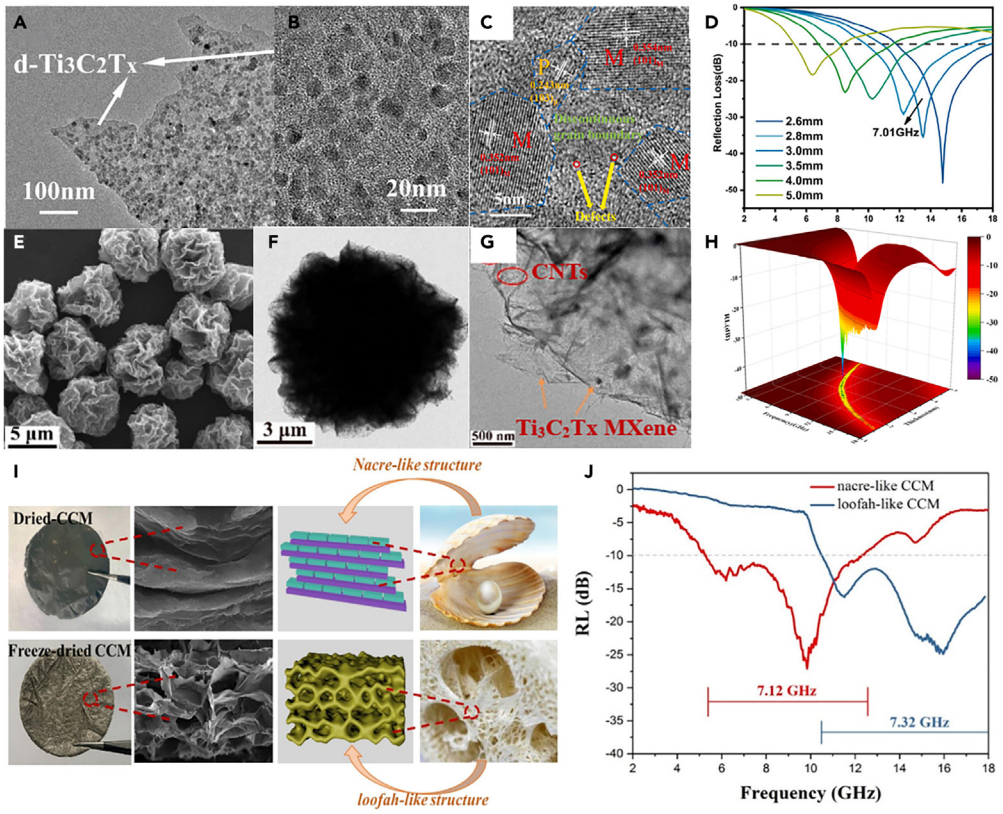

Figure 5. Microstructure characterization and EM absorption performance of MXene-based composites with 0D carbon nanoparticles and 1D CNTs

(A–C) SEM and (B and C) HRTEM images of carbon nanoparticles/MXene composite.

(D) RL curves of carbon nanoparticles/MXene composite.

(E) SEM and (F and G) TEM images of porous CNTs/MXene microspheres.

(H) 3D RL map of porous CNTs/MXene microspheres.

(I) Schematic illustration of nacre-like and loofah-like CNFs/MXene membranes.

(J) RL curves of nacre-like and loofah-like CNFs/MXene membranes.

(A–D) Reproduced with permission.[203] Copyright 2022, Elsevier Ltd.

(E–H) Reproduced with permission.[204] Copyright 2021, Elsevier Ltd.

(I and J) Reproduced with permission.[205] Copyright 2021, Elsevier Ltd.

CNTs/CNFs matrix with MXene suspension, so that MXene nanosheets can uniformly deposit on the surface of CNTs/CNFs.[210,215] With a simple electrophoretic deposition technique, Yang et al. made MXene nanosheets highly disperse in CNTs buckypaper, and the full contact of MXene nanosheets and CNTs matrix resulted in strong shielding performance in X band, where the contribution of EM absorption reached up to 69%.[216] Weng et al. assembled $Ti_3C_2T_x$ MXene-CNTs composite films through spin spray layer-by-layer technique, and when the composite film contained 300 MXene-CNTs bilayers, it could extremely high shielding effectiveness of 58187 dB cm^2 g^{-1} with overwhelming absorption contribution in X band.[206]

Earlier in this review, we mention more than once the positive role of microstructure in promoting EM absorption, and thus it is also of great interest to assemble MXene and CNTs into composite aerogel.[212,217,218] For example, Hu et al. mixed $Ti_3C_2T_x$ suspension and CNTs suspension, then induced the assemble of $Ti_3C_2T_x$ and CNTs by adding HCl solution, and finally harvested $Ti_3C_2T_x$/CNTs composite aerogel.[219] The final composite aerogel could display minimum RL of −44.4 dB and EAB of 5.44 GHz with an absorber thickness of 1.92 mm. More recently, Peng et al. compared EM absorption performance of nacre-like and loofah-like CNFs/MXene membranes, which were prepared through oven-drying or freeze-drying, respectively (Figure 5I).[205] The results indicated that the maximum EABs of nacre-like and loofah-like CNFs/MXene membranes were 7.12 and 7.32 GHz, respectively, and the corresponding absorber thicknesses were 3.6 and 2.5 mm, which again verified that the presence of loose and porous microstructure was helpful to produce good EM absorption performance (Figure 5J).

The stability of MXene is always one of the issues concerned by worldwide researchers, and the abundant O-containing terminating groups and the thin size are easily responsible for the oxidation of MXene nanosheets at high temperature even under inert atmosphere.[220,221] Therefore, many studies typically do not induce the growth of CNTs on MXene nanosheets directly, and instead, they prefer to conduct the growth of CNTs on some intermediate supports, i.e., ZIF-67, CoNi LDH, $Ni(OH)_2$, and then embed these resultant CNTs

clusters into MXene matrix.[222–225] Although the combination of MXene nanosheets and CNTs in this way can also promote EM absorption to some extent, it is essentially not different from physical mixing. *In situ* growth of CNTs in MXene matrix is still a desirable manner to power the EM performance of MXene, because researchers always expect the growth of carbon nanotubes to further enlarge the interlayer distance of MXene nanosheets, creating crosslinked and porous microscopic networks favorable for the propagation and attenuation of incident EM wave. To date, several groups have made some breakthroughs on the suppression of MXene oxidation during the growth of CNTs through vacuum pretreatment to remove O-related molecules as far as possible.[226–229] For example, Li et al. selected Ni nanoparticles as the catalyst and C_2H_4 as the gaseous carbon source to conduct the growth of CNTs on MXene nanosheets, and the resultant MXene/CNTs composite gave EAB of 4.5 GHz with the thickness of only 1.55 mm[226]; Che's group utilized the "seed-germination" effect of Ni^{2+} to breed CNTs with melamine as carbon source, and they also found strong RL (*ca.* −40.0 dB) and moderate EAB (*ca.* 4.0 GHz) with a small absorber thickness (1.5 mm).[227] It has to be pointed out that the *in situ* growth of CNTs do not proceed perpendicular to the surface of MXene nanosheets as expected, and conversely, they curve and grow approximately parallel to the surface. This situation leads to a deviation in EM absorption performance of final composites from the expected results, and also remains a challenging task for the following studies.

Composites of MXene and 2 D carbon materials

Both MXene and rGO are very famous 2D functional materials rising in this century.[230,231] The unique lamellar microstructural morphologies determine that there is a great possibility to construct MXene/rGO composites with face-to-face configuration, and their quite different composition, phase, and property may create remarkable interfacial synergy to produce extraordinary EM performance. Due to the negative charges on the surface of MXene and GO/rGO, small organic amine molecules are always necessary to eliminate their strong repulsive interaction during their combination process.[232–234] For example, Wang and his co-works assembled MXene and rGO in the presence of dopamine, and they found that dopamine could promote the dispersion and combination of MXene and rGO nanosheets effectively.[232] The resultant MXene/rGO composite could exhibit better EM absorption performance than the counterpart without dopamine, including stronger RL intensity (−62.6 dB vs. −16.0 dB) and broader EAB (5.6 GHz vs. 4.3 GHz). Yang et al. successfully created a covalent amide bond between rGO and amino-functionalized MXene through an amidation reaction.[233] The formation of this amide bond was confirmed to be favorable for electron migration and impedance matching, and after locating the mass ratio of MXene/rGO at 2: 1, the optimal composite could display RL intensity of −48.0 dB at 6.4 GHz with a thickness of 2.7 mm and wide EAB of 4.1 GHz just with a small matching thickness of 1.4 mm.

In an effort to highlight the microstructure contribution to EM absorption, some elaborately designed schemes have also been applied to the combination of MXene and rGO. As shown in Figure 6A, Li et al. firstly assembled few-layered MXene (2–8 layers) with polymethyl methacrylate (PMMA) nanospheres through hydrogen bonding and van der Waals force, and then the intermediate hybrids were further wrapped by GO nanosheets and treated under high-temperature inert atmosphere.[235] The final MXene/rGO composite presented uniformly spherical morphology and typically hollow microstructure (Figures 6B and 6C), and thus it had ultra-light feature with the density as low as 0.0033 g/cm^3 (Figure 6D). The unique heterogeneous interface associated with core-shell configuration and hollow microstructure rendered the rGO/$Ti_3C_2T_X$ hybrid as promising EWAMs, and especially, its EAB could almost cover the whole X band with the minimum RL intensity of −23.0 dB (Figure 6E). The construction of 3D porous aerogel is also attractive for MXene/rGO composites. For example, Wang et al. obtained 3D porous MXene $Ti_3C_2T_x$/rGO composite aerogel through hydrothermal self-assembly and freeze-drying treatment.[236] The optimal RL and EAB of this composite aerogel could reach −31.2 dB and 5.4 GHz, respectively, and if the absorber thickness was accumulated from 1 to 4 mm, the corresponding integrated EAB would cover the frequency range of 4.9–18.0 GHz. By considering the poor mechanical stability of $Ti_3C_2T_x$/rGO composite aerogels from freeze-drying treatment, some groups prefer to employ organic polymers as a flexible matrix for the combination of MXene and rGO.[237,238] Li et al. introduced polyurethane containing Diels-Alder bonds (PUDA) into MXene/rGO composite aerogel with a vacuum assisted impregnation method, and the resultant not only showed good EM absorption contribution (over −30 dB) in X band, but also maintained its EM function after 5000 bending cycles.[239] Besides those homogeneous MXene/rGO composites, there are also some interests in the fabrication of heterogeneous MXene/rGO composites in recent years. Liao's group prepared 2D porous double-layered carbon nanosheets and then conducted their assembly with $Ti_3C_2T_x$ MXene flakes to generate heterogeneous films with laminated structure.[240] The obtained heterogeneous film displayed the specific shielding effectiveness as high as 33143 dB cm^2 g^{-1} in X band, which was mainly attributed to the unique porous layer-by-layer architecture and the corresponding enhancement in the absorption of EM wave. Du and his co-workers alternately deposited rGO layer and MXene/PMMA microspheres to produce multiple-layers composite film with sandwich-like structure rather than wrapping MXene/PMMA hybrid microspheres with rGO nanosheets.[241] Such a heterogeneous film even could produce good absorption (over 90%) in THz range (0.2–2.0 THz). Li et al. demonstrated the preparation of macroscopic Janus film by filtering MXene suspension on GO film.[242] This Janus film exhibited absorption-dominant EM shielding performance in X band, and more interestingly, it could possess multi-responsive actuation capability, including humidity, light, and electricity.

It is worth noting that some novel techniques are involving into the preparation process of MXene/rGO composites, which may bring about enhanced and even unprecedented properties for final composites. Zheng et al. coupled coaxial wet spinning with freeze-drying treatment to produce an interfused core-shell heterogeneous MXene/rGO aerogel (Figure 6F),[243] and the final aerogel was composed of crosslinked and wrinkled fibers, where MXene nanosheets with poor oxidization resistance were densely coated by rGO nanosheets. The resultant MXene/rGO aerogel had better EM shielding effectiveness (absorption contribution was over 75%) than individual MXene film in X band, and its performance could maintain over 80% after 120 days, indicating hydrophobic rGO sheath provided effective protection for internal MXene nanosheets (Figure 6G). Very interestingly, the resultant MXene/rGO aerogel also showed good compressibility and ultra-low density, as well as excellent oil/water separation and thermal insulation (Figures 6H–6L). Zhang's group designed resilient and lightweight MXene/rGO scaffolds

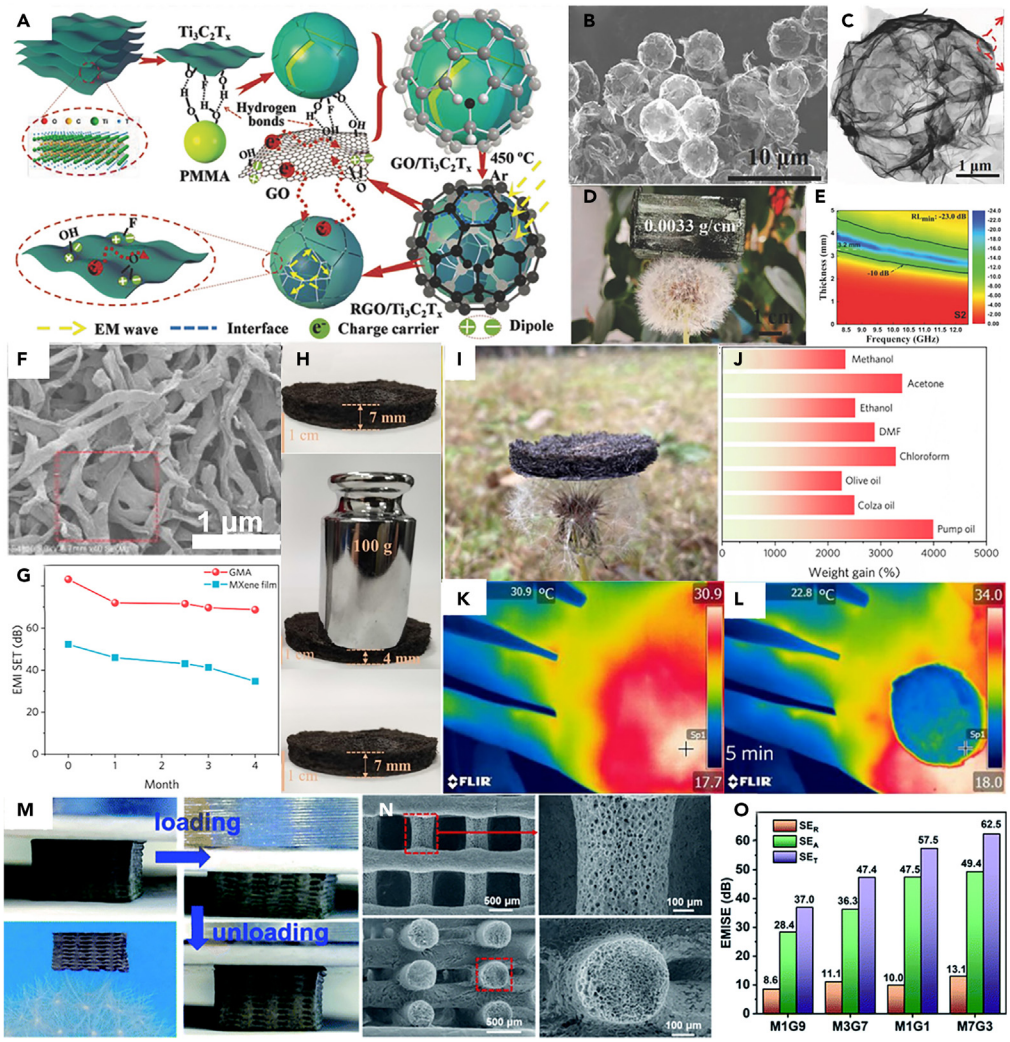

Figure 6. Preparative process, digital photographs, various properties of MXene/rGO aerogels

(A) Schematic illustration for the fabrication of RGO/$Ti_3C_2T_X$ foam.
(B and C) (B) SEM and (C) HRTEM images of RGO/$Ti_3C_2T_X$ foam.
(D) The photograph of free-standing RGO/$Ti_3C_2T_X$ foam (about 23 × 45 × 11 mm^3).
(E) 2D RL map of EM absorption performance of RGO/$Ti_3C_2T_X$ foam.
(F) SEM image of core–shell rGO/MXene fiber.
(G) EMI shielding durability of GMA and MXene film.
(H) Digital images of GMA before and after 100 g loading.
(I) Digital photograph of rGO/MXene fiber aerogel supported on dandelion.
(J) Recyclability of GMA in absorbing organic solvent.
(K and L) Infrared thermal images of naked palm and GMA.
(M) The lightweight MXene/RGO scaffold on a dandelion tip has reversible compressibility.
(N) Top-view and cross-sectional view of the MXene/RGO scaffolds.
(O) The SET, SEA and SER values of MXene/RGO scaffolds.
(A–E) Reproduced with permission.[235] Copyright 2018, Wiley-VCH.
(F–L) Reproduced with permission.[243] Copyright 2022, Elsevier Ltd.
(M–O) Reproduced with permission.[244] Copyright 2013, The Royal Society of Chemistry.

with 3D printing (Figure 6M), and the scaffolds were built up with periodic and porous fibers (Figure 6N).[244] The hierarchical and robust architectures delivered unexpected mechanical properties, and more importantly, they established a broadband tunable and absorption-dominant EM shielding performance (over 60 dB) in 8.2–26.5 GHz (Figure 6O). These eye-catching results can inspire the following studies on the construction of MXene/rGO composites effectively.

Composites of MXene and 3D carbon materials

Although the superiority of 3D porous microstructure toward EM attenuation has been demonstrated in many EWAMs, including MXene/C composites, the assembly of MXene nanosheets and various carbon nanomaterials (i.e., CNTs, CNFs, GO, rGO) usually requires complex processes, especially hydrothermal treatment and freeze-drying treatment in most cases. This situation drives some research groups to employ carbon aerogel/foam with unique 3D porous microstructure as a ready-made scaffold to support MXene nanosheets. A popular method to produce such carbon scaffold is to pyrolyze melamine foam.[245,246] For example, Sun et al. immersed melamine-derived carbon foam into MXene suspension and regulated the loading of MXene nanosheets by controlling MXene concentration, and after solvent removal under vacuum condition, the composite of MXene and carbon foam was further immobilized with epoxy resin.[245] The EM properties of such MXene/carbon foam were highly dependent on the loading of MXene nanosheets, and when the concentration of MXene was 5.0 mg/mL, the corresponding composite would exhibit the strongest RL of −41.5 dB (17.7 GHz, 1.83 mm) accompanied by an EAB of 4.7 GHz (10.6–15.3 GHz). The effective improvement on EM absorption performance was again linked with the unique 3D foam structure, as well as interfacial polarization and dipole polarization in the composite. Biomass-derived carbon materials are another kind of attractive scaffolds for MXene nanosheets. Liang et al. obtained 3D porous carbon scaffold with natural larch wood as the precursor.[191] After loading MXene nanosheets, the composite could produce absorption-dominant shielding effectiveness up to 71.3 dB in X band, and meanwhile, it had a density as low as 0.197 g/cm^3 but anisotropic compressive strength as large as 1.8 MPa. Different from hard carbon scaffold derived from natural larch wood, Jia et al. selected balsa wood as the precursor and removed lignin and hemicellulose therein before high-temperature pyrolysis, so that they harvested compressible carbon foam.[247] The embedment of MXene nanosheets coated with *trans*-l,4-polyisoprene not only increased EM absorption and total shielding effectiveness of the composite, but also endowed the composite with fascinating shape-memory characteristic. In addition to natural wood, recent progress indicated that starch was also a qualified precursor to generate carbon foam.[248] The composite of MXene and starch-derived carbon foam also produce high EM absorption capability over 40 dB in X band, and besides lightweight (0.32 g/cm^3) and compression resistance (4.9 MPa), it presented surprising flame retardancy, suggestive of a new and potential application field of such composite in the future.

As one of the most popular functional materials at present, the studies about MXene-based EWAMs are increasing by exponential growth. The good electrical conductivity of MXene nanosheets means that the required filler loading of MXene-based EWAMs in resin matrix will be drastically decreased, and thus the combination of MXene nanosheets and various carbon materials is considered as one of promising modes for the construction of lightweight EWAMs. However, the stability of MXene nanosheets may be an obstacle for their practical applications, because they easily suffer from phase destruction during preparative processes, especially in those under high-temperature condition. Therefore, an effective method to produce stable MXene nanosheets will further expand their application in the field of EM absorption.

MOLYBDENUM CARBIDE/CARBON COMPOSITES

The achievements made in SiC/C and MXene/C composites cannot completely conceal the dilemmas arising from their production and application processes. On one hand, the formation of SiC and MXene phases always requires rigorous conditions, especially high temperature over 1400°C in most cases, and on the other hand, the large size SiC and MXene may suppress their synergies with carbon components to some extent due to the limited heterogeneous contact. Therefore, the exploration of new carbides/carbon composites becomes an attractive topic in the field of EM absorption in recent years.[249–251] As one of the earth-abundant transition metal carbides, molybdenum carbide with multiple phases has been extensively studied in electrochemical capacitors, hydrogen evolution, and lithium-ion storage due to its unique electronic structure such as those of noble metals,[252–255] and compared with conventional SiC and MXene, the synthesis of molybdenum carbide can be realized under relatively mild conditions (600∼800°C), and thus it is more easy to accommodate ultra-small molybdenum carbide nanoparticles in carbon matrix.[256–258] These merits suggest that molybdenum carbide/carbon composites may also work for EM attenuation effectively, because the tunable electronic structure, small particle size, and uniform dispersion of molybdenum carbide nanoparticles are quite favorable for sufficiently synergistic effects and interfacial polarization.

Dai et al. firstly reported the EM absorption performance of Mo_2C/C composites, which were prepared through Cu-Mo-MOFs transformation and Cu etching.[259] The results indicated that Mo_2C/C composites could produce minimum RL of −49.0 dB at 9.04 GHz (2.60 mm) and maximum EAB of 4.56 GHz (1.7 mm), and such good performance indeed benefitted from the synergistic effect between Mo_2C nanoparticles and carbon matrix. Thanks to the relatively low temperature for the formation of molybdenum carbide phase, molybdenum carbide/carbon composites can be easily obtained through a solid-phase reaction between carbon matrix and Mo-containing salts/oxides. For example, Fan et al. impregnated cotton fiber textile into $(NH_4)_6Mo_7O_{24}\cdot 4H_2O$ solution and then obtained EM functionalized Mo_2C/C composites[260]; Wang et al. mixed MoO_3 with CNTs or CB, and harvested MoC/CNTs and MoC/CB composites, where MoC/CNTs could generate RL of −42.2 dB and EAB of 4.0 GHz with an absorber thickness of 1.5 mm.[261] In order to stimulate the microstructural contribution to EM attenuation, Che's group employed hollow N,P-doped carbon microspheres derived from dry yeast as the carbon matrix, and loaded $(NH_4)_6Mo_7O_{24}\cdot 4H_2O$ through hydrothermal treatment and then converted the intermediate products into final Mo_2C/C composites.[262] It was found that in final composites, hollow N,P-doped carbon microspheres were decorated by heterogeneous nanoflowers with a diameter of ∼50 nm that were actually composed of core-shell Mo_2C@C nanoparticles (∼5 nm). The interfacial polarization between Mo_2C@C nanoflowers and hollow carbon microsphere was clearly recorded by electron holography images, and the optimal composite had minimum RL of −50.6 and maximum EAB of 5.4 GHz. Although the synthesis of Mo_2C/C composites through solid-phase reaction is relatively simple, this way fails to disperse molybdenum carbide nanoparticles uniformly in carbon matrix, and the agglomeration or sintering of nanoparticles is easily detected in final composites, which is essentially unfavorable for EM absorption. Our group realized homogeneous-like dispersion of

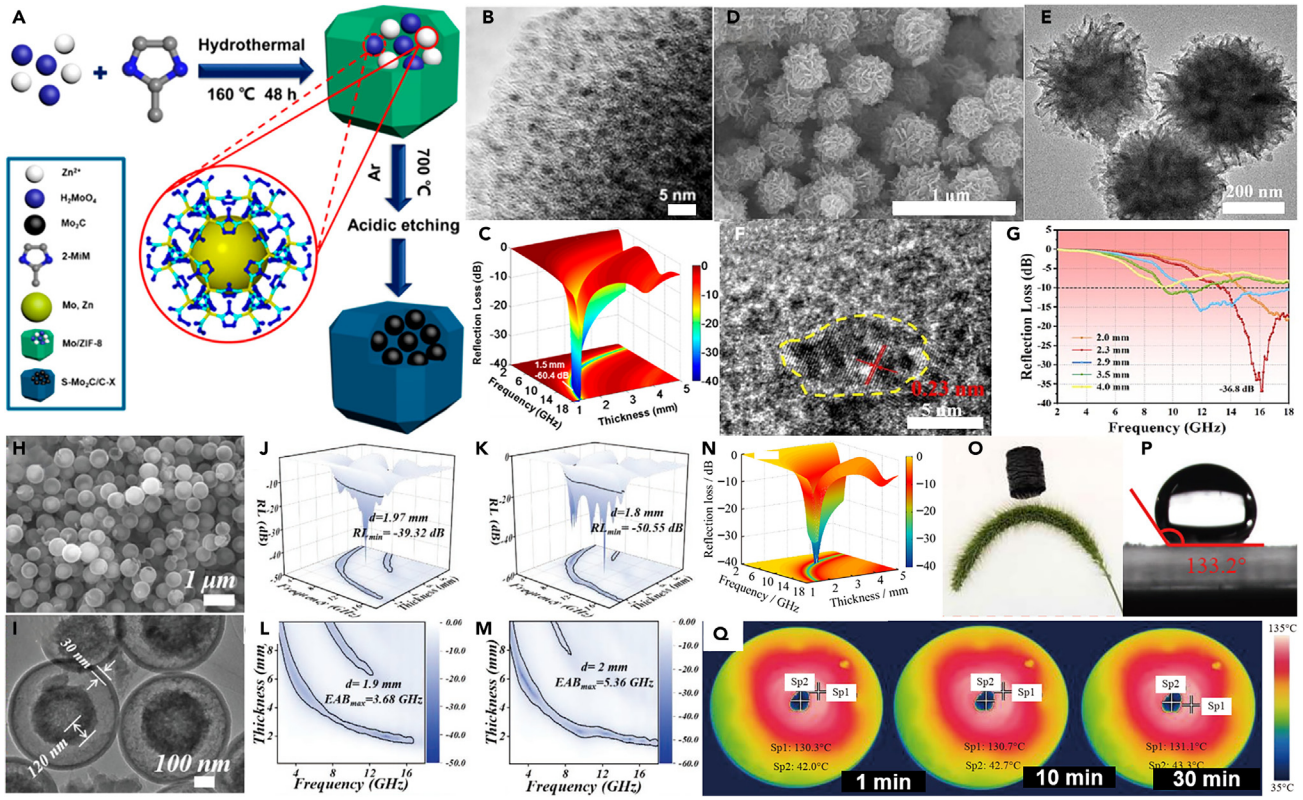

Figure 7. Preparative process, microstructure characterization, and various properties of Mo_2C/C compsoites

(A) Schematic illustration for the preparation of Mo_2C decorated carbon polyhedrons through MOFs transformation.

(B) TEM image of Mo_2C/C composite.

(C) 3D RL map of Mo_2C/C composite.

(D–F) SEM, (E) TEM, and (F) HRTEM images of flower-like Mo_2C/C composite.

(G) RL curves of flower-like Mo_2C/C composite.

(H) SEM and (I) TEM images of MoC_{1-x}/C composites.

(J–M) 3D RL maps of MoC_{1-x}/C composites.

(N) 3D RL map of Mo_2C/rGO aerogel.

(O) Photograph of Mo_2C/rGO aerogel resting on setaria viridis.

(P) Water contact angle test of Mo_2C/rGO aerogel.

(Q) Thermal insulation test of Mo_2C/rGO aerogel.

(A–C) Reproduced with permission.[263] Copyright 2018, American Chemical Society.

(D–G) Reproduced with permission.[264] Copyright 2023, Elsevier Ltd.

(H–M) Reproduced with permission.[265] Copyright 2022, Wiley-VCH.

(N–Q) Reproduced with permission.[60] Copyright 2023, Springer Nature.

Mo_2C nanoparticles by pyrolyzing Mo-substituted ZIF-8 (Figure 7A),[263] and the resultant Mo_2C nanoparticles were evenly distributed throughout the whole carbon skeleton and their average size was only 4.5 nm (Figure 7B). The content of Mo species in initial ZIF-8 just changed the dispersity of Mo_2C nanoparticles, but not their average size. The homogeneous-like dispersion of Mo_2C nanoparticles brought good EM absorption performance (Figure 7C), and with a small thickness of 1.5 mm, it could generate strong RL (−60.4 dB) and broad EAB (4.8 GHz). More importantly, the final Mo_2C/C composite displayed excellent environmental tolerance, and its EM absorption performance was almost unchanged after being treated at 473 K under air atmosphere and in strong acid solution (HCl, 3.0 mol/L) for 24 h.

With the increasing concerns on molybdenum carbide/carbon composites, some novel methods have been continuously developed. For example, we triggered the room temperature polymerization of pyrrole monomer by phosphomolybdic acid (PMo_{12}), and then converted the intermediate PMo_{12}/polypyrrole (PMo_{12}/PPy) nanospheres into pomegranate-like Mo_2C@C nanospheres, where an individual nanosphere was composed of many Mo_2C nanoparticles and a very thin carbon shell less than 10 nm.[266] EM analysis revealed that conductive loss from carbon shells played a dominant role in dielectric loss, and interior Mo_2C nanoparticles improved impedance matching and provided auxiliary polarization loss effects. In addition to these intrinsic loss features, the homogeneous chemical composition, core-shell configuration, and uniform spherical morphology all contributed to the consumption of EM energy to some extent, and thus the final composite showed qualified absorption effectiveness in a very broad frequency range (3.5–18.0 GHz) by manipulating the absorber thickness from

1.0 to 5.0 mm. Similarly, Wang et al. designed flower-like Mo-PDA precursor through the electrostatic interactions between dopamine and $[Mo_7O_{24}]^{6-}$, and further obtained flower-like Mo_2C/C composites assembled by carbon nanosheets and ultra-small Mo_2C nanoparticles (Figures 7D–7F).[264] After refining the loading of Mo_2C nanoparticles, the composite with unique morphology could broaden its EAB up to 7.04 GHz (Figure 7G). More recently, Zhao et al. and Deng et al. almost simultaneously reported the synthesis of double-shell Mo_2C/C hollow microspheres with PDA-coated molybdenum glycerate microspheres as the precursor.[265,267] It was worth noting that Zhao et al. also induced a phase transformation from hexagonal Mo_2C to cubic $Mo_{1-x}C$ by changing the pyrolysis atmosphere (Figures 7H and 7I), and they believed that such a phase transformation strengthened RL intensity from −39.3 to −50.6 dB and extended EAB from 3.68 to 5.36 GHz (Figures 7J–7M).[265] Huang's group manipulated β- and η-phases of molybdenum carbide with different guest clusters (MoO_4 and PMo_{12}) in the precursors, and concluded that η-MoC might be helpful for stronger RL and broader EAB.[268] However, these temporary conclusions cannot serve as the final conclusions yet to guide the fabrication of molybdenum carbide/carbon composites, because they are not based on a strict and systematical comparison, where the influences of carbon content and graphitization degree have not been excluded completely. That is to say, the phase engineering for molybdenum carbide/carbon composites is still a rather challenging task in the following studies.

The advantages of aerogel structure for EM absorption are mentioned more than once earlier in this review, and thus the creation of aerogel structure in molybdenum carbide/carbon composites is also significant. Following this direction, we conducted the assembly of ammonium molybdate and GO with the assistance of glucose through a hydrothermal reaction, and then converted the intermediate MO_2/GO aerogel into Mo_2C/rGO aerogels under high-temperature inert atmosphere.[60] The attachment of Mo_2C nanoparticles enhanced EM absorption performance of rGO aerogel remarkably, and with a low filler loading (9 wt %), Mo_2C/rGO aerogel could produce strong RL of −63.3 dB and EAB of 5.1 GHz (Figure 7N). It was more interesting that the resultant Mo_2C/rGO aerogel did not lose the lightweight feature of pristine rGO aerogel, but also consolidated its hydrophobicity and thermal insulation obviously (Figures 7O–7Q). However, such aerogels from hydrothermal assembly usually have relatively large Mo_2C nanoparticles (*ca.* 20–50 nm) and poor nanoparticles dispersion, and thus some advanced methods are still desirable to produce high-quality molybdenum carbide/carbon composite aerogels with better performance.

Molybdenum carbide has the advantages of ultra-small particle size and uniform dispersion in carbon matrix, which endows molybdenum carbide/carbon composites with strong interfacial polarization. However, the corresponding composites does not exhibit obvious enhancement in EM absorption performance as compared with SiC/C and MXene/C composites, and thus some specific studies on absorption mechanism, such as phase effect, needs to be carried out. In addition, the multifunction features of molybdenum carbide/carbon composites, including hydrophobicity, thermal insulation, and thermal stability, should be fully considered when EWAMs are designed.

OTHER CARBIDES/CARBON COMPOSITES

Although most studies about EM absorption performance of carbides/carbon composites focus on SiC, MXene, and Mo_2C, there are also several groups that attempt to construct novel composites with some uncommon carbides. As a kind of nonmetallic carbide, B_4C has excellent mechanical properties, thermal conductivity, and high hardness, which is widely utilized as abrasive grits, wear-resistance components, bulletproof armors, neutron absorbers.[269,270] Furthermore, extremely low density and tunable band gap render B_4C as a potential attachment of carbon materials to remedy their relatively poor impedance matching. Ma et al. prepared C-encapsulated B_4C nanoparticles by pyrolyzing the mixture of H_3BO_3 and $C_{12}H_{22}O_{11}$ at 1550°C under vacuum condition.[271] The results revealed that B_4C nanoparticles balanced the relationship between attenuation ability and impedance matching, and when B/C atomic ratio in the initial mixture reached 1:1.25, the composite could produce RL intensity as strong as −60 dB with a small thickness of 1.5 mm, while the corresponding EAB was only 1.5 GHz. Wang et al. induced *in situ* growth of B_4C nanowires on activated carbon felt (ACF), and they came to similar conclusion, that is the B_4C/ACF composite just worked for strong RL intensity (below −30.0 dB), but failed to realize broad frequency response.[272] Wang et al. conducted the formation of a thin graphitic layer around B_4C nanosheets with the assistance of NaCl, and they extended the EAB of these core-shell nanosheets to 4.0 GHz.[273] From the limited results available, the EM absorption performance of B_4C/C composites is temporarily lagging behind those of the aforementioned composites, and thus an elaborate design on the composition and microstructure of B_4C/C composites is still necessary to further enhance their performance in the following studies.

Transition metal carbides, excluding 2D MXene, usually have similar properties, such as high melting point, low density, large rigidity, and good environmental stability, and especially for that the occupation of interstitial sites by carbon atom will also change the d-band electron density of metals at Fermi level.[274,275] Therefore, in addition to molybdenum carbide (i.e., $Mo_{1-x}C$, MoC, Mo_2C), many other transition metal carbides can also produce EM absorption characteristics to some extent and emerge as promising EM additives in carbon matrix.[276,277] The arc-discharge method is widely utilized for the preparation of TiC/C composites, because final composites have desirable core-shell configuration in most cases.[278–280] For example, Meng et al. obtained core-shell TiC@C nanocubes in this way, and they found that this composite could produce RL intensity close to −30.0 dB and EAB of 3.9 GHz with the thickness of 2.0 mm and the filler loading of 50 wt %.[278] Very interesting, Yu et al. realized the morphology transformation of TiC from nanocube (Sample A) to truncated octahedron (Sample B) and the prior exposure of low energy (111) facet by adjusting the reaction atmosphere (Figures 8A and 8B).[279] Both experimental data and theoretical calculations identified that the stronger localization of polarized charge might be created at TiC(111)/graphite interface than that at TiC(100)/graphite interface, thus enhancing dielectric loss capacity and absorption coefficient (Figure 8C). As a result, the minimum RL intensity and maximum EAB of Sample B reached −45.1 dB and 5.1 GHz (Figure 8D), respectively, which were superior to those of Sample A (Figure 8E). Of note is that the arc-discharge method is also applicable to the synthesis of VC@C and Er_2C@C nanocomposites, and both of them can produce RL intensity less than −45.0 dB and EAB close to 5.0 GHz.[281,282] Although the arc-discharge method is universal and highly effective for

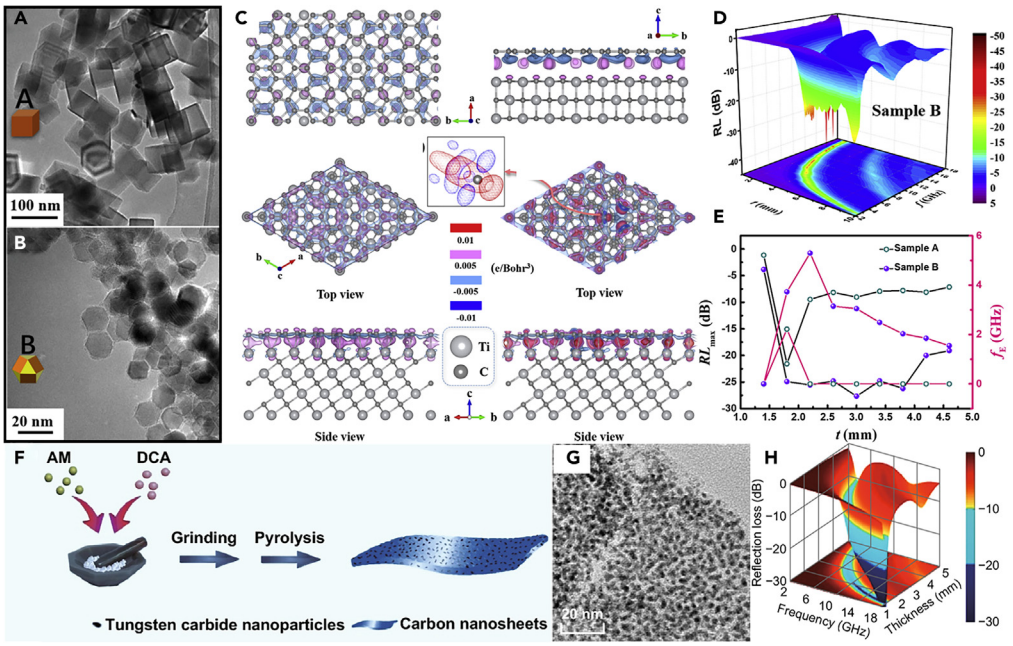

Figure 8. Engineering phase, preparative process, and EM absorption performance of titanium carbide/carbon and tungsten carbide/carbon composites

(A and B)TEM images of (A) Sample A and (B) Sample B.

(C) Charge transferring near different TiC/graphene interface structures.

(D) 3D RL map of sample B.

(E) The dependence of RL_{max} and f_E on the thickness of samples A and samples B.

(F) Schematic illustration for solvent-free synthesis of different tungsten carbide/carbon composites.

(G) TEM image of tungsten carbide/carbon composite.

(H) 3D RL map of tungsten carbide/carbon composite.

(A–E) Reproduced with permission.[279] Copyright 2020, Elsevier Ltd.

(F–H) Reproduced with permission.[285] Copyright 2020, Springer Nature.

various carbides/carbon composites, the adjustability on the composition and microstructure of final composites is usually limited,[283] and thus there still remains considerable interest in developing new methods for carbides/carbon composites. For example, Yuan et al. coated carbon microspheres with TiO_2 and then conducted the conversion of TiO_2 into TiC at 1200°C.[284] The content of TiC nanoparticles could be tailored from 19.9 to 74.1 wt %, and with the optimal loading of TiC nanoparticles, the corresponding composite had minimum RL intensity of −52.4 dB and maximum EAB of 4.3 GHz. Our group recently prepared a series of WC_{1-x}/C composites through a very simple solvent-free strategy, i.e., a direct pyrolysis of the grinding mixture of ammonium metatungstate (AM, tungstate source) and dicyandiamide (DCA, carbon source, Figure 8F).[285] The resultant composites were composed of thin carbon nanosheets and ultrafine WC_{1-x} nanoparticles (3–4 nm, Figure 8G), and their relative contents could be changed just by the weight ratio of DCA to AM. Even with a small absorber thickness (1.50 mm), the optimum composite could generate acceptable EAB of 4.9 GHz, and more importantly, it could maintain good performance in a very broad frequency range of 3.6–18.0 GHz by accumulating the thickness from 1.5 to 5.0 mm (Figure 8H).

As typical transition metal carbides from VIII group, Fe_3C, Co_3C, and Ni_3C have unique magnetic response behavior, that is, they can provide additional magnetic loss mechanism for incident EM wave, and thus they, especially Fe_3C, also receive much attention in the construction of carbides/carbon composites.[286–290] In many cases, Fe_3C is a usually commensal component with metal Fe with body-centered cubic structure from carbothermal reduction due to the occupation of carbon atoms at the interstitial sites of Fe crystals,[36,291,292] and the formation of Fe_3C may moderately decrease the saturation magnetization and magnetic loss capability of metal Fe.[86,293,294] However, Chen's group recently analyzed the density of states (DOS), the charge density differences, and the work function of the models for Fe_3C/N-doped graphene and Fe/N-doped graphene with density functional theory (DFT) and first-principle calculations.[295] Although the results revealed that both Fe_3C and Fe could induce electron migration at their interfaces with carbon layers, the work function difference between Fe_3C and N-doped graphene (1.38 eV) was much higher than that between Fe and N-doped graphene (0.21 eV), which meant that the generation of Fe_3C in carbon matrix would bring stronger interfacial polarization and dielectric loss. Sun et al. further demonstrated the obvious contribution of Fe_3C nanocrystals to oxidation and corrosion resistance for Fe/C related composites.[296] Therefore, the rational construction of Fe_3C/C composites still has its own significance as compared to common Fe/C composites, and however, the controllable formation of absolute Fe_3C phase is always difficult because Fe easily becomes a dominant phase during carbothermal reduction. Literature review suggests that if some polymers are involved in initial precursors, the formation probability of Fe_3C may be remarkably increased,[288,289] which is

possibly attributed to the fact that the gaseous small molecules released from those polymers can promote the infiltration of carbon atoms at high temperature. Despite the lack of support from experimental and theoretical data, more and more groups harvest Fe_3C/C composites successfully following this direction, and one of the most popular strategy is electrospinning, where Fe salts and organic polymers are shaped into 1D fibers and then converted into final Fe_3C/C composites under high-temperature inert atmosphere.[296–300] For example, Liu and his co-workers prepared 1D Fe_3C/C composites with PVP and ferric nitrate as carbon and Fe sources in this way, and the resultant composite displayed minimum RL intensity of −62.6 dB and maximum EAB of 6.5 GHz.[297] Instead of electrospinning, Zhang et al. created 3D foam structure through PVP bubbling in the presence of ferric nitrate, and then converted this intermediate foam into final 3D Fe_3C/C composite by high-temperature pyrolysis.[301] The composition of the composites could be easily manipulated by the weight ratio of PVP to ferric nitrate, and when this ratio was 1:2, the corresponding RL intensity and EAB would be −37.4 dB and 5.6 GHz with an absorber thickness of 2.0 mm. They attributed the good EM absorption performance to the synergy between Fe_3C nanoparticles and 3D carbon frameworks, as well as the structure effect on the aggravated consumption of incident EM wave.

In this section, the EM absorption performance of some uncommon carbides/carbon composites are reviewed. Typical examples include B_4C/C, Fe_3C/C, Er_2C/C, TiC/C, VC/C, WC_{1-x}/C, and so on. It has to be pointed out that these examples are usually from some isolated and episodic reports, and their EM absorption performance is only at a moderate level. That is, more studies on these uncommon carbides/carbon composites are highly encouraged to provide systematic and comprehensive experimental and theoretical data.

MULTICOMPONENT CARBIDES/CARBON COMPOSITES

In theory, each component in composites has its own EM characteristics, which implies that the more kinds of EM components are involved, the stronger synergistic or complementary effects may be generated in final composites. Therefore, it is also of great interest to build multi-component composites based on the combination of carbides and carbon materials.

Carbides/carbon/magnetic component composites

By considering that most carbides are non-magnetic, magnetic materials are extensively selected as the additional components for carbides/carbon composites in a considerable portion of related studies.[249,302–307] The introduction of magnetic materials can bring extra loss mechanisms, such as eddy current loss, natural domain resonance, and ferromagnetic resonance.[10] These effects can irreversibly convert EM energy into heat. More importantly, additional magnetic components can bridge the gap between ε_r and μ_r. When the loss capacities of electric energy and magnetic energy are compatible, the input impedance will be close to the impedance of free space and the reflection of incident EM wave at the interface between EWAMs and free space will be greatly reduced. That is to say, the introduction of magnetic components is helpful to improve impedance matching.[222] Besides, when additional magnetic components are uniformly dispersed in dielectric substrates, there will be more heterogeneous interfaces between dielectric and magnetic components, and the contribution from interfacial polarization will be greatly enhanced.[220] In some cases, the dispersed magnetic metal nanoparticles may also function as carriers for electron migration to strengthen conductive loss.[227] The simplest method is undoubtedly to integrate the as-prepared carbon materials, carbides, and magnetic particles in a physical way.[308–311] Of note is that several groups pay special attention to the microstructure design and the electrostatic interaction among different components for their uniform dispersion and full contact in the latest research.[198,209,302,312,313] For example, Liang et al. assembled positively charged Ni nanochains with MXene and GO nanosheets, and created 3D macroporous skeletons of MXene/GO through the hydrogen bond between MXene and GO and the guidance of unidirectional ice template (Figures 9A and 9B).[198] The resultant ternary Ni/MXene/rGO aerogel exhibited uniform composition distribution, ultralow density and good mechanical property (Figures 9C–9E), and more importantly, the presence of Ni chains brought obvious magnetic resonance behavior. All these merits endowed the final composite aerogel with excellent EM absorption performance, including strong RL of −75.2 dB and broad EAB of 7.3 GHz (Figure 9F). In addition, some unique technologies, such as spray drying,[312,314] electrospinning,[303,315,316] arc discharge,[317–319] are also commonly employed to direct the morphology and composition of multicomponent composites. For example, Che's group fabricated hollow Fe_3O_4/CNTs/MXene microsphere with a spray-drying method (Figures 9G and 9H), whose RL intensity and EAB with a thickness of 2.0 mm were −40.1 dB and 5.8 GHz, respectively (Figure 9I).[314] Electron holography images revealed that CNTs suppressed the re-stacking of $Ti_3C_2T_x$ nanosheets and thus created rich polarization interfaces, and Fe_3O_4 nanospheres confined in the microspheres were responsible for the formation of interconnected 3D magnetic network to broaden response frequency bandwidth. It was interesting that this was a very universal way to produce multicomponent composites, because the relative content of Fe_3O_4, CNTs, and $Ti_3C_2T_x$, even the composition of magnetic particles (Fe_3O_4, FeCo alloy, CoNi alloy, FeCoNi alloy), could be easily manipulated. Zhang et al. demonstrated the synthesis of 1D $Fe_{0.64}Ni_{0.36}$/MXene/CNFs composite with $NiFe_2O_4$/MXene/polyacrylonitrile (PAN) fibers from electrospinning as the precursor, and the complementary loss mechanisms of different components resulted in strong RL intensity (−54.1 dB) and wide EAB (7.8 GHz).[303]

MOFs transformation is currently the most popular strategy to prepare carbon-based composites, and thus many successful examples about magnetic multicomponent carbides/carbon composites are still established on this method. Literature review indicates that there are three common ways to construct magnetic multicomponent carbides/carbon composites through MOFs transformation. The first one is to couple magnetic carbon-based intermediates derived from MOFs with carbides.[320–322] Xiang et al. converted Co-MOFs into sea urchin-like Co/CNTs nanocomposites and modified the intermediate nanocomposites with hexadecyl trimethyl ammonium bromide (CTAB), so that the positively charged nanocomposites could be effectively assembled with MXene nanosheets.[322] The final ternary composites achieved strong RL of −85.8 dB and broad EAB of 6.1 GHz with a relatively small thickness of 1.4 mm. The second way is to induce the growth of MOFs crystals on carbides, and then generate magnetic multicomponent carbides/carbon composites after high-temperature

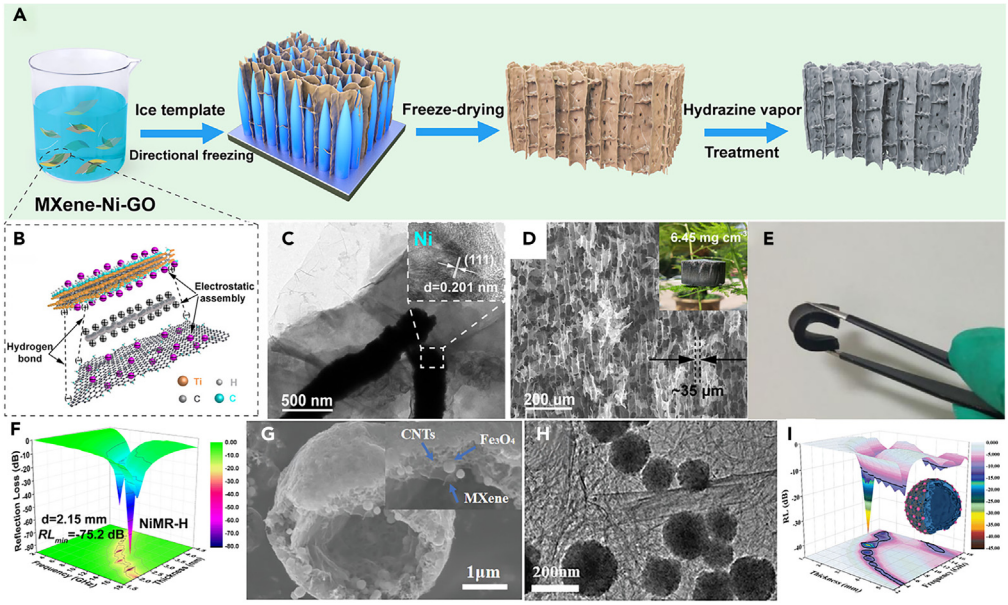

Figure 9. Preparative process and various properties of ternary composites

(A and B) Schematic illustration for the fabrication of Ni/MXene/RGO aerogel.

(C) SEM, photograph (inset), (D) TEM, HRTEM (inset) images of Ni/MXene/RGO aerogel.

(E) Digital photographs of Ni/MXene/RGO aerogel/PDMS after flexible bending for 180°.

(F) 3D RL map of Ni/MXene/RGO aerogel.

(G and H) SEM and (h) TEM images of Fe_3O_4/CNTs/MXene.

(I) 3D RL map of Fe_3O_4/CNTs/MXene.

(A–F) Reproduced with permission.[198] Copyright 2021, American Chemical Society.

(G–I) Reproduced with permission.[314] Copyright 2021, Wiley-VCH.

pyrolysis.[311,323–325] For example, Zou et al. directed the growth of ZIF-67 crystals on exfoliated MXene nanosheets and harvested 0D/1D/2D architectural Co/CNTs/MXene composite under H_2/Ar atmospheres.[222] The multiple synergistic effects and the proper magnetic loss rendered the composite as a promising EM medium with good attenuation ability and impedance matching, whose strongest RL and maximum EAB could reach −50.5 dB and 5.8 GHz, respectively. The third way usually excludes carbides with large particle size (i.e., SiC and MXene), and the mixture of MOFs/metal oxides or MOFs/polyoxometalates will be taken as the precursors, and thus it is a quite flexible route for microstructure design.[249,268,304,326–328] Ji's group pioneered the synthesis of Mo_2C/Co@C through the transformation of MoO_3@ZIF-67, and optimized EM absorption performance (RL: −48.0 dB, EAB: 6.0 GHz) of final composites by the pyrolysis temperature.[304] Huang et al. designed hollow Mo_2C/Co@C polyhedrons with ZIF-8@CoMo-MOFs as the precursor, and further extended EAB to 6.6 GHz.[327] Inspired by the advantages of MOFs transformation, Zhang et al. utilized the supramolecular self-assembly between PMo_{12} and PDA in the presence of $CoFe_2O_4$ nanoparticles to produce hierarchical molybdenum carbide/iron-cobalt alloy/nitrogen-doped carbon (Mo_2C/FeCo/NC).[329] They found that the conductive-dielectric-magnetic loss coupling network generated favorable features for EM absorption, and thus the final ternary composite not only displayed strong RL intensity up to −77.4 dB, but also had wide frequency response with EAB of 7.3 GHz.

Carbides/carbon/nonmagnetic components composites

The introduction of magnetic particles indeed makes solid contribution to EM absorption, while their role is not just the center of magnetic loss, and in many cases, their impact on dielectric loss is much larger than magnetic loss. Inspired by this fact, the construction of multicomponent dielectric media based on carbides/carbon composites also arouses great interest. In the family of dielectric loss materials, conductive polymers are a popular kind of additives for carbides/carbon composites, because they are usually generated under mild condition through the polymerization of organic monomer, and they preferably nucleate on the surface of solid particles at the initial stage of polymerization, which may avoid phase segregation in final composites.[330–332] Yin et al. found that PANI layer on the surface of MXene/CF composite fibers would increase the performance of EM absorption in X band remarkably with negligible influence on reflection performance, thus reinforcing the total shielding effectiveness.[333] Liu et al. directed the *in situ* polymerization of aniline monomer on the surface of hollow SiC/C microspheres, and they harvested radial PANI nanorods with controllable content (Figures 10A–10C). When the weight ratio of hollow SiC/C microspheres to aniline monomer reached 1:1.5, the final composite (SCP-1:1.5) could have EAB of 5.61 GHz with an absorber thickness of 1.88 mm, and the integrated EAB could further broadened to almost 14.0 GHz by accumulating the thickness from 1.0 to 5.0 mm (Figure 10D).[334] Hu's group firstly built up a carbon layer on SiC whiskers through hydrothermal carbonization of glucose, and further created

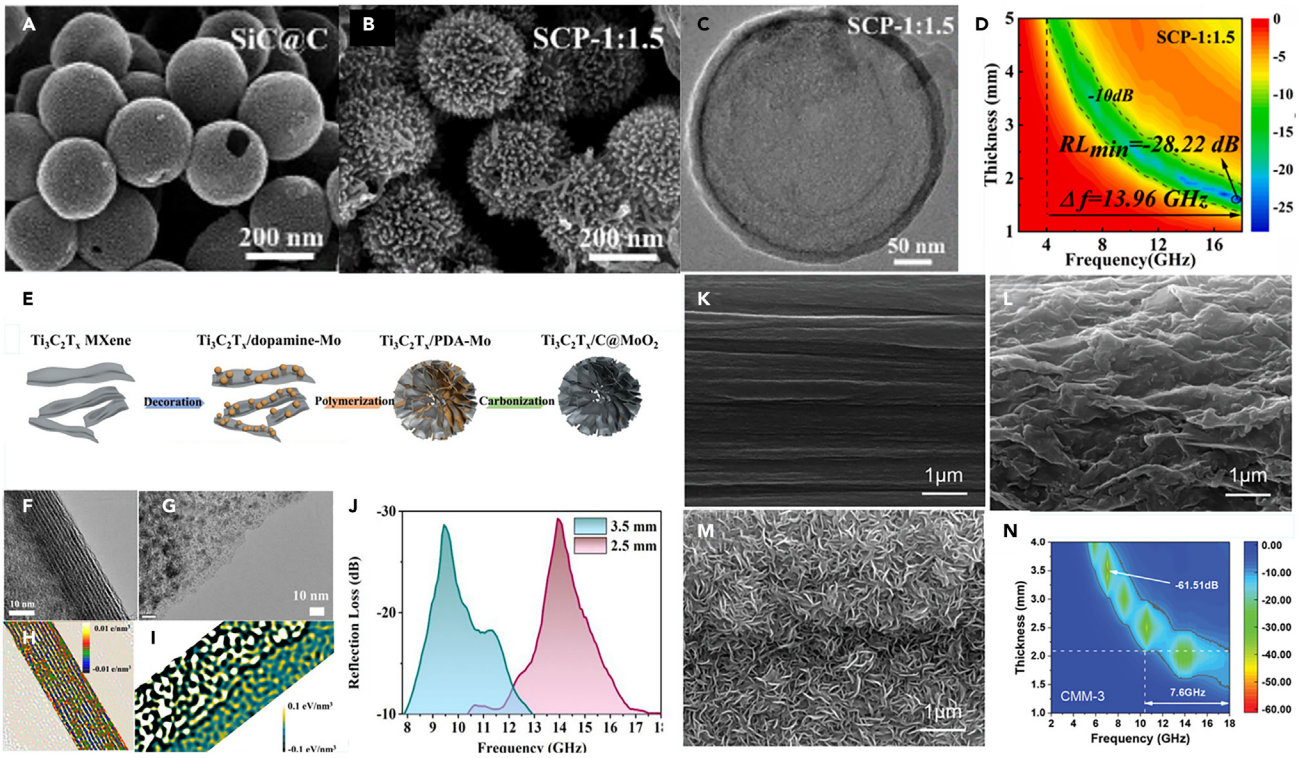

Figure 10. Microstructure characterization and EM absorption performance of ternary dielectric composites

(A and B)SEM images of (A) SiC@C, (B) SiC@C@PANI.

(C) TEM image of SiC@C@PANI.

(D) 2D RL map of EM absorption performance of SiC@C@PANI.

(E–G) Schematic synthesis process and (F and G) TEM images of MXene/C/MoO_2 composites.

(H and I) Charge density distributions at the interfaces between MXene/carbon nanosheets and at the heterojunctions between MoO_2/C and MoO_2/MXene.

(J) The EABs of MXene/C/MoO_2 composites with different absorber thickness.

(K–M) SEM images of CFs, CFs@MXene and CFs@MXene@MoS_2.

(N) 2D RL map of EM absorption performance of CFs@MXene@MoS_2 composites.

(A–D) Reproduced with permission.[334] Copyright 2022, Elsevier Ltd.

(E–J) Reproduced with permission.[337] Copyright 2021, American Chemical Society.

(K–N) Reproduced with permission.[338] Copyright 2020, Wiley-VCH.

a PPy layer through the polymerization of pyrrole monomer.[335,336] The EM characteristics of SiC/C/PPy could be manipulated by the dosage of glucose and the polymerization time of PPy, and the optimized ternary composite had the strongest RL of −52.4 dB and EAB of 8.1 GHz, which were superior to those of the best SiC/C composite (−24.6 dB and 6.8 GHz).[336]

Previous studies point out that transition metal oxides may consume incident EM energy through polarization effects generated from ionic metal-oxygen bonds, non-metrological defect sites, heterogeneous interfaces, and even electron transition,[336,339] and thus some metal oxides, such as ZnO, MoO_2, TiO_2, and Co_3O_4, are usually designed as the inorganic additives for carbides/carbon composites.[337,340–342] For example, Wu et al. embedded MXene nanosheets into flower-like Mo-PDA microspheres, and then converted the intermediate product to final MXene/C/MoO_2 composites with 2D/2D/0D heterojunctions at 600°C under Ar atmosphere (Figures 10E–10G).[337] They recorded the re-equilibrium of charges with a maximum density range of $\pm$0.01 eV/nm^3 at the 2D/2D interfaces between MXene/carbon nanosheets (Figure 10H), as well as the re-equilibrium of charges at the 0D/2D heterojunctions between MoO_2/C and MoO_2/MXene (Figure 10I). These uneven distributions of charges brought intensive interfacial polarization in a wide frequency range, and thus the ternary MXene/C/MoO_2 composites showed EAB as broad as 7.7 GHz (Figure 10J). Compared with those metal oxides, transition metal sulfides may be more favorable for energy consumption, because their relatively narrow band gap can promote electron transition and provide considerable conductive loss.[38,343] Therefore, transition metal sulfides are also popular additives in multicomponent carbides/carbon composites.[344,345] Wang et al. attached MXene nanosheets on CTAB-decorated CFs through electrostatic interaction, and further conducted the growth of MoS_2 nanosheets on the surface of CFs@MXene.[338] SEM images clearly identified the change of surface morphology from CFs to CFs@MXene@MoS_2, where MoS_2 nanosheets were vertically anchored on the surface of CFs@MXene (Figures 10K–10M). Thanks to the powerful synergy among different components, CFs@MXene@MoS_2 not only generated broad EAB (7.6 GHz), but also showed strong RL intensity (−61.5 dB, Figure 10N). Of note is that in addition to metal oxides and sulfides, SiO_2 gradually receives attention in some recent

articles about EM absorption performance of multicomponent carbides/carbon composites.[148,179,346] Although SiO_2 is a kind of wave-transparent materials in essence, it can still regulate the dielectric properties of various composites and improve their impedance matching.[347–349] It is precisely through the functions of SiO_2 that Deng et al. designed hierarchical core-shell SiCnws@SiO_2-carbon foam hybrid composites with highly efficient EM absorption, where the impedance gradient structure coupled with enhanced interfacial polarization made EAB of the composite cover the whole X band.[346]

Inspired by the moderation effect of additional dielectric components, there is also interest in the construction of multicomponent carbides/carbon composites with two different carbon components or carbides.[228,350] It needs be mentioned that when two kinds of carbon components are involved in final composites, one of them is usually utilized as 3D skeleton to afford microstructure effect while improving dielectric properties.[174,351–353] Hou et al. firstly fabricated 3D rGO foams through bidirectional freeze-drying and pyrolysis treatment, and then induced the growths of SiC and CNTs successively with CVI and CVD techniques.[352] The final composites could produce qualified EM absorption in the whole X band superior to many carbides/carbon composites, and the authors confirmed that the significantly enhanced EM absorption performance benefited from multiple heterogeneous interfaces and multi-scale hierarchical architecture. Dai et al. designed CFs-reinforced carbon aerogel with polyacrylamide (PAM) hydrogel as the precursor of carbon skeleton, and then introduced SiC particles with a carbothermal reduction reaction (Figure 11A).[174] The final composite not only inherited extremely low density from carbon aerogel (Figure 11B), but also maintained hierarchically porous microstructure (Figures 11C and 11D), and more importantly, many favorable characteristics, including strong attenuation capability, good impedance matching, and interconnected 3D networks, were together responsible for its excellent EM absorption performance with RL of −52.6 dB and EAB of 8.6 GHz (Figure 11E). As for multicomponent composites with two different carbides, one of them usually refers to those candidates that have very small particle size and are easily available under mild conditions, e.g., Mo_2C and ZrC.[251,350,354,355] For example, Yuan et al. obtained 1D Mo_2C/SiC/C fibers by the pyrolysis of PCS/$MoO_2(acac)_2$/PVP co-electrospinning fibers, and the uniform dispersion of Mo_2C and SiC nanoparticles could generate abundant interfaces, defects, and synergistic effect, thus resulting in broad EM response with EAB of 6.87 GHz.[354] Yang et al. coated MoO_3/PDA microspheres with MXene nanosheets, and converted the intermediate composite into ternary Mo_2C/C/MXene composite, which also displayed strong RL intensity over −60 dB and moderate EAB.[355] More recently, Wang et al. prepared Hollow carbon/MXene/Mo_2C microtubes (HCMM) with polyethylene terephthalate (PET) non-woven fabric as a sacrificing template (Figures 11F–11H).[251] The obtained 1D hierarchical microtube produced a very strong RL of −66.3 dB with an ultra-thin absorber thickness of 1.0 mm (Figure 11I). In order to extend its EAB, the authors designed macroscopic 3D structural metasurface based on the HCMM, and the stimulated results revealed that it could realize an ultra-broad EAB in the range of 3.7–40.0 GHz with a thickness of 5.0 mm (Figure 11J), which laid a solid foundation for the practical application of carbides/carbon composites. Silicon nitride (Si_3N_4) as a kind of famous inorganic ceramics has superior mechanical properties but comparable dielectric properties to SiC, and thus it is also taken as an additive in multicomponent composites sometimes, where the most popular combination is SiC/Si_3N_4/C.[356] In many cases, carbon materials, such as CFs, graphene, carbon foams, still play as the matrix of final composites, and SiC and Si_3N_4 with different morphologies can be introduced through physical mixing and *in-situ* generation.[149,172,357,358] For example, Xiao et al. directed the formation of porous ceramic composites with alternating SiC/C and Si_3N_4 layers, and the final composite could produce strong RL in X band.[358]

It is widely accepted that the synergistic effect between different EM media will produce positive contribution of EM absorption, and thus the rational construction of EWAMs is not limited by binary or ternary composites, and some multicomponent composites with at least four components are also sporadically reported in recent years. For example, Liu et al. employed CoNi-MOF/MXene as the precursor and converted it into quaternary MXene/CNTs/TiO_2/CoNi composites at high temperature under N_2 atmosphere,[325] whose RL intensity and EAB were −54.6 dB and 4.0 GHz, respectively. Although the performance of MXene/CNTs/TiO_2/CoNi was moderate, it required a relatively small absorber thickness of 1.76 mm. Hou et al. conducted the selenylation of CoNi LDH/MXene to generate $NiSe_2$-$CoSe_2$@C/$Ti_3C_2T_x$ composite, and the EAB as broad as 5.68 GHz was attributed to the multi-interface polarization loss from the synergistic effects of different components.[359] Yu's group showed their interests in the construction of multicomponent composites with simple physical mixture.[128,130] For example, they obtained quaternary CNTs/Fe_3Si/Fe/SiOCN nanocomposites by pyrolyzing the mixture of poly(methylvinyl) silazane, ferric acetylacetonate, and carboxylic functionalized CNTs, and the final composite could display minimum RL of −65.3 dB and maximum EAB of 6.0 GHz with the absorber thickness of only 1.6 mm.[130] They could even produce hexahydric Co_2Si@SiC/C/SiOC/SiO_2/Co_3O_4 nanocomposites with the mixture of pitch, $Co_2(CO)_8$, and low-molecular weight PCS as the precursor, and this composites with so many components indeed showed the superiority in RL intensity in X band.[360]

Numerous results indicate that the construction of multicomponent composites based on carbides/carbon composites are helpful for EM absorption. Both of additional dielectric and magnetic components can improve impedance matching and enhance RL characteristics of carbides/carbon composites, especially when some unique microstructures are created in these composites. However, the studies on multicomponent composites is still in a blind stage, and it is extremely difficult to make clear the coupling effects of multiple components and microstructure just by experimental data. In view of this fact, multicomponent carbides/carbon composites only exhibit limited extension in EAB and are still incapable of low-frequency absorption. Therefore, it is urgently demanded to utilize machine learning methods to help for the design of highly effective EWAMs.

Conclusions

Herein, we present a state-of-the-art review on carbides/carbon composites as high-performance electromagnetic wave absorbing materials (EWAMs). Based on these reports, the combination of carbides and carbon materials is an indeed good pathway to enhance EM absorption

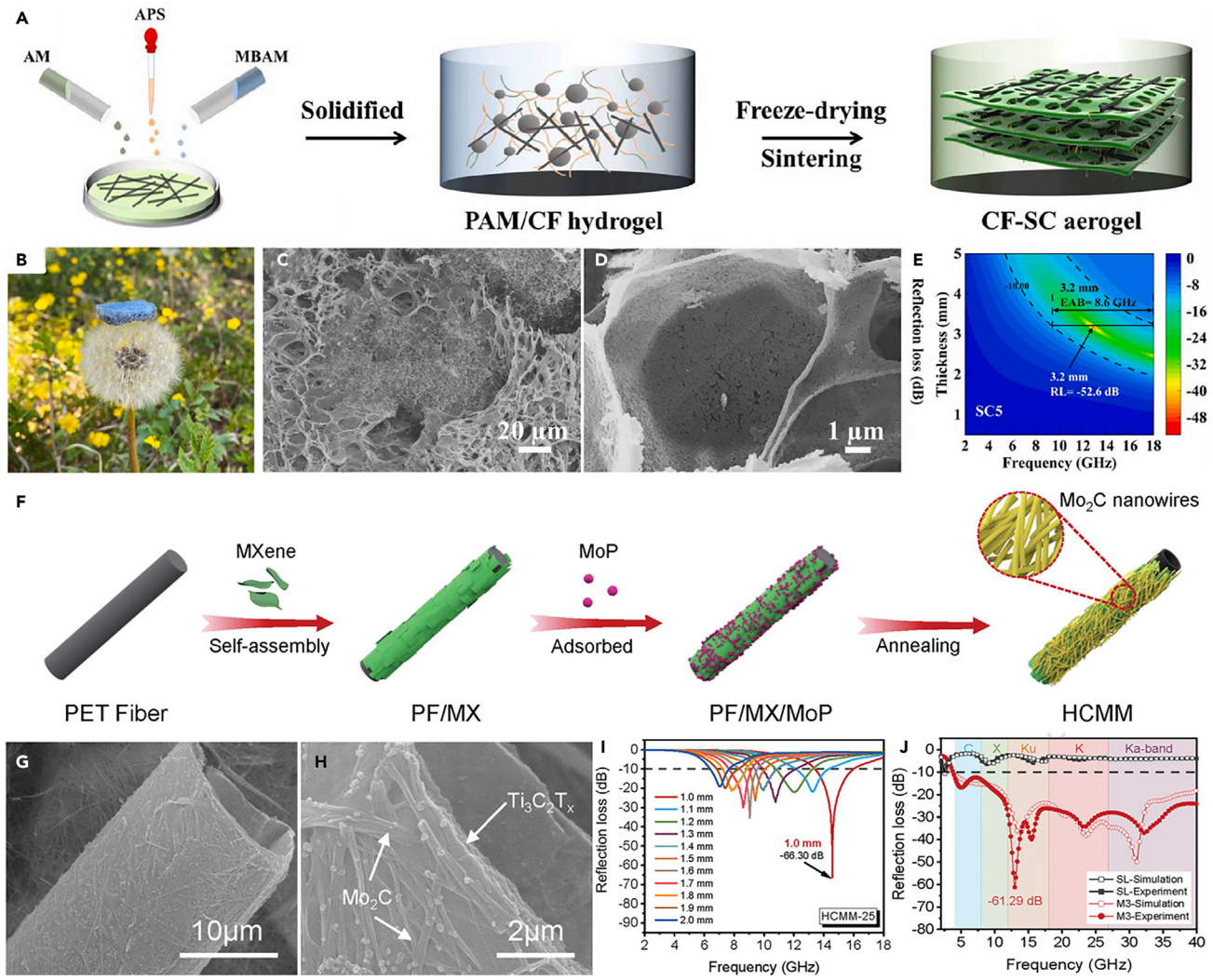

Figure 11. Preparative process and EM absorption performance of ternary dielectric composites with unique microstructure

(A) Schematic illustration for the fabrication of CF-SC aerogel.

(B) Digital photograph of CF-SC aerogel supported on dandelion.

(C and D) SEM images of CF-SC aerogel.

(E) 2D RL map of CF-SC aerogel.

(F) Schematic illustration for the fabrication.

(G and H) SEM images, (I) RL curves of HCMM.

(I) The comparison of simulated and experimental reflectivity of single-layered and multiple-layered HCMM-based EWAMs with metasurface.

(A–E) Reproduced with permission.[174] Copyright 2023, Elsevier Ltd.

(F–I) Reproduced with permission.[251] Copyright 2023, Wiley-VCH.

significantly, because the synergy between them can generate rich EM loss mechanisms and improve impedance matching. To date, the most widely used carbides include SiC, MXene, and Mo_2C, and thus we spend a lot of words to discuss the EM absorption performance of binary composites with these three kinds of carbides. In Table 1, we further filtrate some typical binary composites with excellent performance and make a comprehensive comparison in the frequency range of 2.0–18.0 GHz. Although some SiC/C composites with 0D or 1D morphology (Entry 1–3) may produce good absorption characteristics especially in effective absorption bandwidth (EAB), their performance is still less than those of 3D SiC/C composites (Entry 4 and 5), suggesting that microstructure design may be an important breakthrough point for the fabrication of SiC/C composites. This is because SiC/C composites with 3D microstructure usually have high porosity, which facilitates the reinforcement of interfacial polarization effect and multiple reflection behavior, and both of them can intensify the energy consumption of incident EM wave. As a rising star in carbides, MXene nanosheets have demonstrated their prospect in EM absorption when they are coupled with carbon materials (Entry 6–11). The resultant MXene/C composites have a little inferior performance to SiC/C composites, while

Table 1. Recent progress in carbides/carbon composites as EWAMs

Entry	Category	Absorbers	C-band 4-8 GHz			X-band 8-12 GHz			Ku-band 12-18 GHz			Filler loading	Reference
			d (mm)	Min RL (dB)	EAB (GHz) (RL < −10 dB)	d (mm)	Min RL (dB)	EAB (GHz) (RL < −10 dB)	d (mm)	Min RL (dB)	EAB (GHz) (RL < −10 dB)		
1	SiC/C composites	SiC@C nanowires	4.0	−20.2	2.0 (6.0–8.0)	3.0	−26.6	7.8 (8.0–15.8)	2.8	−50.0	8.0 (8.2–16.2)	50.0 wt %	Liang et al.[110]
2		SiC/rGO nanowires	–	–	–	3.0	−39.7	4.1 (7.8–11.9)	1.9	−56.3	6.2 (11.8–18.0)	35.0 wt %	Wang et al.[137]
3		SiC@C nanoparticles	3.5	−24.5	3.3 (6.6–9.9)	3.0	−24.9	3.9 (8.1–12.0)	2.1	−30.7	5.6 (12.4–18.0)	8.0 wt %	Chen et al.[166]
4		SCNF108[a]	–	–	–	3.0	−52.5	10.1 (7.9–18.0)	2.6	−40.2	8.2 (9.8–18.0)	12.6 wt %	Cai et al.[169]
5		SiC/C-900	–	–	–	3.6	−51.6	10.8 (7.2–18.0)	3.6	−17.7	10.8 (7.2–18.0)	50.0 wt %	Ye et al.[181]
6	MXene/C composites	PCM-50-700[b]	5.0	−18.5	3.2 (5.2–8.4)	3.5	−25.2	5.4 (8.1–13.5)	2.8	−35.7	7.0 (10.8–17.8)	7.50 wt %	Huyan et al.[203]
7		MXene/CNTs	4.3	−29.1	2.1 (4.9–7.0)	2.7	−30.6	3.4 (8.4–11.8)	1.9	−23.7	4.9 (12.7–17.6)	30.0 wt %	Cui et al.[204]
8		TCF[c]	3.72	−29.2	2.1 (5.7–7.8)	2.52	−31.2	3.7 (9.1–12.8)	1.92	−44.4	5.4 (12.6–18.0)	4.00 wt %	Hu et al.[219]
9		loofah-like CCM[d]	5.0	−44.8	3.6 (5.4–9.0)	4.0	−63.8	5.0 (6.4–11.4)	2.5	−24.2	7.3 (10.7–18.0)	15.0 wt %	Peng et al.[205]
10		Ti_3CNCl_2/rGO	–	–	–	3.0	−21.4	7.6 (10.4–18.0)	2.5	−62.6	5.6 (12.4–18.0)	0.70 wt %	Wang et al.[232]
11		$Ti_3C_2T_x$@RGO	4.0	−27.5	2.0 (5.1–7.1)	2.5	−27.2	3.6 (8.8–12.4)	2.0	−26.0	5.4 (11.5–16.9)	15.0 wt %	Wang et al.[236]
12	Molybdenum carbide/carbon composites	Mo_2C/C	–	–	–	2.6	−49.2	3.4 (8.0–11.4)	1.85	−24.1	4.3 (12.0–16.3)	20.0 wt %	Dai et al.[259]
13		Mo_2C/C	3.5	−27.1	1.6 (5.1–6.7)	2.5	−42.2	2.5 (7.4–9.7)	1.5	−60.4	4.8 (13.2–18.0)	50.0 wt %	Wang et al.[263]
14		Mo_2C/C	–	–	–	2.9	−16.1	7.0 (11.0–18.0)	2.3	−36.8	4.7 (13.3–18.0)	10.0 wt %	Wang et al.[264]
15		$Mo_{1-x}C$/C	3.8	−14.3	1.5 (5.4–6.9)	2.8	−17.4	2.2 (7.4–9.6)	1.8	−50.6	4.5 (13.5–17.0)	20.0 wt %	Zhao et al.[265]
16	Other carbides/ carbon composites	TiC/graphite	3.8	−26.4	2.0 (6.0–8.0)	2.6	−25.0	3.2 (9.2–12.4)	1.8	−25.2	3.8 (14.2–18.0)	50.0 wt %	Yu et al.[279]
17		C@TiC	4.0	−50.3	2.2 (5.7–7.9)	3.0	−26.9	3.0 (8.1–11.1)	2.0	−19.8	4.1 (13.0–17.1)	30.0 wt %	Yuan et al.[284]
18		WC_{1-x}/C	3.03	−15.0	2.0 (6.0–8.0)	2.13	−20.5	3.2 (8.8–12.0)	1.5	−26.3	4.9 (13.1–18.0)	45.0 wt %	Lian et al.[285]
19		Fe_3C/C	5.0	−19.4	4.4 (5.8–10.2)	3.6	−62.6	6.5 (8.6–15.1)	3.0	−27.2	6.8 (11.0–17.8)	10.0 wt %	Sun et al.[297]
20		Fe_3C/C	3.5	−40.5	2.5 (6.0–8.5)	2.5	−37.1	4.0 (9.0–13.0)	2.0	−37.4	5.6 (11.4–17.0)	10.0 wt %	Zhang et al.[301]
21	Multicomponent carbides/ carbon composites	CSN[e]	3.1	−10.0	0.1 (7.9–8.0)	3.2	−18.4	4.0 (8.0–12.0)	3.2	−51.3	10.1 (7.9–18.0)	0.55 wt %	Cai et al.[173]
22		Ni/MXene/RGO	5.0	−20.2	2.6 (4.7–7.3)	3.5	−22.6	4.3 (7.2–11.5)	2.5	−37.0	7.3 (10.7–18.0)	0.64 wt %	Liang et al.[198]
23		$Fe_{0.64}Ni_{0.36}$/ MXene/CNF	3.5	−28.6	2.7 (6.1–8.9)	2.7	−54.1	5.4 (8.0–13.4)	2.0	−37.6	7.4 (10.6–18.0)	12.5 wt %	Zhang et al.[303]

(*Continued on next page*)

Table 1. *Continued*

Entry	Category	Absorbers	C-band 4-8 GHz d (mm)	C-band 4-8 GHz Min RL (dB)	C-band 4-8 GHz EAB (GHz) (RL < −10 dB)	X-band 8-12 GHz d (mm)	X-band 8-12 GHz Min RL (dB)	X-band 8-12 GHz EAB (GHz) (RL < −10 dB)	Ku-band 12-18 GHz d (mm)	Ku-band 12-18 GHz Min RL (dB)	Ku-band 12-18 GHz EAB (GHz) (RL < −10 dB)	Filler loading	Reference
24		Fe_3O_4@$Ti_3C_2T_x$/CNTs	3.5	−12.1	1.1 (5.8–6.9)	2.8	−16.1	1.9 (8.1–10.0)	2.0	−40.1	5.8 (10.3–16.1)	20.0 wt %	Zhang et al.[314]
25		CoMo@HNCP[f]	4.0	−18.1	2.3 (5.5–7.8)	2.5	−44.8	5.2 (9.1–14.3)	2.0	−22.2	6.9 (11.1–18.0)	30.0 wt %	Huang et al.[327]
26		Mo_2C/SiC/C	4.5	−62.5	3.6 (6.1–9.7)	3.5	−34.3	5.0 (8.0–13.0)	2.75	−24.7	6.8 (11.2–18.0)	15.0 wt %	Yuan et al.[354]
27		Fe_3Si/Fe/CNTs/SiOCN	3.43	−65.3	1.3 (5.0–6.3)	2.00	−20.4	2.4 (9.0–11.4)	1.35	−53.0	4.3 (13.7–18.0)	60.0 wt %	Yu et al.[130]

[a]SiC@C nanowire foams with a density of 108 mg/cm^3.
[b]PDA derived carbon nanoparticles@MXene composites.
[c]$Ti_3C_2T_x$/carbon nanotubes (CNTs) foam.
[d]carbonized cellulose nanofiber/MXene membrane.
[e]Carbon microtube@SiC nanowire/Ni nanoparticle aerogel.
[f]MoC_2/Co embedded hybrid hollow N-doped carbon polyhedron.

they usually require less filler loading in resin, and thus they may be a good choice for lightweight EWAMs. It is undoubted that excellent electrical conductivity of MXene nanosheets can provide strong conductive loss capability and compensate for the negative effect caused by the decrease in filler loading. Compared with SiC and MXene, Mo_2C nanoparticles seem incapable of generating comparable effect in binary composites, and Mo_2C/C composites even cannot harvest EAB over 6.0 GHz unless the microstructure effect is fully utilized (Entry 14). Other binary composites with some uncommon candidates only produce moderate EM absorption performance and have not showed any possible trends in performance breakthrough yet (Entry 16–20). Very interestingly, ternary composites display obvious enhancements in EM absorption, and many of them can promise both strong RL intensity and broad EAB, and even realize extremely low filler loading (Entry 21 and 22). This is because most ternary composites are created based on elaborate design, and thus the multiple synergies can be developed very well and lead to powerful attenuation capability toward incident EM wave. However, carbides/carbon composites with two or more additives fail to present continuous reinforcement in EM absorption as expected, which may be attributed to the difficulty in the rational arrangement and regulation of multiple components.

CHALLENGES AND PERSPECTIVES

As we introduced in the main text, carbides/carbon composites have made obvious progress in the past decade, while the improvements on EM absorption are still far behind the requirements for practical application. Most composites usually have some advantages in one or two aspects, and few of them can afford all features of small absorber thickness, low density, broad response frequency, and strong absorption. Such a context indicates that there remain some challenges related to the composition and microstructure design on carbides/carbon composites. First, the composition optimization of carbides/carbon composites is highly dependent on the feedback of testing results, while this process is not only time-consuming, but also leads to some deviations from the optimum composition due to human and instrument errors. Second, the EM characteristics of carbides/carbon composites are the results from the linkage effect of composition and microstructure, but to date, there is no an available method to distinguish the contribution of each factor quantitatively, which hinders the design of high-performance EWAMs to some extent. Third, one of the potential advantages in carbides/carbon composites is their excellent environmental tolerance, while most current composites pay more attention to their EM absorption performance and do not fully develop their respective characteristics. Carbon materials have good dielectric loss capability, but they will be burned off at high temperature in the presence of oxygen, and in contrast, carbides are generally famous for their good stability under high-temperature conditions, but their dielectric loss capability are relatively weak. Therefore, a composite that have both good heat stability and dielectric loss capability is highly desirable. Fourth, the microstructure design of the reported carbides/carbon composites is mostly carried out in micro-/nano-scale. Although various unique microstructures can enhance the energy attenuation of incident EM wave to some extent, their effect is much less than that from macroscopic 3D structural metasurface design, which may bring ultra-broadband EAB covering 3.7–40.0 GHz.

In an effort to obtain excellent carbides/carbon composites for EM absorption, some specific perspectives are further proposed at the end of this review. First, some databases related to EM characteristics and machine learning method to assist composition optimization are urgently required for the fabrication of high-performance carbides/carbon composites. With the help of artificial intelligence, the design of EWAMs for different application scenarios will be simpler and more time-saving, and we can also understand EM absorption mechanisms more clearly. Second, a desirable configuration that can simultaneously exert the advantages of carbides and carbon materials should be developed for carbides/carbon composites. Possibly, a core-shell configuration with carbon cores and carbides shells may be useful, because carbon materials as the cores can provide effective dielectric loss and the dense shells composed of carbides are helpful to protect carbon cores at high temperature. It is unfortunate that such a kind of composites are rarely reported to date. At last, microstructure design and macroscopic metasurface design are encouraged to be integrated, because the synergy among the structural effects from different scales will be greatly helpful to realize ultra-broad frequency EM response.

ACKNOWLEDGMENTS

This work is financially supported by National Natural Science Foundation of China (21776053).

DECLARATION OF INTERESTS

The authors declare no competing interests.

REFERENCES

1. Shahzad, F., Alhabeb, M., Hatter, C.B., Anasori, B., Man Hong, S., Koo, C.M., and Gogotsi, Y. (2016). Electromagnetic interference shielding with 2D transition metal carbides (MXenes). Science *353*, 1137–1140. https://doi.org/10.1126/science.aag2421.
2. Liu, L., Deng, H., Tang, X., Lu, Y., Zhou, J., Wang, X., Zhao, Y., Huang, B., and Shi, Y. (2021). Specific electromagnetic radiation in the wireless signal range increases wakefulness in mice. Proc. Natl. Acad. Sci. USA *118*, e2105838118. https://doi.org/10.1073/pnas.2105838118.
3. Cao, M.S., Wang, X.X., Zhang, M., Cao, W.Q., Fang, X.Y., and Yuan, J. (2020). Variable-temperature electron transport and dipole polarization turning flexible multifunctional microsensor beyond electrical and optical energy. Adv. Mater. *32*, 1907156. https://doi.org/10.1002/adma.201907156.
4. Lv, H., Yang, Z., Pan, H., and Wu, R. (2022). Electromagnetic absorption materials: Current progress and new frontiers. Prog. Mater. Sci. *127*, 100946. https://doi.org/10.1016/j.pmatsci.2022.100946.
5. Wu, Z., Cheng, H.W., Jin, C., Yang, B., Xu, C., Pei, K., Zhang, H., Yang, Z., and Che, R. (2022). Dimensional Design and Core-Shell Engineering of Nanomaterials for Electromagnetic Wave Absorption. Adv. Mater. *34*, 2107538. https://doi.org/10.1002/adma.202107538.
6. Zhang, C., Shi, Y., Li, X., Wu, H., Shen, Y., Guo, W., Tian, K., and Wang, H. (2022).

Architecture inspired structure engineering toward carbon nanotube hybrid for microwave absorption promotion. iScience *25*, 105203. https://doi.org/10.1016/j.isci.2022.105203.

7. Chang, Q., Liang, H., Shi, B., and Wu, H. (2022). Microstructure induced dielectric loss in lightweight Fe_3O_4 foam for electromagnetic wave absorption. iScience *25*, 103925. https://doi.org/10.1016/j.isci.2022.103925.
8. Qin, F., and Brosseau, C. (2012). A review and analysis of microwave absorption in polymer composites filled with carbonaceous particles. J. Appl. Phys. *111*, 061301. https://doi.org/10.1063/1.3688435.
9. Micheli, D., Vricella, A., Pastore, R., and Marchetti, M. (2014). Synthesis and electromagnetic characterization of frequency selective radar absorbing materials using carbon nanopowders. Carbon *77*, 756–774. https://doi.org/10.1016/j.carbon.2014.05.080.
10. Green, M., and Chen, X. (2019). Recent progress of nanomaterials for microwave absorption. J. Materiomics *5*, 503–541. https://doi.org/10.1016/j.jmat.2019.07.003.
11. Gai, L., Zhao, H., Wang, F., Wang, P., Liu, Y., Han, X., and Du, Y. (2022). Advances in core-shell engineering of carbon-based composites for electromagnetic wave absorption. Nano Res. *15*, 9410–9439. https://doi.org/10.1007/s12274-022-4695-6.
12. Kong, L.B., Li, Z.W., Liu, L., Huang, R., Abshinova, M., Yang, Z.H., Tang, C.B., Tan, P.K., Deng, C.R., and Matitsine, S. (2013). Recent progress in some composite materials and structures for specific electromagnetic applications. Int. Mater. Rev. *58*, 203–259. https://doi.org/10.1179/1743280412y.0000000011.
13. Duan, W., Li, X., Wang, Y., Qiang, R., Tian, C., Wang, N., Han, X., and Du, Y. (2018). Surface functionalization of carbonyl iron with aluminum phosphate coating toward enhanced anti-oxidative ability and microwave absorption properties. Appl. Surf. Sci. *427*, 594–602. https://doi.org/10.1016/j.apsusc.2017.08.034.
14. Guo, Y., Zhang, X., Feng, X., Jian, X., Zhang, L., and Deng, L. (2018). Non-isothermal oxidation kinetics of FeSiAl alloy powder for microwave absorption at high temperature. Composites, Part B *155*, 282–287. https://doi.org/10.1016/j.compositesb.2018.08.112.
15. Qing, Y., Zhou, W., Luo, F., and Zhu, D. (2009). Microwave-absorbing and mechanical properties of carbonyl-iron/epoxy-silicone resin coatings. J. Magn. Magn Mater. *321*, 25–28. https://doi.org/10.1016/j.jmmm.2008.07.011.
16. Wang, H., Li, M., and Li, X. (2016). Influence of external magnetic field on the microwave absorption properties of carbonyl iron and polychloroprene composites film. AIP Adv. *6*, 125030. https://doi.org/10.1063/1.4972239.
17. Halilov, S.V., Eschrig, H., Perlov, A.Y., and Oppeneer, P.M. (1998). Adiabatic spin dynamics from spin-density-functional theory: Application to Fe, Co, and Ni. Phys. Rev. B *58*, 293–302. https://doi.org/10.1103/PhysRevB.58.293.
18. Jiang, X., Wan, W., Wang, B., Zhang, L., Yin, L., Van Bui, H., Xie, J., Zhang, L., Lu, H., and Deng, L. (2022). Enhanced anti-corrosion and microwave absorption performance with carbonyl iron modified by organic fluorinated chemicals. Appl. Surf. Sci. *572*, 151320. https://doi.org/10.1016/j.apsusc.2021.151320.
19. Jia, T., Qi, X., Wang, L., Yang, J.L., Gong, X., Chen, Y., Qu, Y., Peng, Q., and Zhong, W. (2023). Constructing mixed-dimensional lightweight flexible carbon foam/carbon nanotubes-based heterostructures: An effective strategy to achieve tunable and boosted microwave absorption. Carbon *206*, 364–374. https://doi.org/10.1016/j.carbon.2023.02.046.
20. Qiang, R., Du, Y., Wang, Y., Wang, N., Tian, C., Ma, J., Xu, P., and Han, X. (2016). Rational design of yolk-shell C@C microspheres for the effective enhancement in microwave absorption. Carbon *98*, 599–606. https://doi.org/10.1016/j.carbon.2015.11.054.
21. Liang, Q., Wang, L., Qi, X., Peng, Q., Gong, X., Chen, Y., Xie, R., and Zhong, W. (2023). Hierarchical engineering of CoNi@Air@C/SiO_2@Polypyrrole multicomponent nanocubes to improve the dielectric loss capability and magnetic-dielectric synergy. J. Mater. Sci. Technol. *147*, 37–46. https://doi.org/10.1016/j.jmst.2022.10.069.
22. Chandrasekhar, P., and Naishadham, K. (1999). Broadband microwave absorption and shielding properties of a poly(aniline). Synth. Met. *105*, 115–120. https://doi.org/10.1016/s0379-6779(99)00085-5.
23. Xia, T., Zhang, C., Oyler, N.A., and Chen, X. (2013). Hydrogenated TiO_2 nanocrystals: a novel microwave absorbing material. Adv. Mater. *25*, 6905–6910. https://doi.org/10.1002/adma.201303088.
24. Yang, J., Zhang, J., Liang, C., Wang, M., Zhao, P., Liu, M., Liu, J., and Che, R. (2013). Ultrathin $BaTiO_3$ nanowires with high aspect ratio: a simple one-step hydrothermal synthesis and their strong microwave absorption. ACS Appl. Mater. Interfaces *5*, 7146–7151. https://doi.org/10.1021/am4014506.
25. Xiao, J., Qi, X., Gong, X., Peng, Q., Chen, Y., Xie, R., and Zhong, W. (2022). Defect and interface engineering in core@shell structure hollow carbon@MoS_2 nanocomposites for boosted microwave absorption performance. Nano Res. *15*, 7778–7787. https://doi.org/10.1007/s12274-022-4625-7.
26. Xiao, J., Qi, X., Gong, X., Peng, Q., Chen, Y., Xie, R., and Zhong, W. (2023). Tunable and improved microwave absorption of flower-like core@shell MFe_2O_4@MoS_2 (M = Mn, Ni and Zn) nanocomposites by defect and interface engineering. J. Mater. Sci. Technol. *139*, 137–146. https://doi.org/10.1016/j.jmst.2022.08.022.
27. Cao, M.S., Cai, Y.Z., He, P., Shu, J.C., Cao, W.Q., and Yuan, J. (2019). 2D MXenes: Electromagnetic property for microwave absorption and electromagnetic interference shielding. Chem. Eng. J. *359*, 1265–1302. https://doi.org/10.1016/j.cej.2018.11.051.
28. Chiu, S.C., Yu, H.C., and Li, Y.Y. (2010). High electromagnetic wave absorption performance of silicon carbide nanowires in the gigahertz range. J. Phys. Chem. C *114*, 1947–1952. https://doi.org/10.1021/jp905127t.
29. Zhang, Y., Huang, Y., Zhang, T., Chang, H., Xiao, P., Chen, H., Huang, Z., and Chen, Y. (2015). Broadband and Tunable High-Performance Microwave Absorption of an Ultralight and Highly Compressible Graphene Foam. Adv. Mater. *27*, 2049–2053. https://doi.org/10.1002/adma.201405788.
30. Wu, N., Hu, Q., Wei, R., Mai, X., Naik, N., Pan, D., Guo, Z., and Shi, Z. (2021). Review on the electromagnetic interference shielding properties of carbon based materials and their novel composites: Recent progress, challenges and prospects. Carbon *176*, 88–105. https://doi.org/10.1016/j.carbon.2021.01.124.
31. Wang, F., Cui, L., Zhao, H., Han, X., and Du, Y. (2021). High-efficient electromagnetic absorption and composites of carbon microspheres. J. Appl. Phys. *130*, 230902. https://doi.org/10.1063/5.0068122.
32. Zimmerle, B., Wu, M., Liu, J., and Chen, X. (2023). The microwave absorption performance of candle soots. Carbon *212*, 118124. https://doi.org/10.1016/j.carbon.2023.118124.
33. Zhao, H., Xu, X., Fan, D., Xu, P., Wang, F., Cui, L., Han, X., and Du, Y. (2021). Anchoring porous carbon nanoparticles on carbon nanotubes as a high-performance composite with a unique core-sheath structure for electromagnetic pollution precaution. J. Mater. Chem. A *9*, 22489–22500. https://doi.org/10.1039/d1ta06147j.
34. Green, M., Tran, A.T.V., and Chen, X. (2020). Maximizing the microwave absorption performance of polypyrrole by data-driven discovery. Compos. Sci. Technol. *199*, 108332. https://doi.org/10.1016/j.compscitech.2020.108332.
35. Green, M., Tran, A.T., and Chen, X. (2020). Obtaining strong, broadband microwave absorption of polyaniline through data-driven materials discovery. Adv. Mater. Interfac. *7*, 2000658. https://doi.org/10.1002/admi.202000658.
36. Qiang, R., Du, Y., Zhao, H., Wang, Y., Tian, C., Li, Z., Han, X., and Xu, P. (2015). Metal organic framework-derived Fe/C nanocubes toward efficient microwave absorption. J. Mater. Chem. A *3*, 13426–13434. https://doi.org/10.1039/c5ta01457c.
37. Shi, B., Liang, H., Xie, Z., Chang, Q., and Wu, H. (2023). Dielectric loss enhancement induced by the microstructure of $CoFe_2O_4$ foam to realize broadband electromagnetic wave absorption. Int. J. Miner. Metall. Mater. *30*, 1388–1397. https://doi.org/10.1007/s12613-023-2599-4.
38. Cui, L., Han, X., Wang, F., Zhao, H., and Du, Y. (2021). A review on recent advances in carbon-based dielectric system for microwave absorption. J. Mater. Sci. *56*, 10782–10811. https://doi.org/10.1007/s10853-021-05941-y.
39. Li, C., Qi, X., Gong, X., Peng, Q., Chen, Y., Xie, R., and Zhong, W. (2022). Magnetic-dielectric synergy and interfacial engineering to design yolk–shell structured CoNi@void@C and CoNi@void@C@MoS_2 nanocomposites with tunable and strong wideband microwave absorption. Nano Res. *15*, 6761–6771. https://doi.org/10.1007/s12274-022-4468-2.
40. Cui, L., Tian, C., Tang, L., Han, X., Wang, Y., Liu, D., Xu, P., Li, C., and Du, Y. (2019). Space-confined synthesis of core-shell $BaTiO_3$@carbon microspheres as a high-performance binary dielectric system for microwave absorption. ACS Appl. Mater. Interfaces *11*, 31182–31190. https://doi.org/10.1021/acsami.9b09779.
41. Zhang, F., Jia, Z., Wang, Z., Zhang, C., Wang, B., Xu, B., Liu, X., and Wu, G. (2021). Tailoring nanoparticles composites derived

from metal-organic framework as electromagnetic wave absorber. Mater. Today Phys. *20*, 100475. https://doi.org/10.1016/j.mtphys.2021.100475.

42. Wang, P., Gai, L., Hu, B., Liu, Y., Wang, F., Xu, P., Han, X., and Du, Y. (2023). Topological MOFs deformation for the direct preparation of electromagnetic functionalized Ni/C aerogels with good hydrophobicity and thermal insulation. Carbon *212*, 118132. https://doi.org/10.1016/j.carbon.2023.118132.
43. Chen, J.G. (1996). Carbide and nitride overlayers on early transition metal surfaces: Preparation, characterization, and reactivities. Chem. Rev. *96*, 1477–1498. https://doi.org/10.1021/cr950232u.
44. Ordine, A., Achete, C.A., Mattos, O.R., Margarit, I.C.P., Camargo, S.S., and Hirsch, T. (2000). Magnetron sputtered SiC coatings as corrosion protection barriers for steels. Surf. Coat. Technol. *133–134*, 583–588. https://doi.org/10.1016/s0257-8972(00)00976-2.
45. Izawa, M., Koseki, T., Kamiya, Y., and Toyomasu, T. (1995). Characteristics of a SiC microwave absorber for a damped cavity. Rev. Sci. Instrum. *66*, 1910–1912. https://doi.org/10.1063/1.1145821.
46. Ishikawa, T., Ichikawa, H., Hayase, T., Nagata, Y., and Imai, Y. Electromagnetic wave absorber with silicon carbide fibre layer pref. on metal plate and opt. laminated with resin or ceramic. patent DE3311001-A; GB2117569-A; FR2524719-A; JP58169997-A; SE8301747-A; US4507354-A; GB2117569-B; CA1203873-A; SE455451-B; IT1163181-B; JP91035840-B; DE3311001-C2, patent application DE3311001-A DE3311001 25 Mar 1983 GB2117569-A GB008111 24 Mar 1983 US4507354-A US477249 21 Mar 1983 JP91035840-B JP051034 31 Mar 1982 DE3311001-C2 DE3311001 25 Mar 1983, DE3311001-A 06 Oct 1983 H01Q-017/00 198341 Pages: 14 German GB2117569-A 12 Oct 1983 H01Q-017/00 198341 English FR2524719-A 07 Oct 1983 H01Q-017/00 198345 French JP58169997-A 06 Oct 1983 198346 Japanese SE8301747-A 31 Oct 1983 H01Q-017/00 198346 Swedish US4507354-A 26 Mar 1985 B32B-007/00 198515 English CA1203873-A 29 Apr 1986 H01Q-017/00 198622 English IT1163181-B 08 Apr 1987 H01Q-000/00 198925 Italian JP91035840-B 29 May 1991 199125 Japanese DE3311001-C2 07 Jul 1994 H01Q-017/00 199425 Pages: 6 German.
47. Gao, H., Luo, F., Deng, H., Nan, H., and Qing, Y. (2019). Fabrication of SiC_f/SiC-mullite composite with improved pretreatment condition via precursor infiltration-sintering combined with infiltration-pyrolysis process. Ceram. Int. *45*, 16062–16069. https://doi.org/10.1016/j.ceramint.2019.05.122.
48. Lan, X., Liang, C., Wu, M., Wu, N., He, L., Li, Y., and Wang, Z. (2018). Facile synthesis of highly defected silicon carbide sheets for efficient absorption of electromagnetic waves. J. Phys. Chem. C *122*, 18537–18544. https://doi.org/10.1021/acs.jpcc.8b05339.
49. Chen, J., Li, X., Feng, M., Luo, K., Yang, J., and Zhang, B. (2017). Improved microwave absorption performance of modified SiC in the 2-18 GHz frequency range. CrystEngComm *409*, 519–528. https://doi.org/10.1039/c6ce02285e.
50. Green, M., Liu, Z., Smedley, R., Nawaz, H., Li, X., Huang, F., and Chen, X. (2018). Graphitic carbon nitride nanosheets for microwave absorption. Mater. Today Phys. *5*, 78–86. https://doi.org/10.1016/j.mtphys.2018.06.005.
51. Jian, X., Tian, W., Li, J., Deng, L., Zhou, Z., Zhang, L., Lu, H., Yin, L., and Mahmood, N. (2019). High-temperature oxidation-resistant $ZrN_{0.4}B_{0.6}$/SiC nanohybrid for enhanced microwave absorption. ACS Appl. Mater. Interfaces *11*, 15869–15880. https://doi.org/10.1021/acsami.8b22448.
52. Hou, Y., Cheng, L., Zhang, Y., Du, X., Zhao, Y., and Yang, Z. (2021). High temperature electromagnetic interference shielding of lightweight and flexible ZrC/SiC nanofiber mats. Chem. Eng. J. *404*, 126521. https://doi.org/10.1016/j.cej.2020.126521.
53. Long, X., Shao, C., and Wang, J. (2019). Continuous SiCN fibers with interfacial SiC_xN_y phase as structural materials for electromagnetic absorbing applications. ACS Appl. Mater. Interfaces *11*, 22885–22894. https://doi.org/10.1021/acsami.9b06819.
54. Wu, Q., Shui, W.J., and Wang, G.S. (2017). The enhanced wave absorbing properties of SiC/PVDF composites affected by the SiC sizes. Sci. Adv. Mater. *9*, 1401–1407. https://doi.org/10.1166/sam.2017.3109.
55. Xiao, T., Kuang, J., Pu, H., Zheng, Q., Lu, Y., Liu, W., and Cao, W. (2021). Hollow SiC microtube with multiple attenuation mechanisms for broadband electromagnetic wave absorption. J. Alloys Compd. *862*, 158032. https://doi.org/10.1016/j.jallcom.2020.158032.
56. Yang, H.J., Yuan, J., Li, Y., Hou, Z.L., Jin, H.B., Fang, X.Y., and Cao, M.S. (2013). Silicon carbide powders: Temperature-dependent dielectric properties and enhanced microwave absorption at gigahertz range. Solid State Commun. *163*, 1–6. https://doi.org/10.1016/j.ssc.2013.03.004.
57. Iqbal, A., Shahzad, F., Hantanasirisakul, K., Kim, M.K., Kwon, J., Hong, J., Kim, H., Kim, D., Gogotsi, Y., and Koo, C.M. (2020). Anomalous absorption of electromagnetic waves by 2D transition metal carbonitride Ti_3CNT_x (MXene). Science *369*, 446–450. https://doi.org/10.1126/science.aba7977.
58. Liu, J., Wei, X., Gao, L., Tao, J., Xu, L., Peng, G., Jin, H., Wang, Y., Yao, Z., and Zhou, J. (2023). An overview of C-SiC microwave absorption composites serving in harsh environments. J. Eur. Ceram. Soc. *43*, 1237–1254. https://doi.org/10.1016/j.jeurceramsoc.2022.11.040.
59. Xiang, Z., Wang, X., Zhang, X., Shi, Y., Cai, L., Zhu, X., Dong, Y., and Lu, W. (2022). Self-assembly of nano/microstructured 2D Ti_3CNT_x MXene-based composites for electromagnetic pollution elimination and Joule energy conversion application. Carbon *189*, 305–318. https://doi.org/10.1016/j.carbon.2021.12.075.
60. Wang, J., Zheng, Y., Wang, Y., Zhang, C., Jiang, Y., Suo, C., Cui, M., Zhang, T., Chen, X., and Xu, K. (2023). Reduced graphene oxide aerogel decorated with Mo_2C nanoparticles toward multifunctional properties of hydrophobicity, thermal insulation and microwave absorption. J. Transl. Med. *21*, 536–547. https://doi.org/10.1007/s12613-022-2570-9.
61. Tokumitsu, K. (1997). Synthesis of metastable Fe_3C, Co_3C and Ni_3C by mechanical alloying method. Mater. Sci. Forum *235–238*, 127–132. https://doi.org/10.4028/www.scientific.net/MSF.235-238.127.
62. Liu, D., Qiang, R., Du, Y., Wang, Y., Tian, C., and Han, X. (2018). Prussian blue analogues derived magnetic FeCo alloy/carbon composites with tunable chemical composition and enhanced microwave absorption. J. Colloid Interface Sci. *514*, 10–20. https://doi.org/10.1016/j.jcis.2017.12.013.
63. Wen, B., Cao, M.S., Hou, Z.L., Song, W.L., Zhang, L., Lu, M.M., Jin, H.B., Fang, X.Y., Wang, W.Z., and Yuan, J. (2013). Temperature dependent microwave attenuation behavior for carbon-nanotube/silica composites. Carbon *65*, 124–139. https://doi.org/10.1016/j.carbon.2013.07.110.
64. Green, M., Liu, Z., Xiang, P., Liu, Y., Zhou, M., Tan, X., Huang, F., Liu, L., and Chen, X. (2018). Doped, conductive SiO_2 nanoparticles for large microwave absorption. Light Sci. Appl. *7*, 87. https://doi.org/10.1038/s41377-018-0088-8.
65. Qin, M., Zhang, L., and Wu, H. (2022). Dielectric loss mechanism in electromagnetic wave absorbing materials. Adv. Sci. *9*, 2105553. https://doi.org/10.1002/advs.202105553.
66. Zhao, H., Xu, X., Wang, Y., Fan, D., Liu, D., Lin, K., Xu, P., Han, X., and Du, Y. (2020). Heterogeneous interface induced the formation of hierarchically hollow carbon microcubes against electromagnetic pollution. Small *16*, 2003407. https://doi.org/10.1002/smll.202003407.
67. Quan, B., Gu, W., Sheng, J., Lv, X., Mao, Y., Liu, L., Huang, X., Tian, Z., and Ji, G. (2021). From intrinsic dielectric loss to geometry patterns: Dual-principles strategy for ultrabroad band microwave absorption. Nano Res. *14*, 1495–1501. https://doi.org/10.1007/s12274-020-3208-8.
68. Green, M., Thi Van Tran, A., and Chen, X. (2020). Realizing maximum microwave absorption of poly(3,4-ethylenedioxythiophene) with a data-driven method. ACS Appl. Electron. Mater. *2*, 2937–2944. https://doi.org/10.1021/acsaelm.0c00573.
69. Liu, X., Zhang, Z., Wu, Y., and Wang, J. (2011). Absorption properties of carbon black/silicon carbide microwave absorbers. Composites, Part B *42*, 326–329. https://doi.org/10.1016/j.compositesb.2010.11.009.
70. Zhou, W., Long, L., Xiao, P., Li, Y., Luo, H., Hu, W.D., and Yin, R.M. (2017). Silicon carbide nano-fibers in-situ grown on carbon fibers for enhanced microwave absorption properties. Ceram. Int. *43*, 5628–5634. https://doi.org/10.1016/j.ceramint.2017.01.095.
71. Wang, C., Han, X., Xu, P., Zhang, X., Du, Y., Hu, S., Wang, J., and Wang, X. (2011). The electromagnetic property of chemically reduced graphene oxide and its application as microwave absorbing material. Appl. Phys. Lett. *98*, 072906. https://doi.org/10.1063/1.3555436.
72. Wang, L., Yu, X., Li, X., Zhang, J., Wang, M., and Che, R. (2020). MOF-derived yolk-shell Ni@C@ZnO Schottky contact structure for enhanced microwave absorption. Chem. Eng. J. *383*, 123099. https://doi.org/10.1016/j.cej.2019.123099.
73. Sha, L., Gao, P., Wu, T., and Chen, Y. (2017). Chemical Ni-C bonding in Ni-carbon nanotube composite by a microwave welding method and its. induced

high-frequency radar frequency electromagnetic wave absorption. ACS Appl. Mater. Interfaces *9*, 40412–40419. https://doi.org/10.1021/acsami.7b07136.
74. Kittel, C. (2018). Introduction to Solid State Physics, 8th Edition (John Wiley and Sons).
75. Ohlan, A., Singh, K., Chandra, A., and Dhawan, S.K. (2010). Microwave absorption behavior of core-shell structured poly (3,4-ethylenedioxy thiophene)-barium ferrite nanocomposites. ACS Appl. Mater. Interfaces *2*, 927–933. https://doi.org/10.1021/am900893d.
76. Kuriakose, M., Longuemart, S., Depriester, M., Delenclos, S., and Sahraoui, A.H. (2014). Maxwell-Wagner-Sillars effects on the thermal-transport properties of polymer-dispersed liquid crystals. Phys. Rev. E *89*, 022511. https://doi.org/10.1103/PhysRevE.89.022511.
77. Quan, B., Liang, X., Ji, G., Cheng, Y., Liu, W., Ma, J., Zhang, Y., Li, D., and Xu, G. (2017). Dielectric polarization in electromagnetic wave absorption: Review and perspective. J. Alloys Compd. *728*, 1065–1075. https://doi.org/10.1016/j.jallcom.2017.09.082.
78. Wang, Y., Du, Y., Qiang, R., Tian, C., Xu, P., and Han, X. (2016). Interfacially engineered sandwich-like rGO/carbon microspheres/rGO composite as an efficient and durable microwave absorber. Adv. Mater. Interfac. *3*, 1500684. https://doi.org/10.1002/admi.201500684.
79. Wang, Y., Du, Y., Guo, D., Qiang, R., Tian, C., Xu, P., and Han, X. (2017). Precursor-directed synthesis of porous cobalt assemblies with tunable close-packed hexagonal and face-centered cubic phases for the effective enhancement in microwave absorption. J. Mater. Sci. *52*, 4399–4411. https://doi.org/10.1007/s10853-016-0687-9.
80. Quan, B., Shi, W., Ong, S.J.H., Lu, X., Wang, P.L., Ji, G., Guo, Y., Zheng, L., and Xu, Z.J. (2019). Defect engineering in two common types of dielectric materials for electromagnetic absorption applications. Adv. Funct. Mater. *29*, 1901236. https://doi.org/10.1002/adfm.201901236.
81. Zhao, B., Du, Y., Yan, Z., Rao, L., Chen, G., Yuan, M., Yang, L., Zhang, J., and Che, R. (2023). Structural defects in phase-regulated high-entropy oxides toward superior microwave absorption properties. Adv. Funct. Mater. *33*. https://doi.org/10.1002/adfm.202209924.
82. Wang, F., Gu, W., Chen, J., Wu, Y., Zhou, M., Tang, S., Cao, X., Zhang, P., and Ji, G. (2022). The point defect and electronic structure of K doped $LaCo_{0.9}Fe_{0.1}O_3$ perovskite with enhanced microwave absorbing ability. Nano Res. *15*, 3720–3728. https://doi.org/10.1007/s12274-021-3955-1.
83. Lv, H., Zhou, X., Wu, G., Kara, U.I., and Wang, X. (2021). Engineering defects in 2D g-C_3N_4 for wideband, efficient electromagnetic absorption at elevated temperature. J. Mater. Chem. A *9*, 19710–19718. https://doi.org/10.1039/d1ta02785a.
84. Hou, L.J., Xie, M.Y., Ye, W., Zhao, G.J., Yan, L., Zhang, C., Huang, G., Yang, F., and Li, Y. (2021). Intrinsic defect-rich porous carbon nanosheets synthesized from potassium citrate toward advanced supercapacitors and microwave absorption. Carbon *328*, 176–186. https://doi.org/10.1016/j.carbon.2021.06.072.
85. Qin, M., Zhang, L., Zhao, X., and Wu, H. (2021). Defect induced polarization loss in multi-shelled spinel hollow spheres for electromagnetic wave absorption application. Adv. Sci. *8*, 2004640. https://doi.org/10.1002/advs.202004640.
86. Xu, Z., Du, Y., Liu, D., Wang, Y., Ma, W., Wang, Y., Xu, P., and Han, X. (2019). Pea-like Fe/Fe_3C nanoparticles embedded in nitrogen-doped carbon nanotubes with tunable dielectric/magnetic loss and efficient electromagnetic absorption. ACS Appl. Mater. Interfaces *11*, 4268–4277. https://doi.org/10.1021/acsami.8b19201.
87. Su, H., Zhang, K.X., Zhang, B., Wang, H.H., Yu, Q.Y., Li, X.H., Antonietti, M., and Chen, J.S. (2017). Activating cobalt nanoparticles via the Mott-Schottky effect in nitrogen-rich carbon shells for base-free aerobic oxidation of alcohols to esters. J. Am. Chem. Soc. *139*, 811–818. https://doi.org/10.1021/jacs.6b10710.
88. Peng, L., Su, L., Yu, X., Wang, R., Cui, X., Tian, H., Cao, S., Xia, B.Y., and Shi, J. (2022). Electron redistribution of ruthenium-tungsten oxides Mott-Schottky heterojunction for enhanced hydrogen evolution. Appl. Catal., B *308*, 121229. https://doi.org/10.1016/j.apcatb.2022.121229.
89. Wang, B., Huang, F., Wu, H., Xu, Z., Wang, S., Han, Q., Liu, F., Li, S., and Zhang, H. (2022). Enhanced interfacial polarization of defective porous carbon confined CoP nanoparticles forming Mott-Schottky heterojunction for efficient electromagnetic wave absorption. Nano Res. *16*, 4160–4169. https://doi.org/10.1007/s12274-022-4779-3.
90. Li, T., Xia, L., Yang, H., Wang, X., Zhang, T., Huang, X., Xiong, L., Qin, C., and Wen, G. (2021). Construction of a Cu-Sn heterojunction interface derived from a schottky junction in Cu@Sn/rGO composites as a highly efficient dielectric microwave absorber. ACS Appl. Mater. Interfaces *13*, 11911–11919. https://doi.org/10.1021/acsami.0c22049.
91. Liu, J., Jia, Z., Dong, Y., Li, J., Cao, X., and Wu, G. (2022). Structural engineering and compositional manipulation for high-efficiency electromagnetic microwave absorption. Mater. Today Phys. *27*, 100801. https://doi.org/10.1016/j.mtphys.2022.100801.
92. Wu, R., Zhou, K., Yue, C.Y., Wei, J., and Pan, Y. (2015). Recent progress in synthesis, properties and potential applications of SiC nanomaterials. Prog. Mater. Sci. *72*, 1–60. https://doi.org/10.1016/j.pmatsci.2015.01.003.
93. Anasori, B., Shi, C., Moon, E.J., Xie, Y., Voigt, C.A., Kent, P.R.C., May, S.J., Billinge, S.J.L., Barsoum, M.W., and Gogotsi, Y. (2016). Control of electronic properties of 2D carbides (MXenes) by manipulating their transition metal layers. Nanoscale Horiz. *1*, 227–234. https://doi.org/10.1039/c5nh00125k.
94. Dong, J., Shi, Y., Huang, C., Wu, Q., Zeng, T., and Yao, W. (2019). A New and stable Mo-Mo_2C modified g-C_3N_4 photocatalyst for efficient visible light photocatalytic H_2 production. Appl. Catal., B *243*, 27–35. https://doi.org/10.1016/j.apcatb.2018.10.016.
95. He, N., Liu, M., Qi, J., Tong, J., Sao, W., Yang, X., Shi, L., and Tong, G. (2019). Plasmon resonance strategy to enhance permittivity and microwave absorbing performance of Cu/C core-shell nanowires. Chem. Eng. J. *378*, 122160. https://doi.org/10.1016/j.cej.2019.122160.
96. Han, N., Liu, K., Zhang, X., Wang, M., Du, P., Huang, Z., Zhou, D., Zhang, Q., Gao, T., Jia, Y., et al. (2019). Highly efficient and stable solar-powered desalination by tungsten carbide nanoarray film with sandwich wettability. Sci. Bull. *64*, 391–399. https://doi.org/10.1016/j.scib.2019.03.008.
97. Sun, B., Han, Y., Li, S., Xu, P., Han, X., Nafady, A., Ma, S., and Du, Y. (2021). Cotton cloth supported tungsten carbide/carbon nanocomposites as a Janus film for solar driven interfacial water evaporation. J. Mater. Chem. A *9*, 23140–23148. https://doi.org/10.1039/d1ta06707a.
98. Goodenough, J.B. (2002). Summary of losses in magnetic materials. IEEE Trans. Magn. *38*, 3398–3408. https://doi.org/10.1109/tmag.2002.802741.
99. Kovalčíková, A., Sedláček, J., Lenčéš, Z., Bystrický, R., Dusza, J., and Šajgalík, P. (2016). Oxidation resistance of SiC ceramics prepared by different proceessing routes. J. Eur. Ceram. Soc. *36*, 3783–3793. https://doi.org/10.1016/j.jeurceramsoc.2016.03.016.
100. Zhang, W. (2022). Tribology of SiC ceramics under lubrication: Features, developments, and perspectives. Curr. Opin. Solid State Mater. Sci. *26*, 101000. https://doi.org/10.1016/j.cossms.2022.101000.
101. Kim, Y.W., Kultayeva, S., Sedláček, J., Hanzel, O., Tatarko, P., Lenčéš, Z., and Šajgalík, P. (2020). Thermal and electrical properties of additive-free rapidly hot-pressed SiC ceramics. J. Eur. Ceram. Soc. *40*, 234–240. https://doi.org/10.1016/j.jeurceramsoc.2019.10.015.
102. Baitalik, S., and Kayal, N. (2019). Thermal shock and chemical corrosion resistance of oxide bonded porous SiC ceramics prepared by infiltration technique. J. Alloys Compd. *781*, 289–301. https://doi.org/10.1016/j.jallcom.2018.12.046.
103. Lan, X., Liang, C., Wu, M., Wu, N., He, L., Li, Y., and Wang, Z. (2018). Facile Synthesis of Highly Defected Silicon Carbide Sheets for Efficient Absorption of Electromagnetic Waves. J. Phys. Chem. C *122*, 18537–18544. https://doi.org/10.1021/acs.jpcc.8b05339.
104. Liang, C., Liu, C., Wang, H., Wu, L., Jiang, Z., Xu, Y., Shen, B., and Wang, Z. (2014). SiC-Fe_3O_4 dielectric-magnetic hybrid nanowires: controllable fabrication, characterization and electromagnetic wave absorption. J. Mater. Chem. A *2*, 16397–16402. https://doi.org/10.1039/c4ta02907k.
105. Hou, Y., Cheng, L., Zhang, Y., Yang, Y., Deng, C., Yang, Z., Chen, Q., Wang, P., and Zheng, L. (2017). Electrospinning of Fe/SiC hybrid fibers for highly efficient microwave absorption. ACS Appl. Mater. Interfaces *9*, 7265–7271. https://doi.org/10.1021/acsami.6b15721.
106. Cai, Z., Su, L., Niu, M., Wang, L., Ni, Z., Wang, H., Peng, K., and Zhuang, L. (2022). Ultralight and resilient bicontinuous Si_3N_4/SiC nanowire network for tunable and highly efficient electromagnetic wave absorption in extreme conditions. Adv. Mater. Interfac. *9*. https://doi.org/10.1002/admi.202201553.
107. Han, M., Yin, X., Hou, Z., Song, C., Li, X., Zhang, L., and Cheng, L. (2017). Flexible and thermostable graphene/SiC nanowire foam composites with tunable electromagnetic wave absorption properties. ACS Appl. Mater. Interfaces *9*, 11803–11810. https://doi.org/10.1021/acsami.7b00951.
108. Jiang, Y., Chen, Y., Liu, Y.J., and Sui, G.X. (2018). Lightweight spongy bone-like

graphene@SiC aerogel composites for high-performance microwave absorption. Chem. Eng. J. *337*, 522–531. https://doi.org/10.1016/j.cej.2017.12.131.

109. Zhu, H.L., Bai, Y.J., Liu, R., Lun, N., Qi, Y.X., Han, F.D., and Bi, J.Q. (2011). In situ synthesis of one-dimensional MWCNT/SiC porous nanocomposites with excellent microwave absorption properties. J. Mater. Chem. *21*, 13581–13587. https://doi.org/10.1039/c1jm11747e.
110. Liang, C., and Wang, Z. (2017). Controllable fabricating dielectric-dielectric SiC@C core-shell nanowires for high-performance electromagnetic wave attenuation. ACS Appl. Mater. Interfaces *9*, 40690–40696. https://doi.org/10.1021/acsami.7b13063.
111. Wan, F., Luo, F., Wang, H., Huang, Z., Zhou, W., and Zhu, D. (2014). Effects of carbon black (CB) and alumina oxide on the electromagnetic- and microwave-absorption properties of SiC fiber/aluminum phosphate matrix composites. Ceram. Int. *40*, 15849–15857. https://doi.org/10.1016/j.ceramint.2014.07.113.
112. Singh, S., Kumar, A., and Singh, D. (2020). Enhanced microwave absorption performance of SWCNT/SiC composites. J. Electron. Mater. *49*, 7279–7291. https://doi.org/10.1007/s11664-020-08460-9.
113. Zhao, J.M., An, W.X., Li, D.A., and Yang, X. (2011). Synthesis and microwave absorption properties of SiC-carbon fibers composite in S and C band. Synth. Met. *161*, 2144–2148. https://doi.org/10.1016/j.synthmet.2011.08.016.
114. Fang, X., Pan, L., Yao, J., Yin, S., Wang, Y., Li, Q., and Yang, J. (2021). Controllable dielectric properties and strong electromagnetic wave absorption properties of SiC/spherical graphite-AlN microwave-attenuating composite ceramics. Ceram. Int. *47*, 22636–22645. https://doi.org/10.1016/j.ceramint.2021.04.277.
115. Li, J.S., Wang, S.C., and Hwang, C.C. (2020). Preparation and high-temperature microwave absorbing properties of 6H-SiC/MWCNT/silicon resin composites. mat. express *10*, 1–9. https://doi.org/10.1166/mex.2020.1612.
116. Hu, S.H., Yuan, J.J., Dai, H., Liu, Y.Y., He, J., and Tu, J.L. (2022). Preparation of a flexible X-band radar-wave-absorbing composite material by using beta-silicon carbide and polyurethane as substrates and multiwalled carbon nanotubes as additives. Symmetry *14*, 2144. https://doi.org/10.3390/sym14102144.
117. Kuang, J., Hou, X., Xiao, T., Li, Y., Wang, Q., Jiang, P., and Cao, W. (2019). Three-dimensional carbon nanotube/SiC nanowire composite network structure for high-efficiency electromagnetic wave absorption. Ceram. Int. *45*, 6263–6267. https://doi.org/10.1016/j.ceramint.2018.12.107.
118. Hasegawa, Y., and Okamura, K. (1985). SiC-C composite-materials synthesized by pyrolysis of polycarbosilane. J. Mater. Sci. Lett. *4*, 356–358. https://doi.org/10.1007/bf00719814.
119. Bouillon, E., Langlais, F., Pailler, R., Naslain, R., Cruege, F., Huong, P.V., Sarthou, J.C., Delpuech, A., Laffon, C., Lagarde, P., et al. (1991). Conversion mechanisms of a polycarbosilane precursor into an SiC-based ceramic material. J. Mater. Sci. *26*, 1333–1345. https://doi.org/10.1007/bf00544474.
120. Jian, K., Chen, Z.H., Ma, Q.S., and Zheng, W.W. (2005). Effects of pyrolysis processes on the microstructures and mechanical properties of C_f/SiC composites using polycarbosilane. Mater. Sci. Eng. A-Struct. Mater. Prop. Microstruct. Process *390*, 154–158. https://doi.org/10.1016/j.msea.2004.07.064.
121. Li, Q., Yin, X., Duan, W., Kong, L., Hao, B., and Ye, F. (2013). Electrical, dielectric and microwave-absorption properties of polymer derived SiC ceramics in X band. J. Alloys Compd. *565*, 66–72. https://doi.org/10.1016/j.jallcom.2013.02.176.
122. Wang, Y., Wang, H., Deng, P., Chen, W., Guo, Y., Tao, T., and Qin, J. (2018). Microstructures, dielectric response and microwave absorption properties of polycarbosilane derived SiC powders. Lab. Chip. *18*, 3606–3616. https://doi.org/10.1016/j.ceramint.2017.11.101.
123. Jia, Y., Rahman Chowdhury, M.A., and Xu, C. (2020). Electromagnetic property of polymer derived SiC-C solid solution formed at ultra-high temperature. Carbon *162*, 74–85. https://doi.org/10.1016/j.carbon.2020.02.036.
124. Han, M., Yin, X., Duan, W., Ren, S., Zhang, L., and Cheng, L. (2016). Hierarchical graphene/SiC nanowire networks in polymer-derived ceramics with enhanced electromagnetic wave absorbing capability. J. Eur. Ceram. Soc. *36*, 2695–2703. https://doi.org/10.1016/j.jeurceramsoc.2016.04.003.
125. Chen, Q., Li, D., Yang, Z., Jia, D., Zhou, Y., Riedel, R., Zhang, T., and Gao, C. (2021). SiBCN-reduced graphene oxide (rGO) ceramic composites derived from single-source-precursor with enhanced and tunable microwave absorption performance. Carbon *179*, 180–189. https://doi.org/10.1016/j.carbon.2021.03.057.
126. Wen, Q., Feng, Y., Yu, Z., Peng, D.L., Nicoloso, N., Ionescu, E., and Riedel, R. (2016). Microwave absorption of SiC/HfC_xN_{1-x}/C ceramic nanocomposites with HfC_xN_{1-x}-carbon core-shell Particles. J. Am. Ceram. Soc. *99*, 2655–2663. https://doi.org/10.1111/jace.14256.
127. Chen, L., Zhao, J., Wang, L., Peng, F., Liu, H., Zhang, J., Gu, J., and Guo, Z. (2019). In-situ pyrolyzed polymethylsilsesquioxane multi-walled carbon nanotubes derived ceramic nanocomposites for electromagnetic wave absorption. Ceram. Int. *45*, 11756–11764. https://doi.org/10.1016/j.ceramint.2019.03.052.
128. Gu, C., Guo, C., Dong, X., Hu, Z., Wu, P., Su, Z., Lu, Y., Xu, B., Yu, Z., and Liu, A. (2019). Core-shell structured iron-containing ceramic nanoparticles: Facile fabrication and excellent electromagnetic absorption properties. J. Am. Ceram. Soc. *102*, 7098–7107. https://doi.org/10.1111/jace.16619.
129. Hou, Y., Xiao, B., Sun, Z., Yang, W., Wu, S., Qi, S., Wen, G., and Huang, X. (2019). High temperature anti-oxidative and tunable wave absorbing SiC/Fe_3Si/CNTs composite ceramic derived from a novel polysilyacetylene. Ceram. Int. *45*, 16369–16379. https://doi.org/10.1016/j.ceramint.2019.05.165.
130. Yu, Z., Zhu, Q., Li, F., Chen, T., and Du, H. (2022). Single-source-precursor derived multicomponent CNTs/Fe_3Si/Fe/SiOCN ceramic nanocomposites: microstructural evolution and excellent electromagnetic wave absorbing properties. J. Mater. Chem. C *10*, 6252–6262. https://doi.org/10.1039/d1tc05916e.
131. Huo, Y., Zhao, K., Xu, Z., and Tang, Y. (2020). Electrospinning synthesis of SiC/Carbon hybrid nanofibers with satisfactory electromagnetic wave absorption performance. J. Alloys Compd. *815*, 152458. https://doi.org/10.1016/j.jallcom.2019.152458.
132. Huang, Z., Wang, C., Song, M., Xia, W., and Liu, W. (2022). Synthesis of SiC/graphene nanocomposites by atmospheric plasmas for improving efficient of microwave absorption. Fullerenes, Nanotub. Carbon Nanostruct. *30*, 1212–1220. https://doi.org/10.1080/1536383x.2022.2084082.
133. Wang, Z., Wang, P., Zhang, Y., and Shen, G. (2017). One-dimensional carbon/SiC nanocomposites with tunable dielectric and broadband electromagnetic wave absorption properties. Carbon *28*, 207. https://doi.org/10.1016/j.carbon.2017.09.052.
134. Wang, P., Cheng, L., Zhang, Y., and Zhang, L. (2017). Synthesis of SiC nanofibers with superior electromagnetic wave absorption performance by electrospinning. J. Alloys Compd. *716*, 306–320. https://doi.org/10.1016/j.jallcom.2017.05.059.
135. Huo, Y., Tan, Y., Zhao, K., Lu, Z., Zhong, L., and Tang, Y. (2021). Enhanced electromagnetic wave absorption properties of Ni magnetic coating-functionalized SiC/C nanofibers synthesized by electrospinning and magnetron sputtering technology. Chem. Phys. Lett. *763*, 138230. https://doi.org/10.1016/j.cplett.2020.138230.
136. Wang, P., Kankala, R.K., Fan, J., Long, R., Liu, Y., and Wang, S. (2018). Electrospinning of graphite/SiC hybrid nanowires with tunable dielectric and microwave absorption characteristics. Composites, Part A *29*, 68–80. https://doi.org/10.1016/j.compositesa.2017.10.012.
137. Wang, P., Morgan, B., Packard, P., Goode, V., and Tola, D. (2020). SiC/rGO core-shell nanowire as a lightweight, highly efficient gigahertz electromagnetic wave absorber. ACS Appl. Electron. Mater. *88*, 473–478. https://doi.org/10.1021/acsaelm.9b00721.
138. Zhang, Y., Wang, J., Wei, P., Zhang, J., Zhang, G., Pan, C., Zhu, Y., Sun, X., and Cui, J. (2021). Flexible SiC-CNTs hybrid fiber mats for tunable and broadband microwave absorption. Ceram. Int. *10*, 8123–8133. https://doi.org/10.1016/j.ceramint.2020.11.167.
139. Wang, C., Huang, Z., Zhou, J., Song, M., Chen, X., Zheng, Y., Yang, C., Xia, W., and Xia, W. (2022). One-step synthesis of SiC/C nanocomposites by atmospheric thermal plasmas for efficient microwave absorption. Ceram. Int. *48*, 10391–10402. https://doi.org/10.1016/j.ceramint.2021.12.106.
140. Wang, C., You, T., Zhang, Y., Song, M., Huang, Z., and Xia, W. (2023). Synthesis of N-doped SiC nano-powders with effective microwave absorption and enhanced photoluminescence. J. Alloys Compd. *932*, 167699. https://doi.org/10.1016/j.jallcom.2022.167699.
141. Zhao, H., Wang, F., Cui, L., Xu, X., Han, X., and Du, Y. (2021). Composition optimization and microstructure eesign in MOFs-eerived magnetic carbon-based microwave absorbers: A review. Nano-Micro Lett. *13*, 208. https://doi.org/10.1007/s40820-021-00734-z.

142. Li, G., Xie, T., Yang, S., Jin, J., and Jiang, J. (2012). Microwave absorption enhancement of porous carbon fibers compared with carbon nanofibers. J. Phys. Chem. C *116*, 9196–9201. https://doi.org/10.1021/jp300050u.
143. Li, Z., Han, X., Ma, Y., Liu, D., Wang, Y., Xu, P., Li, C., and Du, Y. (2018). MOFs-derived hollow Co/C microspheres with enhanced microwave absorption performance. ACS Sustainable Chem. Eng. *6*, 8904–8913. https://doi.org/10.1021/acssuschemeng.8b01270.
144. Liu, Q., Cao, Q., Bi, H., Liang, C., Yuan, K., She, W., Yang, Y., and Che, R. (2016). CoNi@SiO_2@TiO_2 and CoNi@Air@TiO_2 microspheres with strong wideband microwave absorption. Adv. Mater. *28*, 486–490. https://doi.org/10.1002/adma.201503149.
145. Liu, D., Du, Y., Wang, F., Wang, Y., Cui, L., Zhao, H., and Han, X. (2020). MOFs-derived multi-chamber carbon microspheres with enhanced microwave absorption. Carbon *157*, 478–485. https://doi.org/10.1016/j.carbon.2019.10.056.
146. Liu, J., Tao, J., Gao, L., He, X., Wei, B., Gu, Y., Yao, Z., and Zhou, J. (2022). Morphology-size synergy strategy of SiC@C nanoparticles towards lightweight and efficient microwave absorption. Chem. Eng. J. *433*, 134484. https://doi.org/10.1016/j.cej.2021.134484.
147. Wu, R., Yang, Z., Fu, M., and Zhou, K. (2016). In-situ growth of SiC nanowire arrays on carbon fibers and their microwave absorption properties. J. Alloys Compd. *687*, 833–838. https://doi.org/10.1016/j.jallcom.2016.06.106.
148. Yan, L., Hong, C., Sun, B., Zhao, G., Cheng, Y., Dong, S., Zhang, D., and Zhang, X. (2017). In Situ Growth of Core-Sheath Heterostructural SiC Nanowire Arrays on Carbon Fibers and Enhanced Electromagnetic Wave Absorption Performance. ACS Appl. Mater. Interfaces *9*, 6320–6331. https://doi.org/10.1021/acsami.6b15795.
149. Qian, J., Du, B., Cai, M., He, C., Wang, X., Xiong, H., and Shui, A. (2021). Preparation of SiC nanowire/carbon fiber composites with enhanced electromagnetic wave absorption performance. Adv. Eng. Mater. *23*, 2100434. https://doi.org/10.1002/adem.202100434.
150. Qian, J., Shui, A., Du, B., Cai, M., He, C., Zeng, S., Zhong, X., and Lou, J. (2022). Synthesis and tunable electromagnetic shielding and absorption performance of the three-dimensional SiC nanowires/carbon fiber composites. J. Eur. Ceram. Soc. *42*, 4154–4161. https://doi.org/10.1016/j.jeurceramsoc.2022.03.058.
151. Xie, S., Jin, G.Q., Meng, S., Wang, Y.W., Qin, Y., and Guo, X.Y. (2012). Microwave absorption properties of in situ grown CNTs/SiC composites. J. Alloys Compd. *520*, 295–300. https://doi.org/10.1016/j.jallcom.2012.01.050.
152. Ren, F., Xue, J., Liu, X., and Cheng, L. (2020). In situ construction of CNWs/SiC-NWs hybrid network reinforced SiCN with excellent electromagnetic wave absorption properties in X band. Carbon *168*, 278–289. https://doi.org/10.1016/j.carbon.2020.06.081.
153. Xu, J., Xia, L., Luo, J., Lu, S., Huang, X., Zhong, B., Zhang, T., Wen, G., Wu, X., Xiong, L., and Wang, G. (2020). High-performance electromagnetic wave absorbing CNT/SiC_f composites: synthesis, tuning, and mechanism. ACS Appl. Mater. Interfaces *12*, 20775–20784. https://doi.org/10.1021/acsami.9b19281.
154. Bu, A., Zhang, Y., Xiang, Y., Chen, W., Cheng, H., and Wang, L. (2020). Enhanced antioxidation and microwave absorbing properties of SiC/SiO_2 coating on carbon fiber. J. Mater. Sci. Mater. Electron. *31*, 17067–17074. https://doi.org/10.1007/s10854-020-04264-z.
155. Zhou, W., Li, Y., Long, L., Luo, H., and Wang, Y. (2020). High-temperature electromagnetic wave absorption properties of C_f/SiCNFs/Si_3N_4 composites. J. Am. Ceram. Soc. *103*, 6822–6832. https://doi.org/10.1111/jace.17389.
156. Qian, J., Du, B., He, C., Cai, M., Zhong, X., Xiong, H., Zeng, S., and Shui, A. (2022). Multiscale SiCnw and carbon fiber reinforced SiOC ceramic with enhanced mechanical and microwave absorption properties. J. Am. Ceram. Soc. *105*, 3456–3468. https://doi.org/10.1111/jace.18338.
157. Su, J., Wang, B., Cao, X., Yang, R., Zhao, H., Zhang, P., Wang, W., and Wang, C. (2022). Simultaneously enhancing mechanical and microwave absorption properties of C_f/SiC composites via SiC nanowires additions. Ceram. Int. *48*, 36238–36248. https://doi.org/10.1016/j.ceramint.2022.08.181.
158. Liu, D., Du, Y., Xu, P., Wang, F., Wang, Y., Cui, L., Zhao, H., and Han, X. (2021). Rationally designed hierarchical N-doped carbon nanotubes wrapping waxberry-like Ni@C microspheres for efficient microwave absorption. J. Mater. Chem. A *9*, 5086–5096. https://doi.org/10.1039/d0ta10942h.
159. Du, B., Qian, J., Hu, P., He, C., Cai, M., Wang, X., and Shui, A. (2020). Fabrication of C-doped SiC nanocomposites with tailoring dielectric properties for the enhanced electromagnetic wave absorption. Carbon *157*, 788–795. https://doi.org/10.1016/j.carbon.2019.10.029.
160. Dong, S., Zhang, W., Zhang, X., Hu, P., and Han, J. (2018). Designable synthesis of core-shell SiCw@C heterostructures with thickness-dependent electromagnetic wave absorption between the whole X-band and Ku-band. Chem. Eng. J. *354*, 767–776. https://doi.org/10.1016/j.cej.2018.08.062.
161. Liu, M., Lu, J., Gong, H., Sheng, M., Jing, J., Sun, S., Wang, G., and Miao, Y. (2022). Enhanced microwave absorbing performance of Ni-containing SiCN ceramics by constructing multiple interfaces and in-situ generating MWCNTs. Ceram. Int. *48*, 33871–33883. https://doi.org/10.1016/j.ceramint.2022.07.335.
162. Zhang, H., Xu, Y., Zhou, J., Jiao, J., Chen, Y., Wang, H., Liu, C., Jiang, Z., and Wang, Z. (2015). Stacking fault and unoccupied densities of state dependence of electromagnetic wave absorption in SiC nanowires. J. Mater. Chem. C *3*, 4416–4423. https://doi.org/10.1039/c5tc00405e.
163. Li, N., Liu, X., Sun, X., Ye, F., Liu, Y., and Cheng, L. (2016). Flexible thin SiC fiber fabrics using carbon nanotube modification for improving electromagnetic shielding properties. Mater. Des. *54*, 68–75. https://doi.org/10.1016/j.matdes.2016.05.005.
164. Huang, B., Yue, J., Fan, B., Liu, Y., and Huang, X. (2022). Vertical carbon nanotubes arrays with controlled morphology on silicon carbide fibers for electromagnetic wave absorption. Ceram. Int. *48*, 19375–19381. https://doi.org/10.1016/j.ceramint.2022.03.232.
165. Lan, X., and Wang, Z. (2020). Efficient high-temperature electromagnetic wave absorption enabled by structuring binary porous SiC with multiple interfaces. Carbon *170*, 517–526. https://doi.org/10.1016/j.carbon.2020.08.052.
166. Chen, J.P., Du, Y.F., Wang, Z.F., Liang, L.L., Jia, H., Liu, Z., Xie, L.J., Zhang, S.C., and Chen, C.M. (2021). Anchoring of SiC whiskers on the hollow carbon microspheres inducing interfacial polarization to promote electromagnetic wave attenuation capability. Carbon *175*, 11–19. https://doi.org/10.1016/j.carbon.2020.12.073.
167. Li, Y., Liu, X., Nie, X., Yang, W., Wang, Y., Yu, R., and Shui, J. (2019). Multifunctional organic-inorganic hybrid aerogel for self-cleaning, heat-insulating, and highly efficient microwave absorbing material. Adv. Funct. Mater. *29*, 1807624. https://doi.org/10.1002/adfm.201807624.
168. Qin, M., Zhang, L., Zhao, X., and Wu, H. (2021). Lightweight Ni foam-based ultra-broadband electromagnetic wave absorber. Adv. Funct. Mater. *31*, 2103436. https://doi.org/10.1002/adfm.202103436.
169. Cai, Z., Su, L., Wang, H., Niu, M., Gao, H., Lu, D., and Li, M. (2020). Hydrophobic SiC@C nanowire foam with broad-band and mechanically controlled electromagnetic wave absorption. ACS Appl. Mater. Interfaces *12*, 8555–8562. https://doi.org/10.1021/acsami.9b20636.
170. Hao, B., Tao, Z., Yan, X., Liu, W., Luo, Y., Liu, Z., and Jiang, D. (2022). Synthesis and wave absorption characterization of SiC nanowires/expanded graphite composites. Carbon *196*, 540–551. https://doi.org/10.1016/j.carbon.2022.05.022.
171. Liu, D., Gui, K., Wang, M., Zhu, M., Niu, J., and Bao, Y. (2022). A novel hierarchical structure comprised of biomass-derived porous carbon and silicon carbide nanowires for highly efficient microwave absorption. Ceram. Int. *48*, 16033–16041. https://doi.org/10.1016/j.ceramint.2022.02.147.
172. Dong, S., Hu, P., Zhang, X., Han, J., Zhang, Y., and Luo, X. (2018). Carbon foams modified with in-situ formation of Si3N4 and SiC for enhanced electromagnetic microwave absorption property and thermostability. Ceram. Int. *44*, 7141–7150. https://doi.org/10.1016/j.ceramint.2018.01.156.
173. Cai, Z., Su, L., Wang, H., Xie, Q., Gao, H., Niu, M., and Lu, D. (2022). Hierarchically assembled carbon microtube@SiC nanowire/Ni nanoparticle aerogel for highly efficient electromagnetic wave absorption and multifunction. Carbon *191*, 227–235. https://doi.org/10.1016/j.carbon.2022.01.036.
174. Dai, D., Lan, X., and Wang, Z. (2023). Hierarchical carbon fiber reinforced SiC/C aerogels with efficient electromagnetic wave absorption properties. Composites, Part B *248*, 110376. https://doi.org/10.1016/j.compositesb.2022.110376.
175. Ye, X., Chen, Z., Li, M., Wang, T., Zhang, J., Wu, C., Zhou, Q., Liu, H., and Cui, S. (2019). Reticulated SiC coating reinforced carbon foam with tunable electromagnetic microwave absorption performance. Composites, Part B *178*, 107479. https://doi.org/10.1016/j.compositesb.2019.107479.

176. Mao, B., Xia, X., Qin, R., Xu, D., Wang, X., and Lv, H. (2021). Synthesis and microwave absorption properties of multilayer SiC/C foam with alternating distribution of C and SiC. J. Alloys Compd. *879*, 160440. https://doi.org/10.1016/j.jallcom.2021.160440.
177. Ye, X., Chen, Z., Zhang, J., Wu, C., Zhou, Q., Ai, S., Liu, H., and Cui, S. (2019). Double network nested foam composites with tunable electromagnetic wave absorption performances. Inorg. Chem. Front. *6*, 1579–1586. https://doi.org/10.1039/c9qi00398c.
178. Ye, X., Chen, Z., Ai, S., Hou, B., Zhang, J., Liang, X., Zhou, Q., Liu, H., and Cui, S. (2019). Porous SiC/melamine-derived carbon foam frameworks with excellent electromagnetic wave absorbing capacity. J. Adv. Ceram. *8*, 479–488. https://doi.org/10.1007/s40145-019-0328-2.
179. Ye, X., Chen, Z., Ai, S., Hou, B., Zhang, J., Liang, X., Zhou, Q., Liu, H., and Cui, S. (2019). Novel Three-Dimensional SiC/Melamine-Derived Carbon Foam Reinforced SiO_2 Aerogel Composite with Low Dielectric Loss and High Impedance Matching Ratio. ACS Sustainable Chem. Eng. *7*, 2774–2783. https://doi.org/10.1021/acssuschemeng.8b05966.
180. Ye, X., Chen, Z., Ai, S., Hou, B., Zhang, J., Liang, X., Zhou, Q., Liu, H., and Cui, S. (2019). Effects of SiC coating on microwave absorption of novel three-dimensional reticulated SiC/porous carbon foam. Ceram. Int. *45*, 8660–8668. https://doi.org/10.1016/j.ceramint.2019.01.186.
181. Ye, X., Chen, Z., Li, M., Wang, T., Wu, C., Zhang, J., Zhou, Q., Liu, H., and Cui, S. (2019). Microstructure and Microwave Absorption Performance Variation of SiC/C Foam at Different Elevated-Temperature Heat Treatment. ACS Sustainable Chem. Eng. *7*, 18395–18404. https://doi.org/10.1021/acssuschemeng.9b04062.
182. Cheng, Y., Tan, M., Hu, P., Zhang, X., Sun, B., Yan, L., Zhou, S., and Han, W. (2018). Strong and thermostable SiC nanowires/graphene aerogel with enhanced hydrophobicity and electromagnetic wave absorption property. Appl. Surf. Sci. *448*, 138–144. https://doi.org/10.1016/j.apsusc.2018.04.132.
183. Li, H., Deng, W., Li, T., Niu, R., and He, D. (2022). Construction of SiCnws/carbon foam composites with multiple loss mechanisms for excellent electromagnetic wave absorption. Synth. Met. *291*, 117207. https://doi.org/10.1016/j.synthmet.2022.117207.
184. Xiao, S., Mei, H., Han, D., Dassios, K.G., and Cheng, L. (2017). Ultralight lamellar amorphous carbon foam nanostructured by SiC nanowires for tunable electromagnetic wave absorption. Carbon *122*, 718–725. https://doi.org/10.1016/j.carbon.2017.07.023.
185. Naguib, M., Mochalin, V.N., Barsoum, M.W., and Gogotsi, Y. (2014). 25th anniversary article: MXenes: a new family of two-dimensional materials. Adv. Mater. *26*, 992–1005. https://doi.org/10.1002/adma.201304138.
186. Ghidiu, M., Lukatskaya, M.R., Zhao, M.Q., Gogotsi, Y., and Barsoum, M.W. (2014). Conductive two-dimensional titanium carbide 'clay' with high volumetric capacitance. Nature *516*, 78–81. https://doi.org/10.1038/nature13970.
187. Li, Z., and Wu, Y. (2019). 2D early transition metal carbides (MXenes) for catalysis. Small *15*, 1804736. https://doi.org/10.1002/smll.201804736.
188. Pei, Y., Zhang, X., Hui, Z., Zhou, J., Huang, X., Sun, G., and Huang, W. (2021). $Ti_3C_2T_X$ MXene for sensingapplications: recent progress, design principles, and future perspectives. ACS Nano *15*, 3996–4017. https://doi.org/10.1021/acsnano.1c00248.
189. Mahmud, S.T., Hasan, M.M., Bain, S., Rahman, S.T., Rhaman, M., Hossain, M.M., and Ordu, M. (2022). Multilayer MXene heterostructures and nanohybrids for multifunctional applications: a review. ACS Mater. Lett. *4*, 1174–1206. https://doi.org/10.1021/acsmaterialslett.2c00175.
190. Liu, J., Zhang, H.B., Sun, R., Liu, Y., Liu, Z., Zhou, A., and Yu, Z.Z. (2017). Hydrophobic, flexible, and lightweight MXene foams for high-performance electromagnetic-interference shielding. Adv. Mater. *29*, 1702367. https://doi.org/10.1002/adma.201702367.
191. Liang, C., Qiu, H., Song, P., Shi, X., Kong, J., and Gu, J. (2020). Ultra-light MXene aerogel/wood-derived porous carbon composites with wall-like "mortar/brick" structures for electromagnetic interference shielding. Sci. Bull. *65*, 616–622. https://doi.org/10.1016/j.scib.2020.02.009.
192. Zeng, Z., Wang, C., Siqueira, G., Han, D., Huch, A., Abdolhosseinzadeh, S., Heier, J., Nüesch, F., Zhang, C.J., and Nyström, G. (2020). Nanocellulose-MXene biomimetic aerogels with orientation-tunable electromagnetic interference shielding performance. Adv. Sci. *7*, 2000979. https://doi.org/10.1002/advs.202000979.
193. Jin, Z., Fang, Y., Wang, X., Xu, G., Liu, M., Wei, S., Zhou, C., Zhang, Y., and Xu, Y. (2019). Ultra-efficient electromagnetic wave absorption with ethanol-thermally treated two-dimensional Nb_2CT_x nanosheets. J. Colloid Interface Sci. *537*, 306–315. https://doi.org/10.1016/j.jcis.2018.11.034.
194. Wu, J., Feng, Y., Xia, Y., Zhu, Q., Luo, L., Ma, L., Li, H., Yan, H., and Qi, S. (2022). Fabrication of S-doped $Ti_3C_2T_x$ materials with enhanced electromagnetic wave absorbing properties. J. Alloys Compd. *891*, 161942. https://doi.org/10.1016/j.jallcom.2021.161942.
195. Xiaodan, X., Yanxiang, W., Yang, Y., Chengjuan, W., Zhenhao, X., and Dongming, L. (2022). Dopants versus defects: Intense confrontation of nitrogen-doped $Ti_3C_2T_x$ for enhanced electromagnetic interference shielding. Compos. Commun. *35*, 101301. https://doi.org/10.1016/j.coco.2022.101301.
196. Rajavel, K., Yu, X., Zhu, P., Hu, Y., Sun, R., and Wong, C. (2020). Exfoliation and defect control of two-Dimensional few-Layer MXene $Ti_3C_2T_x$ for electromagnetic interference shielding coatings. ACS Appl. Mater. Interfaces *12*, 49737–49747. https://doi.org/10.1021/acsami.0c12835.
197. Han, M., Yin, X., Hantanasirisakul, K., Li, X., Iqbal, A., Hatter, C.B., Anasori, B., Koo, C.M., Torita, T., Soda, Y., et al. (2019). Anisotropic MXene aerogels with a mechanically tunable ratio of electromagnetic wave reflection to absorption. Adv. Opt. Mater. *7*, 1900267. https://doi.org/10.1002/adom.201900267.
198. Liang, L., Li, Q., Yan, X., Feng, Y., Wang, Y., Zhang, H.B., Zhou, X., Liu, C., Shen, C., and Xie, X. (2021). Multifunctional magnetic $Ti_3C_2T_x$ MXene/graphene aerogel with superior electromagnetic wave absorption performance. ACS Nano *15*, 6622–6632. https://doi.org/10.1021/acsnano.0c09982.
199. Song, Q., Ye, F., Kong, L., Shen, Q., Han, L., Feng, L., Yu, G., Pan, Y., and Li, H. (2020). Graphene and MXene nanomaterials: toward high-performance electromagnetic wave absorption in gigahertz band range. Adv. Funct. Mater. *30*, 2000475. https://doi.org/10.1002/adfm.202000475.
200. Li, Y., Meng, F., Mei, Y., Wang, H., Guo, Y., Wang, Y., Peng, F., Huang, F., and Zhou, Z. (2020). Electrospun generation of $Ti_3C_2T_x$ MXene@graphene oxide hybrid aerogel microspheres for tunable high-performance microwave absorption. Chem. Eng. J. *391*, 123512. https://doi.org/10.1016/j.cej.2019.123512.
201. Fan, X., Li, M., Li, X., Ye, F., Xue, J., Zhang, L., and Cheng, L. (2020). Electromagnetic interference shielding Ti3C2Tx-bonded carbon black films with enhanced absorption performance. Chin. Chem. Lett. *31*, 1026–1029. https://doi.org/10.1016/j.cclet.2020.01.030.
202. Xu, X., Wang, Y., Yue, Y., Wang, C., Xu, Z., and Liu, D. (2022). Core-shell MXene/nitrogen-doped C heterostructure for wide-band electromagnetic wave absorption at thin thickness. Ceram. Int. *48*, 30317–30324. https://doi.org/10.1016/j.ceramint.2022.06.304.
203. Huyan, W., Yao, J., Tao, J., Yang, F., Tao, X., Yao, Z., Zhou, J., and Jiao, Z. (2022). MXene@C heterogeneous nanocomposites with the 2D-0D structure for ultra-light and broadband electromagnetic wave absorption. Carbon *197*, 444–454. https://doi.org/10.1016/j.carbon.2022.06.070.
204. Cui, Y., Wu, F., Wang, J., Wang, Y., Shah, T., Liu, P., Zhang, Q., and Zhang, B. (2021). Three dimensional porous MXene/CNTs microspheres: Preparation, characterization and microwave absorbing properties. Composites, Part A *145*, 106378. https://doi.org/10.1016/j.compositesa.2021.106378.
205. Peng, H., He, M., Zhou, Y., Song, Z., Wang, Y., Feng, S., Chen, X., Zhang, X., and Chen, H. (2022). Low-temperature carbonized biomimetic cellulose nanofiber/MXene composite membrane with excellent microwave absorption performance and tunable absorption bands. Chem. Eng. J. *433*, 133269. https://doi.org/10.1016/j.cej.2021.133269.
206. Weng, G.M., Li, J., Alhabeb, M., Karpovich, C., Wang, H., Lipton, J., Maleski, K., Kong, J., Shaulsky, E., Elimelech, M., et al. (2018). Layer-by-layer assembly of cross-functional semi-transparent MXene-carbon nanotubes composite films for next-generation electromagnetic interference shielding. Adv. Funct. Mater. *28*, 1803360. https://doi.org/10.1002/adfm.201803360.
207. Wu, H., Zhu, C., Li, X., Hu, X., Xie, H., Lu, X., and Qu, J.P. (2022). Layer-by-layer assembly of multifunctional NR/MXene/CNTs composite films with exceptional electromagnetic interference shielding performances and excellent mechanical properties. Macromol. Rapid Commun. *43*, 2200387. https://doi.org/10.1002/marc.202200387.
208. Cao, W., Ma, C., Tan, S., Ma, M., Wan, P., and Chen, F. (2019). Ultrathin and flexible CNTs/MXene/cellulose nanofibrils composite paper for electromagnetic interference shielding. Nano-Micro Lett. *11*, 72. https://doi.org/10.1007/s40820-019-0304-y.
209. Zhu, L., Mo, R., Yin, C.G., Guo, W., Yu, J., and Fan, J. (2022). Synergistically constructed

electromagnetic network of magnetic particle-decorated carbon nanotubes and MXene for efficient electromagnetic shielding. ACS Appl. Mater. Interfaces *14*, 56120–56131. https://doi.org/10.1021/acsami.2c17696.

210. Duan, N., Shi, Z., Wang, Z., Zou, B., Zhang, C., Wang, J., Xi, J., Zhang, X., Zhang, X., and Wang, G. (2022). Mechanically robust $Ti_3C_2T_x$ MXene/Carbon fiber fabric/Thermoplastic polyurethane composite for efficient electromagnetic interference shielding applications. Mater. Des. *214*, 110382. https://doi.org/10.1016/j.matdes.2022.110382.
211. Yu, L.P., Zhou, X.H., Lu, L., Xu, L., and Wang, F.J. (2021). MXene/Carbon Nanotube Hybrids: Synthesis, Structures, Properties, and Applications. ChemSusChem *14*, 5079–5111. https://doi.org/10.1002/cssc.202101614.
212. Sambyal, P., Iqbal, A., Hong, J., Kim, H., Kim, M.K., Hong, S.M., Han, M., Gogotsi, Y., and Koo, C.M. (2019). Ultralight and Mechanically Robust $Ti_3C_2T_x$ Hybrid Aerogel Reinforced by Carbon Nanotubes for Electromagnetic Interference Shielding. ACS Appl. Mater. Interfaces *11*, 38046–38054. https://doi.org/10.1021/acsami.9b12550.
213. Deng, Z., Tang, P., Wu, X., Zhang, H.B., and Yu, Z.Z. (2021). Superelastic, ultralight, and conductive $Ti_3C_2T_x$ MXene/acidified carbon nanotube anisotropic aerogels for electromagnetic interference shielding. ACS Appl. Mater. Interfaces *13*, 20539–20547. https://doi.org/10.1021/acsami.1c02059.
214. Min Jeon, S., Hongyue, J., Jae Song, Y., and Lee, S. (2022). Enhanced electromagnetic absorption of cement composites by controlling the effective cross-sectional area of MXene flakes with diffuse reflection based on carbon fibers. Construct. Build. Mater. *348*, 128711. https://doi.org/10.1016/j.conbuildmat.2022.128711.
215. Sun, Y., Li, B., Zheng, H., Rong, K., Fan, W., and Li, D. (2023). MXene-decorated carbonized jute composite for high-performance electromagnetic interference shielding. J. Mater. Res. Technol. *22*, 658–667. https://doi.org/10.1016/j.jmrt.2022.11.160.
216. Yang, R., Gui, X., Yao, L., Hu, Q., Yang, L., Zhang, H., Yao, Y., Mei, H., and Tang, Z. (2021). Ultrathin, lightweight, and flexible CNT buckypaper enhanced using MXenes for electromagnetic interference shielding. Nano-Micro Lett. *13*, 66. https://doi.org/10.1007/s40820-021-00597-4.
217. Zhou, B., Li, Y., Li, Z., Ma, J., Zhou, K., Liu, C., Shen, C., and Feng, Y. (2021). Fire/heat-resistant, anti-corrosion and folding $Ti_2C_3T_x$ MXene/single-walled carbon nanotube films for extreme-environmental EMI shielding and solar-thermal conversion applications. J. Mater. Chem. C *9*, 10425–10434. https://doi.org/10.1039/d1tc00289a.
218. Cui, Y., Yang, K., Zhang, F., Lyu, Y., Zhang, Q., and Zhang, B. (2022). Ultra-light MXene/CNTs/PI aerogel with neat arrangement for electromagnetic wave absorption and photothermal conversion. Composites, Part A *158*, 106986. https://doi.org/10.1016/j.compositesa.2022.106986.
219. Hu, K., Wang, H., Cheng, W., Rao, Y., Pan, L., Zhang, C.J., Wang, Y., Li, Q., and Yang, J. (2022). Lightweight and robust $Ti_3C_2T_x$/carbon nanotubes foam with tuneable and highly efficient microwave absorption performance. Ceram. Int. *48*, 31129–31137. https://doi.org/10.1016/j.ceramint.2022.05.325.
220. Deng, B., Xiang, Z., Xiong, J., Liu, Z., Yu, L., and Lu, W. (2020). Sandwich-like Fe&TiO_2@C nanocomposites derived from MXene/Fe-MOFs hybrids for electromagnetic absorption. Nano-Micro Lett. *12*, 55. https://doi.org/10.1007/s40820-020-0398-2.
221. Hou, T., Jia, Z., Dong, Y., Liu, X., and Wu, G. (2022). Layered 3D structure derived from MXene/magnetic carbon nanotubes for ultra-broadband electromagnetic wave absorption. Chem. Eng. J. *431*, 133919. https://doi.org/10.1016/j.cej.2021.133919.
222. Zou, Z., Ning, M., Lei, Z., Zhuang, X., Tan, G., Hou, J., Xu, H., Man, Q., Li, J., and Li, R.W. (2022). 0D/1D/2D architectural Co@C/MXene composite for boosting microwave attenuation performance in 2-18 GHz. Carbon *193*, 182–194. https://doi.org/10.1016/j.carbon.2022.03.017.
223. Zhou, J., Guo, F., Luo, J., Hao, G., Liu, G., Hu, Y., Zhang, G., Guo, H., Zhou, H., and Jiang, W. (2022). Designed 3D heterostructure with 0D/1D/2D hierarchy for low-frequency microwave absorption in the S-band. J. Mater. Chem. C *10*, 1470–1478. https://doi.org/10.1039/d1tc04881c.
224. Huang, M., Wang, L., Zhao, B., Chen, G., and Che, R. (2023). Engineering the electronic structure on MXenes via multidimensional component interlayer insertion for enhanced electromagnetic shielding. J. Mater. Sci. Technol. *138*, 149–156. https://doi.org/10.1016/j.jmst.2022.07.047.
225. Zhou, J., Zhang, G., Luo, J., Hu, Y., Hao, G., Guo, H., Guo, F., Wang, S., and Jiang, W. (2021). A MOFs-derived 3D superstructure nanocomposite as excellent microwave absorber. Chem. Eng. J. *426*, 130725. https://doi.org/10.1016/j.cej.2021.130725.
226. Li, X., Yin, X., Han, M., Song, C., Xu, H., Hou, Z., Zhang, L., and Cheng, L. (2017). Ti_3C_2 MXenes modified with in situ grown carbon nanotubes for enhanced electromagnetic wave absorption properties. J. Mater. Chem. C *5*, 4068–4074. https://doi.org/10.1039/c6tc05226f.
227. Li, X., You, W., Xu, C., Wang, L., Yang, L., Li, Y., and Che, R. (2021). 3D seed-germination-like MXene with in situ growing CNTs/Ni heterojunction for enhanced microwave absorption via polarization and magnetization. Nano-Micro Lett. *13*, 157. https://doi.org/10.1007/s40820-021-00680-w.
228. Yue, Y., Wang, Y., Xu, X., Wang, C., Yao, Z., and Liu, D. (2022). In-situ growth of bamboo-shaped carbon nanotubes and helical carbon nanofibers on $Ti_3C_2T_x$ MXene at ultra-low temperature for enhanced electromagnetic wave absorption properties. Ceram. Int. *48*, 6338–6346. https://doi.org/10.1016/j.ceramint.2021.11.176.
229. Cheng, J., Liu, B., Wang, Y., Zhao, H., and Wang, Y. (2022). Growing CoNi nanoalloy@N-doped carbon nanotubes on MXene sheets for excellent microwave absorption. J. Mater. Sci. Technol. *130*, 157–165. https://doi.org/10.1016/j.jmst.2022.05.013.
230. Naguib, M., Kurtoglu, M., Presser, V., Lu, J., Niu, J., Heon, M., Hultman, L., Gogotsi, Y., and Barsoum, M.W. (2011). Two-dimensional nanocrystals produced by exfoliation of Ti_3AlC_2. Adv. Mater. *23*, 4248–4253. https://doi.org/10.1002/adma.201102306.
231. Novoselov, K.S., Geim, A.K., Morozov, S.V., Jiang, D., Zhang, Y., Dubonos, S.V., Grigorieva, I.V., and Firsov, A.A. (2004). Electric field effect in atomically thin carbon films. Science *306*, 666–669. https://doi.org/10.1126/science.1102896.
232. Wang, K., Chu, W., Li, H., Chen, Y., Cai, Y., and Liu, H. (2021). Ferromagnetic Ti_3CNCl_2-decorated RGO aerogel: From 3D interconnecting conductive network construction to ultra-broadband microwave absorber with thermal insulation property. J. Colloid Interface Sci. *604*, 402–414. https://doi.org/10.1016/j.jcis.2021.05.166.
233. Yang, F., Huang, Y., Han, X., Zhang, S., Yu, M., Zhang, J., and Sun, X. (2023). Covalent bonding of MXene/reduced graphene oxide composites for efficient electromagnetic wave absorption. ACS Appl. Nano Mater. *6*, 3367–3377. https://doi.org/10.1021/acsanm.2c05150.
234. Lee, D.E., Lee, G.H., Son, N.R., Zhang, H.X., and Yoon, K.B. (2023). Polyamide 6/MXene-grafted graphene oxide hybrid nanocomposites. Iran. Polym. J. (Engl. Ed.) *32*, 377–388. https://doi.org/10.1007/s13726-022-01119-8.
235. Li, X., Yin, X., Song, C., Han, M., Xu, H., Duan, W., Cheng, L., and Zhang, L. (2018). Self-Assembly Core-Shell Graphene-Bridged Hollow MXenes Spheres 3D Foam with Ultrahigh Specific EM Absorption Performance. Adv. Funct. Mater. *28*, 1803938. https://doi.org/10.1002/adfm.201803938.
236. Wang, L., Liu, H., Lv, X., Cui, G., and Gu, G. (2020). Facile synthesis 3D porous MXene $Ti_3C_2T_x$@RGO composite aerogel with excellent dielectric loss and electromagnetic wave absorption. J. Alloys Compd. *828*, 154251. https://doi.org/10.1016/j.jallcom.2020.154251.
237. Raagulan, K., Braveenth, R., Jang, H.J., Seon Lee, Y., Yang, C.M., Mi Kim, B., Moon, J.J., and Chai, K.Y. (2018). Electromagnetic shielding by MXene-graphene-PVDF composite with hydrophobic, lightweight and flexible graphene coated fabric. Materials *11*, 1803. https://doi.org/10.3390/ma11101803.
238. Tang, X., Luo, J., Hu, Z., Lu, S., Liu, X., Li, S., Zhao, X., Zhang, Z., Lan, Q., Ma, P., et al. (2022). Ultrathin, flexible, and oxidation-resistant MXene/graphene porous films for efficient electromagnetic interference shielding. Nano Res. *16*, 1755–1763. https://doi.org/10.1007/s12274-022-4841-1.
239. Li, H., Ru, X., Song, Y., Wang, H., Yang, C., Gong, L., Liu, Z., Zhang, Q., and Chen, Y. (2022). Flexible and self-healing 3D MXene/reduced graphene oxide/polyurethane composites for high-performance electromagnetic interference shielding. Compos. Sci. Technol. *227*, 109602. https://doi.org/10.1016/j.compscitech.2022.109602.
240. Li, B., Luo, S., Anwer, S., Chan, V., and Liao, K. (2022). Heterogeneous films assembled from $Ti_3C_2T_x$ MXene and porous double-layered carbon nanosheets for high-performance electromagnetic interference shielding. Appl. Surf. Sci. *599*, 153944. https://doi.org/10.1016/j.apsusc.2022.153944.
241. Li, S., Xu, S., Pan, K., Du, J., and Qiu, J. (2022). Ultra-thin broadband terahertz

absorption and electromagnetic shielding properties of MXene/rGO composite film. Carbon *194*, 127–139. https://doi.org/10.1016/j.carbon.2022.03.048.

242. Li, L., Zhao, S., Luo, X.J., Zhang, H.B., and Yu, Z.Z. (2021). Smart MXene-Based Janus films with multi-responsive actuation capability and high electromagnetic interference shielding performances. Carbon *175*, 594–602. https://doi.org/10.1016/j.carbon.2020.10.090.
243. Zheng, X., Tang, J., Wang, P., Wang, Z., Zou, L., and Li, C. (2022). Interfused core-shell heterogeneous graphene/MXene fiber aerogel for high-performance and durable electromagnetic interference shielding. J. Colloid Interface Sci. *628*, 994–1003. https://doi.org/10.1016/j.jcis.2022.08.019.
244. Dai, Y., Wu, X., Li, L., Zhang, Y., Deng, Z., Yu, Z.Z., and Zhang, H.B. (2022). 3D printing of resilient, lightweight and conductive MXene/reduced graphene oxide architectures for broadband electromagnetic interference shielding. J. Mater. Chem. A *10*, 11375–11385. https://doi.org/10.1039/d2ta01388f.
245. Sun, T., Liu, Z., Li, S., Liu, H., Chen, F., Wang, K., and Zhao, Y. (2021). Effective improvement on microwave absorbing performance of epoxy resin-based composites with 3D MXene foam prepared by one-step impregnation method. Composites, Part A *150*, 106594. https://doi.org/10.1016/j.compositesa.2021.106594.
246. Wang, Y., Yang, J., Chen, Z., and Hu, Y. (2019). A new flexible and ultralight carbon foam/$Ti_3C_2T_X$ MXene hybrid for high-performance electromagnetic wave absorption. RSC Adv. *9*, 41038–41049. https://doi.org/10.1039/c9ra09817h.
247. Jia, X., Shen, B., Zhang, L., and Zheng, W. (2021). Construction of shape-memory carbon foam composites for adjustable EMI shielding under self-fixable mechanical deformation. Chem. Eng. J. *405*, 126927. https://doi.org/10.1016/j.cej.2020.126927.
248. Qi, F., Wang, L., Zhang, Y., Ma, Z., Qiu, H., and Gu, J. (2021). Robust $Ti_3C_2T_x$ MXene/starch derived carbon foam composites for superior EMI shielding and thermal insulation. Mater. Today Phys. *21*, 100512. https://doi.org/10.1016/j.mtphys.2021.100512.
249. Wang, Y., Li, X., Han, X., Xu, P., Cui, L., Zhao, H., Liu, D., Wang, F., and Du, Y. (2020). Ternary Mo_2C/Co/C composites with enhanced electromagnetic waves absorption. Chem. Eng. J. *387*, 124159. https://doi.org/10.1016/j.cej.2020.124159.
250. Qian, X., Zhang, Y., Wu, Z., Zhang, R., Li, X., Wang, M., and Che, R. (2021). Multi-path electron transfer in 1D double-shelled Sn@Mo_2C/C tubes with enhanced dielectric loss for boosting microwave absorption performance. Small *17*, 2100283. https://doi.org/10.1002/smll.202100283.
251. Wang, J., Wu, Z., Xing, Y., Li, B., Huang, P., and Liu, L. (2023). Multi-Scale Design of Ultra-Broadband Microwave Metamaterial Absorber Based on Hollow Carbon/MXene/Mo_2C Microtube. Small *19*, 2207051. https://doi.org/10.1002/smll.202207051.
252. Morishita, T., Soneda, Y., Hatori, H., and Inagaki, M. (2007). Carbon-coated tungsten and molybdenum carbides for electrode of electrochemical capacitor. Electrochim. Acta *52*, 2478–2484. https://doi.org/10.1016/j.electacta.2006.08.056.
253. Zhu, J., Sakaushi, K., Clavel, G., Shalom, M., Antonietti, M., and Fellinger, T.P. (2015). A general salt-templating method to fabricate vertically aligned graphitic carbon nanosheets and their metal carbide hybrids for superior lithium ion batteries and water splitting. J. Am. Chem. Soc. *137*, 5480–5485. https://doi.org/10.1021/jacs.5b01072.
254. Dinh, K.N., Liang, Q., Du, C.F., Zhao, J., Tok, A.I.Y., Mao, H., and Yan, Q. (2019). Nanostructured metallic transition metal carbides, nitrides, phosphides, and borides for energy storage and conversion. Nano Today *25*, 99–121. https://doi.org/10.1016/j.nantod.2019.02.008.
255. Wan, C., Regmi, Y.N., and Leonard, B.M. (2014). Multiple phases of molybdenum carbide as electrocatalysts for the hydrogen evolution reaction. Angew. Chem. Int. Ed. *53*, 6407–6410. https://doi.org/10.1002/anie.201402998.
256. Liu, Y., Yu, G., Li, G.D., Sun, Y., Asefa, T., Chen, W., and Zou, X. (2015). Coupling Mo_2C with nitrogen-rich nanocarbon leads to efficient hydrogen-evolution electrocatalytic sites. Angew. Chem. Int. Ed. *54*, 10752–10757. https://doi.org/10.1002/anie.201504376.
257. Ji, M., Niu, S., Du, Y., Song, B., and Xu, P. (2018). Anion-induced size selection of beta-Mo_2C supported on nitrogen-doped carbon nanotubes for electrocatalytic hydrogen evolution. ACS Sustainable Chem. Eng. *6*, 11922–11929. https://doi.org/10.1021/acssuschemeng.8b02194.
258. Qian, J., Xing, Y., Yang, Y., Li, Y., Yu, K., Li, W., Zhao, T., Ye, Y., Li, L., Wu, F., and Chen, R. (2021). Enhanced electrochemical kinetics with highly dispersed conductive and electrocatalytic mediators for lithium-sulfur batteries. Adv. Mater. *33*, 2100810. https://doi.org/10.1002/adma.202100810.
259. Dai, S., Cheng, Y., Quan, B., Liang, X., Liu, W., Yang, Z., Ji, G., and Du, Y. (2018). Porous-carbon-based Mo_2C nanocomposites as excellent microwave absorber: a new exploration. Nanoscale *10*, 6945–6953. https://doi.org/10.1039/c8nr01244j.
260. Fan, X., Zhan, Y., Xu, H., Hou, Z., Liu, X., and Riedel, R. (2020). Highly flexible, light-weight and mechanically enhanced $(Mo_2C/PyC)_f$ fabrics for efficient electromagnetic interference shielding. Composites, Part A *136*, 105955. https://doi.org/10.1016/j.compositesa.2020.105955.
261. Wang, W., Sun, G., Sun, X., Huang, M., Liang, Y., and Bi, J. (2021). Electromagnetic microwave absorption property of MoC synthesized via a facile solid-state reaction method. J. Mater. Sci. Mater. Electron. *32*, 24351–24362. https://doi.org/10.1007/s10854-021-06906-2.
262. Wu, Z., Jin, C., Yang, Z., and Che, R. (2022). Integrating hierarchical interfacial polarization in yeast-derived Mo_2C/C nanoflower/microsphere nanoarchitecture for boosting microwave absorption performance. Carbon *189*, 530–538. https://doi.org/10.1016/j.carbon.2021.12.073.
263. Wang, Y., Li, C., Han, X., Liu, D., Zhao, H., Li, Z., Xu, P., and Du, Y. (2018). Ultrasmall Mo_2C nanoparticle-decorated carbon polyhedrons for enhanced microwave absorption. ACS Appl. Nano Mater. *1*, 5366–5376. https://doi.org/10.1021/acsanm.8b01479.
264. Wang, L., Lu, J., Zhang, J., and Zhu, J. (2023). Facile preparation and high microwave absorption of flower-like carbon nanosheet aggregations embedded with ultrafine Mo_2C. J. Colloid Interface Sci. *641*, 729–736. https://doi.org/10.1016/j.jcis.2023.03.071.
265. Zhao, T., Jia, Z., Zhang, Y., and Wu, G. (2023). Multiphase molybdenum carbide doped carbon hollow sphere engineering: the superiority of unique double-shell structure in microwave absorption. Small *19*, 2206323. https://doi.org/10.1002/smll.202206323.
266. Wang, Y., Han, X., Xu, P., Liu, D., Cui, L., Zhao, H., and Du, Y. (2019). Synthesis of pomegranate-like Mo_2C@C nanospheres for highly efficient microwave absorption. Chem. Eng. J. *372*, 312–320. https://doi.org/10.1016/j.cej.2019.04.153.
267. Deng, X., Wang, Y., Ma, L., Li, Z., Chen, Z., Lv, X., Chang, Y., Liu, Y., and Shi, J. (2022). Construction of dual-shell Mo_2C/C microsphere towards efficient electromagnetic wave absorption. Int. J. Mol. Sci. *23*, 14502. https://doi.org/10.3390/ijms232314502.
268. Huang, W., Chen, J., Gao, W., Wang, L., Liu, P., Zhang, Y., Yin, Z., and Yang, Y. (2022). Host-Guest crystalline Mo/Co-framework induced phase-conversion of MoC_x in carbon hybrids for regulating absorption of electromagnetic wave. Carbon *197*, 129–140. https://doi.org/10.1016/j.carbon.2022.06.031.
269. Chen, M.W., McCauley, J.W., LaSalvia, J.C., and Hemker, K.J. (2005). Microstructural characterization of commercial hot-pressed boron carbide ceramics. J. Am. Ceram. Soc. *88*, 1935–1942. https://doi.org/10.1111/j.1551-2916.2005.00346.x.
270. Domnich, V., Reynaud, S., Haber, R.A., and Chhowalla, M. (2011). Boroncarbide: structure, properties, and stability under stress. J. Am. Ceram. Soc. *94*, 3605–3628. https://doi.org/10.1111/j.1551-2916.2011.04865.x.
271. Ma, M., Yang, R., Zhang, C., Wang, B., Zhao, Z., Hu, W., Liu, Z., Yu, D., Wen, F., He, J., and Tian, Y. (2019). Direct large-scale fabrication of C-encapsulated B_4C nanoparticles with tunable dielectric properties as excellent microwave absorbers. Carbon *148*, 504–511. https://doi.org/10.1016/j.carbon.2019.04.020.
272. Wang, B., Fu, Q., Song, Q., Yu, Z., and Riedel, R. (2020). In situ growth of B_4C nanowires on activated carbon felt to improve microwave absorption performance. Appl. Phys. Lett. *116*, 203101. https://doi.org/10.1063/5.0007332.
273. Zhang, B., Prikhna, T., Hu, C., and Wang, Z. (2021). Graphene-layer-coated boron carbide nanosheets with efficient electromagnetic wave absorption. Appl. Surf. Sci. *560*, 150027. https://doi.org/10.1016/j.apsusc.2021.150027.
274. Kral, C., Lengauer, W., Rafaja, D., and Ettmayer, P. (1998). Critical review on the elastic properties of transition metal carbides, nitrides and carbonitrides. J. Alloys Compd. *265*, 215–233. https://doi.org/10.1016/s0925-8388(97)00297-1.
275. Pang, J., Sun, J., Zheng, M., Li, H., Wang, Y., and Zhang, T. (2019). Transition metal carbide catalysts for biomass conversion: A review. Appl. Catal., B *254*, 510–522. https://doi.org/10.1016/j.apcatb.2019.05.034.
276. Yuan, X., Cheng, L., Kong, L., Yin, X., and Zhang, L. (2014). Preparation of titanium carbide nanowires for application in electromagnetic wave absorption. J. Alloys

Compd. *596*, 132–139. https://doi.org/10.1016/j.jallcom.2014.01.022.

277. Hong, X., Wang, Q., Tang, Z., Khan, W.Q., Zhou, D., and Feng, T. (2016). Synthesis and electromagnetic absorbing properties of titanium carbonitride with quantificational carbon doping. J. Phys. Chem. C *120*, 148–156. https://doi.org/10.1021/acs.jpcc.5b11000.
278. Meng, H., Song, K.P., Wang, H., Jiang, J.J., Li, D., Han, Z., and Zhang, Z.D. (2011). Dielectric response of carbon coated TiC nanocubes at 2-18 GHz frequencies. J. Alloys Compd. *509*, 490–493. https://doi.org/10.1016/j.jallcom.2010.09.074.
279. Yu, J., Su, R., Yu, J., Liu, X., Zhang, X., and Dong, X. (2020). Regulation of dielectric loss by different exposed crystal facets in graphite-coated titanium carbide nanocomposites. Ceram. Int. *46*, 18339–18346. https://doi.org/10.1016/j.ceramint.2020.04.150.
280. Yu, J., Liu, X., Su, R., Zhang, X., and Dong, X. (2021). Optimized microwave absorption properties by tailoring the morphology of carbon coated TiC nanoparticles by N_2 pressure. Ceram. Int. *47*, 23950–23957. https://doi.org/10.1016/j.ceramint.2021.05.104.
281. Sun, Y., Liu, X., Jin, C., Xia, A., Zhao, S., Li, W., Feng, C., Xiao, F., and Wu, Y. (2013). A facile route to carbon-coated vanadium carbide nanocapsules as microwave absorbers. RSC Adv. *3*, 18082–18086. https://doi.org/10.1039/c3ra42544d.
282. Rong, H., Zhang, Z., Li, Y., Zhang, X., and Li, L. (2019). Significant magnetocaloric and microwave absorption performances in ultrafine ErC_2@C core-shell structural nanocomposites. Compos. Commun. *12*, 123–127. https://doi.org/10.1016/j.coco.2019.01.011.
283. Wang, P., Liu, D., Cui, L., Hu, B., Han, X., and Du, Y. (2021). A review of recent advancements in Ni-related materials used for microwave absorption. J. Phys. D Appl. Phys. *54*, 473003. https://doi.org/10.1088/1361-6463/ac196d.
284. Yuan, X., Huang, S., Li, B., Sha, A., Zhao, H., Chen, X., Zhang, Y., and Guo, S. (2022). Tunable microwave absorption band via rational design of C@TiC nanospheres. Ceram. Int. *48*, 15576–15581. https://doi.org/10.1016/j.ceramint.2022.02.091.
285. Lian, Y., Han, B., Liu, D., Wang, Y., Zhao, H., Xu, P., Han, X., and Du, Y. (2020). Solvent-free synthesis of ultrafine tungsten carbide nanoparticles-decorated carbon nanosheets for microwave absorption. Nano-Micro Lett. *12*, 153. https://doi.org/10.1007/s40820-020-00491-5.
286. Bateer, B., Wang, L., Zhao, L., Yu, P., Tian, C., Pan, K., and Fu, H. (2015). A novel Fe_3C/graphitic carbon composite with electromagnetic wave absorption properties in the C-band. RSC Adv. *5*, 60135–60140. https://doi.org/10.1039/c5ra08623j.
287. Xu, Z., Wang, S., Xie, Y., Xing, Z., Li, Q., Qi, L., Pan, K., and Chen, Y. (2022). Monodisperse branched nickel carbide nanoparticles in situ grown on reduced graphene oxide with excellent electromagnetic absorption properties. J. Alloys Compd. *900*, 163453. https://doi.org/10.1016/j.jallcom.2021.163453.
288. Ban, Q., Li, Y., Qin, Y., Zheng, Y., Xie, X., Yu, Z., and Kong, J. (2022). Hierarchical engineering of Large-caliber carbon Nanotube/Mesoporous Carbon/Fe_3C nanoparticle hybrid nanocomposite towards Ultra-lightweight electromagnetic microwave absorber. J. Colloid Interface Sci. *616*, 618–630. https://doi.org/10.1016/j.jcis.2022.02.104.
289. Gao, S., Yang, S.H., Wang, H.Y., Wang, G.S., and Yin, P.G. (2020). Excellent electromagnetic wave absorbing properties of two-dimensional carbon-based nanocomposite supported by transition metal carbides Fe_3C. Carbon *162*, 438–444. https://doi.org/10.1016/j.carbon.2020.02.031.
290. Tang, H., Jian, X., Wu, B., Liu, S., Jiang, Z., Chen, X., Lv, W., He, W., Tian, W., Wei, Y., et al. (2016). Fe_3C/helical carbon nanotube hybrid: Facile synthesis and spin-induced enhancement in microwave-absorbing properties. Composites, Part B *107*, 51–58. https://doi.org/10.1016/j.compositesb.2016.09.003.
291. Fan, G., Jiang, Y., Xin, J., Zhang, Z., Fu, X., Xie, P., Cheng, C., Liu, Y., Qu, Y., Sun, K., and Fan, R. (2019). Facile synthesis of Fe@Fe_3C/C nanocomposites derived from bulrush for excellent electromagnetic wave-absorbing properties. ACS Sustainable Chem. Eng. *7*, 18765–18774. https://doi.org/10.1021/acssuschemeng.9b02913.
292. Li, N., Liu, L., Duan, Y., Gu, H., Huang, J., Dong, C., Guan, H., and Chen, G. (2023). Exploration of magnetic media modulation engineering on heterogeneous carbon spheres for optimized electromagnetic wave absorption. J. Alloys Compd. *943*, 169109. https://doi.org/10.1016/j.jallcom.2023.169109.
293. Wang, L., Xiong, H., Ur Rehman, S., Chen, Y., Tan, Q., Zhang, L., Zhong, M., and Zhong, Z. (2019). Optimized microstructure and impedance matching for improving the absorbing properties of core-shell C@Fe_3C/Fe nanocomposites. J. Alloys Compd. *780*, 552–557. https://doi.org/10.1016/j.jallcom.2018.12.001.
294. Niu, Y., Li, X., Dong, W., Zhang, C., Zhao, K., Wang, F., and Wang, H. (2020). Synthesis of N-doped carbon with embedded Fe/Fe_3C particles for microwave absorption. J. Mater. Sci. *55*, 11970–11983. https://doi.org/10.1007/s10853-020-04918-7.
295. Xu, C., Xu, H., Yang, Z., Guo, C., Zhang, X., Zhu, C., Zhang, X., and Chen, Y. (2023). Fabrication of N-doped carbon nanotube/carbon fiber dendritic composites with abundant interfaces for electromagnetic wave absorption. Carbon *40*, 234–245. https://doi.org/10.1016/j.carbon.2022.09.033.
296. Sun, Y., Wang, Y., Ma, H., Zhou, Y., Xing, H., Feng, W., Feng, J., Shi, Z., Zong, Y., Li, X., and Zheng, X. (2021). Fe_3C nanocrystals encapsulated in N-doped carbon nanofibers as high-efficient microwave absorbers with superior oxidation/corrosion resistance. Carbon *178*, 515–527. https://doi.org/10.1016/j.carbon.2021.03.032.
297. Sun, C., Guo, Y., Xu, X., Du, Q., Duan, H., Chen, Y., Li, H., and Liu, H. (2017). In situ preparation of carbon/Fe_3C composite nanofibers with excellent electromagnetic wave absorption properties. Composites, Part A *92*, 33–41. https://doi.org/10.1016/j.compositesa.2016.10.033.
298. Liu, H., Li, Y., Yuan, M., Sun, G., Liao, Q., and Zhang, Y. (2018). Solid and macroporous Fe_3C/N-C nanofibers with enhanced electromagnetic wave absorbability. Sci. Rep. *8*, 16832. https://doi.org/10.1038/s41598-018-35078-z.
299. Jiang, Y., Fu, X., Zhang, Z., Du, W., Xie, P., Cheng, C., and Fan, R. (2019). Enhanced microwave absorption properties of Fe_3C/C nanofibers prepared by electrospinning. J. Alloys Compd. *804*, 305–313. https://doi.org/10.1016/j.jallcom.2019.07.038.
300. Wang, C., Zong, L., Li, N., Pan, Y., Liu, Q., Zhang, F., Qiao, L., Wang, J., and Jian, X. (2021). Light-weight 1D heteroatoms-doped Fe_3C@C nanofibers for microwave absorption with a thinner matching thickness. J. Alloys Compd. *885*, 160968. https://doi.org/10.1016/j.jallcom.2021.160968.
301. Zhang, Y., Liu, W., Quan, B., Ji, G., Ma, J., Li, D., and Meng, W. (2017). Achieving the interfacial polarization on C/Fe_3C heterojunction structures for highly efficient lightweight microwave absorption. J. Colloid Interface Sci. *508*, 462–468. https://doi.org/10.1016/j.jcis.2017.08.074.
302. Li, X., Wu, Z., You, W., Yang, L., and Che, R. (2022). Self-Assembly MXene-rGO/CoNi Film with Massive Continuous Heterointerfaces and Enhanced Magnetic Coupling for Superior Microwave Absorber. Nano-Micro Lett. *14*, 73. https://doi.org/10.1007/s40820-022-00811-x.
303. Zhang, S., Jia, Z., Zhang, Y., and Wu, G. (2022). Electrospun $Fe_{0.64}Ni_{0.36}$/MXene/CNFs nanofibrous membranes with multicomponent heterostructures as flexible electromagnetic wave absorbers. Nano Res. *16*, 3395–3407. https://doi.org/10.1007/s12274-022-5368-1.
304. Dai, S., Quan, B., Zhang, B., Liang, X., and Ji, G. (2018). Constructing multi-interface Mo_2C/Co@C nano-rods for a microwave response based on a double attenuation mechanism. Dalton Trans. *47*, 14767–14773. https://doi.org/10.1039/c8dt03282c.
305. Zeng, X., Zhao, C., Nie, T., Shen, Z.Y., Yu, R., and Stucky, G.D. (2022). Construction of 0D/1D/2D MXene nanoribbons-NiCo@NC hierarchical network and their coupling effect on electromagnetic wave absorption. Mater. Today Phys. *28*, 100888. https://doi.org/10.1016/j.mtphys.2022.100888.
306. Javid, M., Qu, X., Huang, F., Li, X., Farid, A., Shah, A., Duan, Y., Zhang, Z., Dong, X., and Pan, L. (2021). In-situ synthesis of SiC/Fe nanowires coated with thin amorphous carbon layers for excellent electromagnetic wave absorption in GHz range. Carbon *171*, 785–797. https://doi.org/10.1016/j.carbon.2020.09.066.
307. Nguyen, V.T., Min, B.K., Yi, Y., Kim, S.J., and Choi, C.G. (2020). MXene($Ti_3C_2T_x$)/graphene/PDMS composites for multifunctional broadband electromagnetic interference shielding skins. Chem. Eng. J. *393*, 124608. https://doi.org/10.1016/j.cej.2020.124608.
308. Ghanbari, F., Moradi Dehaghi, S., and Mahdavi, H. (2020). Epoxy-based multilayered coating containing carbon nanotube (CNT), silicon carbide (SiC), and carbonyl iron (CI) particles: as efficient microwave absorbing materials. J. Coating Technol. Res. *17*, 815–826. https://doi.org/10.1007/s11998-019-00309-z.
309. Liu, H., Wang, Z., Yang, Y., Wu, S., Wang, C., You, C., and Tian, N. (2022). Thermally conductive MWCNTs/Fe_3O_4/$Ti_3C_2T_x$ MXene multi-layer films for broadband electromagnetic interference shielding.

J. Mater. Sci. Technol. *130*, 75–85. https://doi.org/10.1016/j.jmst.2022.05.009.

310. Gordani, G.R., Loghman Estarki, M.R., Kiani, E., and Torkian, S. (2022). The effects of strontium ferrite micro-and nanoparticles on the microstructure, phase, magnetic properties, and electromagnetic waves absorption of graphene oxide-$SrFe_{12}O_{19}$-SiC aerogel nanocomposite. J. Magn. Magn Mater. *545*, 168667. https://doi.org/10.1016/j.jmmm.2021.168667.
311. Wang, J., Hu, S., Tang, Q., Xu, J., Xu, N., Yu, S., Wang, X., and Tian, H. (2022). One-pot hydrothermally prepared rGO/SiC/$CoFe_2O_4$ composites with strong microwave absorption at different thicknesses. Ceram. Int. *48*, 30640–30650. https://doi.org/10.1016/j.ceramint.2022.07.007.
312. Cui, Y., Yang, K., Wang, J., Shah, T., Zhang, Q., and Zhang, B. (2021). Preparation of pleated RGO/MXene/Fe_3O_4 microsphere and its absorption properties for electromagnetic wave. Carbon *172*, 1–14. https://doi.org/10.1016/j.carbon.2020.09.093.
313. Cui, C., Guo, R., Ren, E., Xiao, H., Zhou, M., Lai, X., Qin, Q., Jiang, S., and Qin, W. (2021). MXene-based rGO/Nb_2CT_x/Fe_3O_4 composite for high absorption of electromagnetic wave. Chem. Eng. J. *405*, 126626. https://doi.org/10.1016/j.cej.2020.126626.
314. Zhang, C., Wu, Z., Xu, C., Yang, B., Wang, L., You, W., and Che, R. (2022). Hierarchical $Ti_3C_2T_x$ MXene/Carbon Nanotubes Hollow Microsphere with Confined Magnetic Nanospheres for Broadband Microwave Absorption. Small *18*, 2104380. https://doi.org/10.1002/smll.202104380.
315. Huo, Y., Zhao, K., Peng, M., Li, F., Lu, Z., Meng, Q., and Tang, Y. (2022). Anchoring of SiC and Fe_3Si nanocrystallines in carbon nanofibers inducing interfacial polarization to promote microwave attenuation ability. J. Alloys Compd. *891*, 162006. https://doi.org/10.1016/j.jallcom.2021.162006.
316. Chen, S., Dong, X., Yao, X., Wu, P., Liu, A., and Yu, Z. (2021). Fabrication, microstructural evolution and excellent EMW absorbing properties of SiC fibers with high iron content. J. Mater. Chem. C *9*, 13509–13519. https://doi.org/10.1039/d1tc03281j.
317. Zhou, Y., Muhammad, J., Zhang, X., Wang, D., Duan, Y., Dong, X., and Zhang, Z. (2018). Novel nanocapsules with Co-TiC twin cores and regulable graphitic shells for superior electromagnetic wave absorption. RSC Adv. *8*, 6397–6405. https://doi.org/10.1039/c8ra00040a.
318. Zhou, Y., Muhammad, J., Zhou, T., Wang, D., Wang, X., Duan, Y., Zhang, X., Dong, X., and Zhang, Z. (2019). Incorporation of magnetic component to construct (TiC/Ni)@C ternary composite with heterogeneous interface for enhanced microwave absorption. J. Alloys Compd. *778*, 779–786. https://doi.org/10.1016/j.jallcom.2018.11.237.
319. Li, H., Gao, S., Tong, H., Liu, Y., Wu, A., and Hao, H. (2022). The capacitive loss of microwave energy in Ni@SiC@C core/bi-shell nanoparticles. Chem. Eng. J. *434*, 134655. https://doi.org/10.1016/j.cej.2022.134655.
320. Wang, H., Zhao, J., Yu, J., and Wang, Z. (2023). Metal organic framework-derived hierarchical 0D/1D CoPC/CNTs architecture interlaminated in 2D MXene layers for superior absorption of electromagnetic waves. Synth. Met. *292*, 117215. https://doi.org/10.1016/j.synthmet.2022.117215.
321. Gao, X., Hao, M., Tan, Q., Wang, J., Li, Y., Chen, J., Sun, W., and Li, Y. (2022). Highly performant electromagnetic absorption at the X band based on Co@NCS/$Ti_3C_2T_x$ composites. ACS Appl. Mater. Interfaces *14*, 56213–56225. https://doi.org/10.1021/acsami.2c19926.
322. Xiang, Z., Shi, Y., Zhu, X., Cai, L., and Lu, W. (2021). Flexible and Waterproof 2D/1D/0D Construction of MXene-Based Nanocomposites for Electromagnetic Wave Absorption, EMI Shielding, and Photothermal Conversion. Nano-Micro Lett. *13*, 150. https://doi.org/10.1007/s40820-021-00673-9.
323. Ling, X., Wang, K., Zhang, W., Wu, Y., Jin, Q., and Zhang, D. (2022). Bio-inspired, bimetal ZIF-derived hollow carbon/MXene microstructure aim for superior microwave absorption. J. Colloid Interface Sci. *625*, 317–327. https://doi.org/10.1016/j.jcis.2022.06.011.
324. Guo, Z., Ren, P., Yang, F., Wu, T., Zhang, L., Chen, Z., Huang, S., and Ren, F. (2023). MOF-derived Co/C and MXene co-decorated cellulose-cerived hybrid carbon aerogel with a multi-interface architecture toward absorption-dominated ultra-efficient electromagneticinterference shielding. ACS Appl. Mater. Interfaces *15*, 7308–7318. https://doi.org/10.1021/acsami.2c22447.
325. Liu, Z., Chen, J., Que, M., Zheng, H., Yang, L., Yuan, H., Ma, Y., Li, Y., and Yang, X. (2022). 2D $Ti_3C_2T_x$ MXene/MOFs composites derived CoNi bimetallic nanoparticles for enhanced microwave absorption. Chem. Eng. J. *450*, 138442. https://doi.org/10.1016/j.cej.2022.138442.
326. Yang, G., Wen, B., Wang, Y., Zhou, X., Liu, X., and Ding, S. (2023). In situ construction of ZIF-67 derived Mo_2C@cobalt/carbon composites toward excellent electromagnetic wave absorption properties. Nanotechnology *34*, 185704. https://doi.org/10.1088/1361-6528/acb655.
327. Huang, W., Zhang, X., Zhao, Y., Zhang, J., and Liu, P. (2020). Hollow N-doped carbon polyhedra embedded Co and Mo_2C nanoparticles for high-efficiency and wideband microwave absorption. Carbon *167*, 19–30. https://doi.org/10.1016/j.carbon.2020.05.073.
328. Zhao, B., Wu, N., Yao, S., Yao, Y., Lian, Y., Li, B., Zeng, Z., and Liu, J. (2022). Molybdenum carbide/cobalt composite nanorods via a "MOFs plus MOFs" strategy for high-efficiency microwave absorption. ACS Appl. Nano Mater. *5*, 18697–18707. https://doi.org/10.1021/acsanm.2c04460.
329. Zhang, N., Chen, P., Wang, Y., Zong, M., and Chen, W. (2022). Supramolecular self-assembly derived Mo_2C/FeCo/NC hierarchical nanostructures with excellent wideband microwave absorption properties. Compos. Sci. Technol. *221*, 109325. https://doi.org/10.1016/j.compscitech.2022.109325.
330. Du, L., Du, Y., Li, Y., Wang, J., Wang, C., Wang, X., Xu, P., and Han, X. (2010). Surfactant-assisted solvothermal synthesis of $Ba(CoTi)_xFe_{12-2x}O_{19}$ nanoparticles and enhancement in microwave absorption properties of polyaniline. J. Phys. Chem. C *114*, 19600–19606. https://doi.org/10.1021/jp1067268.
331. Cao, M.S., Yang, J., Song, W.L., Zhang, D.Q., Wen, B., Jin, H.B., Hou, Z.L., and Yuan, J. (2012). Ferroferric oxide/multiwalled carbon nanotube vs polyaniline/ferroferric oxide/multiwalled carbon nanotube multiheterostructures for highly effective microwave absorption. ACS Appl. Mater. Interfaces *4*, 6949–6956. https://doi.org/10.1021/am3021069.
332. Wu, F., Xie, A., Sun, M., Wang, Y., and Wang, M. (2015). Reduced graphene oxide (RGO) modified spongelike polypyrrole (PPy) aerogel for excellent electromagnetic absorption. J. Mater. Chem. A *3*, 14358–14369. https://doi.org/10.1039/c5ta01577d.
333. Yin, G., Wang, Y., Wang, W., and Yu, D. (2020). Multilayer structured PANI/MXene/CF fabric for electromagnetic interference shielding constructed by layer-by-layer strategy. Colloids Surf., A *601*, 125047. https://doi.org/10.1016/j.colsurfa.2020.125047.
334. Liu, J., Gu, Y., Gao, L., Tao, J., Tan, R., Duan, L., Yao, Z., and Zhou, J. (2023). Hollow multi-shell SiC@C@PANI nanoparticles with broadband microwave absorption performance. Appl. Surf. Sci. *613*, 156098. https://doi.org/10.1016/j.apsusc.2022.156098.
335. Dong, S., Zhang, X., Zhang, W., Han, J., and Hu, P. (2018). A multiscale hierarchical architecture of a SiC whiskers- graphite nanosheets/polypyrrole ternary composite for enhanced electromagnetic wave absorption. J. Mater. Chem. C *6*, 10804–10814. https://doi.org/10.1039/c8tc03683g.
336. Dong, S., Zhang, X., Hu, P., Zhang, W., Han, J., and Hu, P. (2019). Biomass-derived carbon and polypyrrole addition on SiC whiskers for enhancement of electromagnetic wave absorption. Chem. Eng. J. *359*, 882–893. https://doi.org/10.1016/j.cej.2018.11.101.
337. Wu, Z., Yang, Z., Jin, C., Zhao, Y., and Che, R. (2021). Accurately Engineering 2D/2D/0D Heterojunction In Hierarchical $Ti_3C_2T_x$ MXene Nanoarchitectures for Electromagnetic Wave Absorption and Shielding. ACS Appl. Mater. Interfaces *13*, 5866–5876. https://doi.org/10.1021/acsami.0c21833.
338. Wang, J., Liu, L., Jiao, S., Ma, K., Lv, J., and Yang, J. (2020). Hierarchical carbon fiber@MXene@MoS_2 core-sheath synergistic microstructure for tunable and efficient microwave absorption. Adv. Funct. Mater. *30*, 2002595. https://doi.org/10.1002/adfm.202002595.
339. Tian, L., Xu, J., Just, M., Green, M., Liu, L., and Chen, X. (2017). Broad range energy absorption enabled by hydrogenated TiO_2 nanosheets: from optical to infrared and microwave. J. Mater. Chem. C *5*, 4645–4653. https://doi.org/10.1039/c7tc01189j.
340. Han, X., Huang, Y., Gao, S., Zhang, G., Li, T., and Liu, P. (2021). A hierarchical carbon Fiber@MXene@ZnO core-sheath synergistic microstructure for efficient microwave absorption and photothermal conversion. Carbon *183*, 872–883. https://doi.org/10.1016/j.carbon.2021.07.072.
341. Wang, J., Zhang, F., Li, Y., Ahmad, M., Liu, P., Zhang, Q., and Zhang, B. (2022). Constructing TCNFs/MXene/TiO_2 microspheres with wrinkled surface for excellent electromagnetic wave absorption. J. Alloys Compd. *918*, 165623. https://doi.org/10.1016/j.jallcom.2022.165623.

342. Cai, Z., Ma, Y., Zhao, K., Yun, M., Wang, X., Tong, Z., Wang, M., Suhr, J., Xiao, L., Jia, S., and Chen, X. (2023). $Ti_3C_2T_x$ MXene/graphene oxide/Co_3O_4 nanorods aerogels with tunable and broadband electromagnetic wave absorption. Chem. Eng. J. *462*, 142042. https://doi.org/10.1016/j.cej.2023.142042.

343. Tao, F., Green, M., Tran, A.T.V., Zhang, Y., Yin, Y., and Chen, X. (2019). Plasmonic Cu_9S_5 nanonets for microwave absorption. ACS Appl. *Nano Mater. 2*, 3836–3847. https://doi.org/10.1021/acsanm.9b00700.

344. Hou, T., Jia, Z., Wang, B., Li, H., Liu, X., Bi, L., and Wu, G. (2021). MXene-based accordion 2D hybrid structure with Co_9S_8/C/$Ti_3C_2T_x$ as efficient electromagnetic wave absorber. Chem. Eng. J. *414*, 128875. https://doi.org/10.1016/j.cej.2021.128875.

345. Li, S., Tang, X., Zhao, X., Lu, S., Luo, J., Chai, Z., Ma, T., Lan, Q., Ma, P., Dong, W., et al. (2023). Hierarchical graphene@MXene composite foam modified with flower-shaped FeS for efficient and broadband electromagnetic absorption. J. Mater. Sci. Technol. *133*, 238–248. https://doi.org/10.1016/j.jmst.2022.06.018.

346. Deng, W., Li, T., Li, H., Niu, R., Dang, A., Cheng, Y., and Wu, H. (2023). In situ construction of hierarchical core-shell SiCnws@SiO_2-carbon foam hybrid composites with enhanced polarization loss for highly efficient electromagnetic wave absorption. Carbon *202*, 103–111. https://doi.org/10.1016/j.carbon.2022.10.081.

347. Wang, L., Huang, Y., Sun, X., Huang, H., Liu, P., Zong, M., and Wang, Y. (2014). Synthesis and microwave absorption enhancement of graphene@Fe_3O_4@SiO_2@NiO nanosheet hierarchical structures. Nanoscale *6*, 3157–3164. https://doi.org/10.1039/c3nr05313j.

348. Chen, Y.J., Gao, P., Zhu, C.L., Wang, R.X., Wang, L.J., Cao, M.S., and Fang, X.Y. (2009). Synthesis, magnetic and electromagnetic wave absorption properties of porous Fe_3O_4/Fe/SiO_2 core/shell nanorods. J. Appl. Phys. *106*, 054303. https://doi.org/10.1063/1.3204958.

349. Jahanaray, M., and Mirzaee, O. (2023). Structural, magnetic and microwave absorption properties of novel hollow core-shell ($SrMnCoFe_{10}O_{19}$/$MnCoFe_2O_4$)/SiO_2 composite microfibers synthesized via electrospinning. Ceram. Int. *49*, 11893–11902. https://doi.org/10.1016/j.ceramint.2022.12.037.

350. Zhao, K., Ye, F., Cheng, L., Liu, R., Liang, J., and Li, X. (2022). Synthesis of embedded ZrC-SiC-C microspheres via carbothermal reduction for thermal stability and electromagnetic wave absorption. Appl. Surf. Sci. *591*, 153105. https://doi.org/10.1016/j.apsusc.2022.153105.

351. Ye, X., Chen, Z., Ai, S., Hou, B., Zhang, J., Zhou, Q., Liu, H., and Cui, S. (2019). Enhanced electromagnetic absorption properties of novel 3D-CF/PyC modified by reticulated SiC coating. ACS Sustainable Chem. Eng. *7*, 11386–11395. https://doi.org/10.1021/acssuschemeng.9b01101.

352. Hou, Z., Xue, J., Wei, H., Fan, X., Ye, F., Fan, S., Cheng, L., and Zhang, L. (2020). Tailorable microwave absorption properties of RGO/SiC/CNT nanocomposites with 3D hierarchical structure. Ceram. Int. *46*, 18160–18167. https://doi.org/10.1016/j.ceramint.2020.04.137.

353. He, X., Feng, L., Zhang, Z., Hou, X., Ye, X., Song, Q., Yang, Y., Suo, G., Zhang, L., Fu, Q.G., and Li, H. (2021). High-performance multifunctional carbon-silicon carbide composites with strengthened reduced graphene oxide. ACS Nano *15*, 2880–2892. https://doi.org/10.1021/acsnano.0c08924.

354. Yuan, X., Li, H., Sha, A., Huang, S., Li, B., and Guo, S. (2022). Flexible Mo_2C-modified SiC/C nanofibers for broadband electromagnetic wave absorption. Adv. Mater. Interfac. *9*, 2200333. https://doi.org/10.1002/admi.202200333.

355. Yang, K., Cui, Y., Wan, L., Wang, Y., Tariq, M.R., Liu, P., Zhang, Q., and Zhang, B. (2022). Preparation of three-dimensional Mo_2C/NC@MXene and its efficient electromagnetic absorption properties. ACS Appl. Mater. Interfaces *14*, 7109–7120. https://doi.org/10.1021/acsami.1c19033.

356. Zhou, W., Long, L., and Li, Y. (2019). Mechanical and electromagnetic wave absorption properties of C-f-Si3N4 ceramics with PyC/SiC interphases. J. Mater. Sci. Technol. *35*, 2809–2813. https://doi.org/10.1016/j.jmst.2019.07.002.

357. Luo, H., Chen, W., Zhou, W., Long, L., Deng, L., Xiao, P., and Li, Y. (2017). Carbon fiber/Si_3N_4 composites with SiC nanofiber interphase for enhanced microwave absorption properties. Ceram. Int. *43*, 12328–12332. https://doi.org/10.1016/j.ceramint.2017.06.096.

358. Xiao, S., Mei, H., Han, D., and Cheng, L. (2020). Sandwich-like SiCnw/C/Si_3N_4 porous layered composite for full X-band electromagnetic wave absorption at elevated temperature. Composites, Part B *183*, 107629. https://doi.org/10.1016/j.compositesb.2019.107629.

359. Hou, T., Jia, Z., Wang, B., Li, H., Liu, X., Chi, Q., and Wu, G. (2021). Metal-organic framework-derived $NiSe_2$-$CoSe_2$@C/$Ti_3C_2T_x$ composites as electromagnetic wave absorbers. Chem. Eng. J. *422*, 130079. https://doi.org/10.1016/j.cej.2021.130079.

360. Wu, Y., Zhong, Y., Guan, Y., Gu, C., Shao, G., Shi, B., Su, Z., Xu, B., Yu, Z., and Liu, A. (2020). Polymer-derived Co_2Si@SiC/C/SiOC/SiO_2/Co_3O_4 nanoparticles: Microstructural evolution and enhanced EM absorbing properties. J. Am. Ceram. Soc. *103*, 6764–6779. https://doi.org/10.1111/jace.17141.